

©Copyright 2018

Molly E. Gear

# Characterization of Marine Mammal Biomechanics to Evaluate Tidal Turbine Collision Impact

Molly E. Gear

A dissertation  
submitted in partial fulfillment of the  
requirements for the degree of

Doctor of Philosophy

University of Washington

2018

Reading Committee:

Michael R. Motley, Chair

Adam P. Summers

Andrea E. Copping

Program Authorized to Offer Degree:  
Civil and Environmental Engineering

University of Washington

## **Abstract**

Characterization of Marine Mammal Biomechanics to Evaluate Tidal Turbine Collision Impact

Molly E. Gear

Chair of the Supervisory Committee:  
Assistant Professor Michael R. Motley  
Civil and Environmental Engineering

Tidal energy has an immense potential for creating renewable energy from the ocean's moving tides and is under investigation worldwide. In this emerging field, potential environmental consequences of installing tidal turbines must be evaluated. Marine mammals often use tidal channels for feeding or traveling and may collide with the spinning blades. In the United States, tidal turbines must comply with the Marine Mammal Protection Act and not threaten or harass marine mammals, thus this risk must be evaluated. Since tidal turbines move relatively slowly, this injury may be non-fatal and sustained to soft tissue. The extent and severity of a turbine strike can be modeled numerically to understand this potential injury before installing tidal turbines. Though some finite element models have been developed for this purpose, improved material models are necessary to more accurately model this interaction. Marine mammals' outer layers are composed of a thin epidermal and dermal layer, skin, then blubber, a thicker subcutaneous fat layer. Uniaxial tensile testing of the skin and blubber layers across a series of species was conducted to determine four material properties: elastic modulus, tensile strength, strain to failure, and yield strength. The skin and blubber compressive elastic modulus were tested using spherical indentation, bulk modulus using volumetric compression, and shear modulus with a rotational test. The results of these tests were analyzed using a principal component analysis to understand the

relationship among the material quantities and differences between species. The material properties are used to represent the soft tissue of each species in a material constitutive model which is validated by comparison with a variety of material tests. Ultimately, a finite element analysis of an impact between a tidal turbine and marine mammal can be created, showing the regions of tissue impacted by a tidal turbine strike. With those models, regulators can evaluate the safety for these protected marine mammals. This result is useful in permitting new tidal turbines, allowing effective management of the ocean's resources.

## TABLE OF CONTENTS

	Page
List of Figures . . . . .	v
List of Tables . . . . .	xi
Chapter 1: Introduction . . . . .	1
1.1 Motivation . . . . .	1
1.2 Environmental Impacts of Tidal Energy . . . . .	1
1.3 Marine Mammal Behavior in Tidal Channels . . . . .	3
1.4 Marine Mammal Potential Injury . . . . .	5
1.5 Finite Element Method Modeling of Soft Tissue . . . . .	8
1.6 Previous Work and Similar Approaches . . . . .	9
1.7 Thesis Outline . . . . .	10
Chapter 2: Tensile Testing of Marine Mammal Soft Tissue . . . . .	12
2.1 Overview . . . . .	12
2.2 Methodology . . . . .	12
2.2.1 Tissue Procurement . . . . .	12
2.2.2 Tensile Tissue Testing . . . . .	14
2.2.3 Data Processing . . . . .	17
2.2.4 Data Analysis . . . . .	18
2.3 Results . . . . .	21
2.3.1 Observations across all tensile testing . . . . .	21
2.3.2 Behavior of Harbor Seal Skin and Blubber . . . . .	22
2.3.3 Multivariate Analysis across Species . . . . .	31
2.4 Summary . . . . .	37

Chapter 3:	Indentation, shear modulus, bulk modulus, density, and histology experiments . . . . .	39
3.1	Overview . . . . .	39
3.2	Indentation Testing . . . . .	40
3.2.1	Overview . . . . .	40
3.2.2	Methodology . . . . .	41
3.2.3	Results . . . . .	44
3.3	Conclusions . . . . .	47
3.4	Bulk Modulus . . . . .	48
3.4.1	Overview . . . . .	48
3.4.2	Methods . . . . .	49
3.4.3	Results . . . . .	54
3.5	Shear Modulus . . . . .	54
3.5.1	Overview . . . . .	54
3.5.2	Methods . . . . .	56
3.5.3	Results . . . . .	59
3.6	Density . . . . .	59
3.6.1	Methods . . . . .	61
3.6.2	Results . . . . .	62
3.7	Histology . . . . .	62
3.7.1	Overview . . . . .	62
3.7.2	Methods . . . . .	62
3.7.3	Results . . . . .	64
3.8	Discussion . . . . .	64
Chapter 4:	Validation of Material Model . . . . .	67
4.1	Overview . . . . .	67
4.2	Methodology . . . . .	68
4.2.1	Material Models . . . . .	68
4.2.2	Blubber Linear Elastic Models . . . . .	70
4.2.3	Blubber Hyperelastic Models . . . . .	71
4.2.4	Skin Linear Elastic Models . . . . .	73
4.2.5	Skin Hyperelastic Models . . . . .	73

4.2.6	Abaqus Setup . . . . .	73
4.2.7	Material Models Tested . . . . .	76
4.3	Results . . . . .	76
4.3.1	Blubber Only Material Modeling . . . . .	76
4.3.2	Skin and Blubber Material Modeling . . . . .	79
4.3.3	Shear and Bulk Modulus Comparison . . . . .	82
Chapter 5:	Parameterization of Material Properties for Finite Element Analysis . .	85
5.1	Overview . . . . .	85
5.2	Parameterization of L112 and J32 . . . . .	87
5.2.1	Methodology . . . . .	87
5.2.2	Finite Element Model Results . . . . .	91
5.2.3	Discussion . . . . .	95
5.3	Comparative Finite Element Method Study . . . . .	95
5.3.1	Methods . . . . .	95
5.3.2	Comparative effect of load on defomation . . . . .	97
Chapter 6:	Conclusions and Future Work . . . . .	99
6.1	Summary and Major Findings . . . . .	99
6.1.1	Tensile Testing . . . . .	99
6.1.2	Indentation Testing . . . . .	100
6.1.3	Bulk and shear modulus . . . . .	100
6.1.4	Histology . . . . .	101
6.1.5	Validation . . . . .	101
6.1.6	Parametric Studies . . . . .	102
6.2	Future Work . . . . .	102
6.2.1	Constructing a complete model . . . . .	102
6.2.2	Material Testing . . . . .	105
6.2.3	Additional Species . . . . .	105
6.2.4	Environmental Monitoring Applications . . . . .	106
6.2.5	Control Theory Applications . . . . .	106
6.2.6	Stakeholder Engagement and Retiring Risk . . . . .	106
Bibliography	. . . . .	108

Appendix A: Tensile Testing Results . . . . .	116
Appendix B: Marine Mammal Parts Permits and Necropsy Reports . . . . .	126



## LIST OF FIGURES

Figure Number	Page
1.1 Structure of juvenile killer whale skin and blubber. . . . .	6
2.1 Schematic of where tissue is collected on the animal (a) and the seal tissue separated into skin and blubber after removing from animal (b) . . . . .	13
2.2 Dimensions and geometry of metal punches used for creating material tensile testing specimens, with (left) a rectangular shaped punch for testing modulus of elasticity and (right) a dogbone shaped punch for testing tensile strength. . . . .	15
2.3 Example stress-strain curve shows the test result of a dogbone shaped sample. 'Tensile stiffness' (also called E, Young's modulus) is measured as the slope of the linear part of this curve. 'Tensile strength' is measured as the maximum strength. The plastic region' of the curve is the region where the curve begins to yield, but has not yet failed completely. The inset shows the test setup for this stress strain curve. . . . .	16
2.4 Stress-strain curves for rectangular shaped tissue specimens from Seal 1 tested at a 10 mm/s test speed. Note that y-axis scale is different for skin (greens) and blubber (blues). Blubber stress-strain curve shows a larger strain to failure and less defined plastic region. . . . .	23
2.5 Tensile stiffness of blubber (blues) and skin (greens) in three adult Harbor Seals (data averaged over orientation). As an overall trend, skin and blubber show a stiffening effect with higher test speeds. . . . .	25
2.6 Elastic modulus and tensile strength shown for fresh and frozen adult harbor seal samples at a test speed of 10 mm/s. Within each animal, the data remains isotropic, as in the fresh samples. . . . .	27
2.7 For every test repeated both on both fresh and frozen data, the data are paired to compare the same angle and animal. For harbor seal skin (A,B), the freezing generally results in larger values for both strength and elastic modulus. For harbor seal blubber (C,D), freezing adult blubber results in a decreased strength and elastic modulus. However, freezing pup blubber overpredicted the fresh pup blubber material properties (C,D). . . . .	28

2.8	Biplot of PCA ordination of all skin material properties with species (Dall's Porpoise, Harbor Porpoise, Harbor Seal, or Killer Whale) denoted. The toothed whales (Dall's Porpoise, Harbor Seal, and Killer Whale) show a clustering separate from the pinniped (Harbor seal) in the ordinate space. The material properties were highly loaded on the first two principal components, with the exact loadings (structure coefficients) in Table 2.1 . . . . .	33
2.9	Boxplots of each of the four material properties over all tests for each species blubber, including both juvenile and adult animals. All marine mammals show the same general trends in the relationship between the relationships between the material properties captured in tensile testing. . . . .	34
2.10	Biplot of PCA ordination of all skin material properties with species (Dall's Porpoise, Harbor Porpoise, or Killer Whale) denoted. The toothed whales still cluster together and overlap even when the seal data is removed. . . . .	35
2.11	Biplot of PCA ordination of all skin material properties with species (Dall's Porpoise, Harbor Porpoise, Harbor Seal, or Killer Whale) denoted. The toothed whales (Dall's Porpoise, Harbor Seal, and Killer Whale) show a clustering separate from the pinniped (Harbor seal) in the ordinate space. The material properties were highly loaded on the first two principal components, with the exact loadings (structure coefficients) in Table 2.1 . . . . .	36
3.1	Example stress-strain curve of compression testing. Inset shows testing setup.	42
3.2	Harbor porpoise ( <i>Phocoena phocoena</i> ) blubber measurements. Lighter orange in the negative direction represents compression tests, while darker orange in the positive direction represents tension testing. Each line represents an individual test, which can be averaged to find the results in Table 3.1. When measured in compression harbor porpoise has an order of magnitude smaller elastic modulus. . . . .	44
3.3	Killer Whale ( <i>Orcinus orca</i> ) blubber measurements. Lighter red in the negative direction represents compression tests, while darker red in the positive direction represents tension testing. Each line represents an individual test, which can be averaged to find the results in Table 3.1. When measured in compression orca has an order of magnitude smaller elastic modulus. As a further difference with harbor porpoise (Figure 3.2), the orca blubber in tension has a much more defined plastic region and overall stiffer values. . . . .	45

3.4	Harbor Seal ( <i>Phocoena vitulina</i> ) blubber measurements. Lighter green in the negative direction represents compression tests, while darker green in the positive direction represents tension testing. Each line represents an individual test, which can be averaged to find the results in Table 3.1. When measured in compression seal has a similar elastic modulus. . . . .	46
3.5	Across all adult orca and harbor porpoise tensile testing, the orca has much stiffer blubber. This trend is also present in compression testing (Figures 3.2-3.3)	47
3.6	Bulk modulus test setup where a downward force is applied to a plate to volumetrically compress a sample . . . . .	50
3.7	Top view of the forces inside the bulk modulus setup once force is applied to sample. Inner ( $r_i$ ) and outer ( $r_o$ ) radius is labeled. . . . .	50
3.8	Clamp design in AutoCAD (a) and after printing on the Formlab Form 2 printer, clamps are rinsed in an alcohol bath (b) . . . . .	52
3.9	Bulk modulus testing results across three animals and two tissues. Middle line of the box plots represent the median of the data, with the box representing the middle 50% of the data. . . . .	55
3.10	Shear modulus plate design in AutoCAD. Left plate is top plate and right is bottom plate compared to Figure 3.11 . . . . .	57
3.11	Shear modulus test setup where motor turns a tissue sample while the force at the outer radius of the top plate is measured. . . . .	58
3.12	Shear modulus testing results across three animals and two tissues. Middle line of the box plots represent the median of the data, with the box representing the middle 50% of the data. . . . .	60
3.13	Density of skin (pictured above) measured through displacing water in a graduated cylinder, measuring the liquid displacement and change in mass. . . .	61
3.14	Microscope photographs of harbor porpoise (a), killer whale (b), and harbor seal (c) skin and blubber layers under polarized light after being preserved in Paraffin wax. . . . .	63
3.15	Microscope photographs of harbor porpoise (a), killer whale (b) skin and blubber layers under polarized light after being preserved in Paraffin wax, highlighting the difference in connection between skin and blubber layers of the two species. . . . .	64
3.16	Structure of juvenile killer whale skin and blubber. . . . .	65
4.1	Force-displacement curve for all blubber only spherical indentation tests . . .	71

4.2	A typical compression curve for blubber is shown in blue. A cubic fit was fit to this data, then a few points were taken on this curve as an input to the Abaqus hyperelastic models. Note that this was modeled in Abaqus as compressive data and thus as negative stress and strain. The oscillations at the beginning come from an artifact of dividing by zero (or very close to zero) in converting the data from force-displacement to stress-strain. . . . .	72
4.3	A typical tensile curve for skin is shown in purple. A fifth order polynomial was fit to this tension testing data (Rectangular sections, tested at 10 mm/s, cut at 0°, per the convention highlighted in Chapter 2), then a few points were taken on this curve as an input to the Abaqus hyperelastic models. . . . .	74
4.4	Abaqus model of the killer whale compressive test for blubber only tests. Mesh is concentrated in center of block, with a rigid plate and sphere to represent the rest of the test. A block with mass is place on top of the sphere to determine the reaction force on the sphere. . . . .	75
4.5	Abaqus model of the killer whale compressive test in two views. Black is skin, pink is blubber, teal is the indentation ball. The indenting ball is modeled as a rigid sphere. . . . .	76
4.6	Spherical indentation raw data tests are shown in gray, with material model results in dotted line for Trial 9 of the J32 killer whale data. . . . .	78
4.7	Spherical indentation raw data tests are shown in gray, with material model results in dotted line for multiple material models tested for the J32 killer whale data. Exact material coefficients can be found in Table 4.1. . . . .	79
4.8	Spherical indentation raw data tests are shown in gray, with material model results in dotted line for multiple material models tested for the HP2 Harbor Porpoise data. Exact material coefficients can be found in Table 4.2. . . . .	80
4.9	Compilation of material models to validate composite behavior of materials. Laboratory data shown in black dashed line. In this case, tension blubber refers to a linear elastic model of the blubber with tension data, compression blubber refers to a linear elastic model applying spherical indentation data, and hyperelastic blubber refers to a hyperelastic model determined from the compression data Trial 9 . . . . .	81
4.10	Compilation of material models highlighting only those using compressive values for blubber. Force displacement curve from laboratory data shown in black line. . . . .	82
4.11	Compilation of bulk and shear modulus generated skin model to validate composite behavior of killer whale tissue. Laboratory data shown in black line. . . . .	84

5.1	L112 orca washed up in Long Beach, WA. February 12th, 2012. Photo by Cascadia Research. . . . .	85
5.2	Three orca specimens have a similar range in their elastic modulus skin values.	87
5.3	Elastic modulus values of orca blubber in tension. L112, a whale observed to be more degraded than other sections, shows a much different blubber pattern.	88
5.4	Stress-strain curves for rectangular shaped tissue specimens from the J32 Orca tested at a 10 mm/s test speed. Blubber stress-strain curve shows a lower strain to failure and less defined plastic region. . . . .	89
5.5	Geometry of each model run. . . . .	90
5.6	Stress (a) and displacement (b) in juvenile orca skin directly under the blade is shown for a model run using average skin elastic modulus values and average blubber values. . . . .	92
5.7	Stress over the course of the model run using high, average, and low orca skin data with low orca blubber data, as prescribed by Table 5.1. In J32, varying the skin doesn't show a strong impact on the results, while the full range of skin values for L112 shows a large amount of variability. . . . .	93
5.8	J32 (a) and L112 (b) skin stress using high, average, and low orca blubber data with high orca skin data, as prescribed by Table 5.1, (c) and (d) show the same for the stress in blubber. The stress in the highest stressed element is reported over the time series of the simulation. In J32, varying the blubber doesn't show a large impact on the results, while the full range of blubber values for L112 shows a large amount of variability especially in skin stress. . . . .	94
5.9	Maximum principal stress under a tensile load of 0.2 MPa on a representative block of layered skin and blubber across four species. Inset describes the finite element method setup for the block of tissue. Black line in A-D denotes interface of skin and blubber. . . . .	97
5.10	Von Mises stress, a formulation of the stress state used to predict the material failure, on a representative block of layered skin and blubber across four species. Inset illustrates the finite element method setup for the block of tissue, where a 10mm diameter rigid ball is indented with 50N of force into the block. Black line in A-D denotes interface of skin and blubber. . . . .	98
6.1	As the blade impacts a killer whale, based on material properties from the parametric study in Chapter 5, the skin experiences the highest stress at the interface between the skin and blubber. . . . .	103

A.1	Box plots show all tensile testing material results from fresh harbor seal ( <i>Phoca vitulina</i> ) tissue at a test speed of 10 mm/s. For each seal, tissue is tested at three orientations. Note that skin (A,B) and blubber (C,D) do not have the same y-scaling. Skin is an order of magnitude stiffer and stronger than the blubber across both the elastic modulus (A,C) and tensile strength (B,D) testing. . . . .	121
A.2	Box plots show all tensile testing material results from frozen Killer whale ( <i>Orcinus orca</i> ) tissue at a test speed of 1 and 10 mm/s. For each whale, tissue is tested at three orientations. Note that skin (A,B) and blubber (C,D) do not have the same y-scaling. Skin is an order of magnitude stiffer and stronger than the blubber across both the elastic modulus (A,C) and tensile strength (B,D) testing. . . . .	122
A.3	Box plots show all tensile testing material results from fresh Harbor Porpoise ( <i>Phocoena phocoena</i> ) and Dall’s Porpoise ( <i>Phocoenoides dalli</i> ), call “H. Porpoise” and “D. Porpoise” respectively. The tissue was tested at speed of 1 and 10 mm/s. For each whale, tissue is tested at three orientations. Note that skin (A,B) and blubber (C,D) do not have the same y-scaling. Skin is an order of magnitude stiffer and stronger than the blubber across both the elastic modulus (A,C) and tensile strength (B,D) testing. . . . .	123
A.4	Example stress strain curves for orca tensile testing in the 0°orientation at 10 mm/s, with blubber in blue and skin in green. . . . .	124
A.5	Example stress strain curves for harbor porpoise tensile testing in the 0°orientation at 10 mm/s, with blubber in blue and skin in green. Note that the two plots are not on the same y-scale and in fact have a different order of magnitude. . . . .	124
A.6	Example stress strain curves for harbor seal tensile testing in the 0°orientation at 10 mm/s, with blubber in blue and skin in green. Note that the two plots are not on the same y-scale and in fact have a different order of magnitude. . . . .	125
B.1	PNNL Authorization from the National Oceanic and Atmospheric Association, which expires January 17, 2018. . . . .	126
B.2	UW Authorization from the National Oceanic and Atmospheric Association, which expires April 1,2020 . . . . .	127
B.3	Necropsy Report from J32, stranded in British Columbia, Canada in December 2014. . . . .	128
B.4	Necropsy Report from Harbor Porpoise, stranded on Orcas Island, Canada in July 2015. . . . .	129

## LIST OF TABLES

Table Number	Page
2.1 Mean and range of each material property variable for both skin and blubber. The structure coefficients (Pearson product-moment correlations) between the material properties variables and the first two principle components, with skin and blubber in separate principal component analyses. . . . .	34
2.2 Results comparing the material properties across groups of orientation, speed, and species. P-values <0.05 are assumed to be significant. . . . .	37
3.1 Comparison of values of elastic modulus in tension and compression. For tension values, the value represents an average across all tissue orientations. Elastic modulus in compression is calculated as the value of E where the strain was 0.1 . . . . .	45
3.2 Parameters used for bulk modulus accuracy calculations. $F$ is set to 450 N to encourage not overloading the MTS Synergie load cell with bulk modulus testing. . . . .	53
3.3 Power and speed used to cut different individual's tissues with laser cutter. . . . .	53
3.4 Summary of averaged bulk modulus results compared to bulk modulus results calculated from estimated poisson's ratio, $\nu$ , and elastic modulus. Numbers are presented as average plus or minus the standard deviation. . . . .	55
3.5 Summary of averaged shear modulus results compared to shear modulus results calculated from estimated poisson's ratio, $\nu$ , and elastic modulus. Numbers are presented as average plus or minus the standard deviation. . . . .	60
3.6 Density measurement for four seals, porpoises, and orca exhibits the expected trend of blubber being less dense than skin. . . . .	62
4.1 For the killer whale skin and blubber, many hyperelastic models were evaluated to determine which best matched the spherical indentation test. In addition, the coefficients calculated here can be compared to shear and bulk modulus testing to further validate the models. . . . .	77

4.2	For the harbor porpoise blubber, hyperelastic models were evaluated to determine which best matched the spherical indentation test. In addition, the coefficients calculated here can be compared to shear and bulk modulus testing to further validate the models. . . . .	78
4.3	For each model created, a bulk modulus and shear modulus can be calculated. In the case of the Ogden model, these are the appropriate values for small strains and the values change as strain increases. . . . .	83
5.1	SRKW Juvenile (L112) and Adult (J32) skin and blubber elastic modulus properties used in ABAQUS modeling. These values were based on the 1 mm/s data because that is what was used in the PNNL modeling. L112's degraded tissue make it's material properties less credible, but the 90°, 1 mm/s test for J32 is also the most variable of any test (Figure 5.2) . . . . .	90
5.2	Skin, Blubber, and Steel material properties used in ABAQUS modeling. . .	90
5.3	Elastic modulus used to compare skin and blubber across four marine mammal species. . . . .	96
A.2	Each animal tested in tension results in data for Elastic Modulus (E), Tensile Strength (TS), Yield Strength (YS), and Strain-to-Failure (STF). Blanks represent missing data. Each animal tested is shown in a different section, delineated by a line. The same animal tested fresh and frozen is also delineated.	116
A.1	Available morphometric data collected at necropsy for animal seal tested. . .	116



## ACKNOWLEDGMENTS

I am deeply grateful for the support of the many mentors that helped guide this work. I appreciate wholeheartedly my committee chair and advisor, Michael Motley. His reassurance and taming of my frenetic energy was fully necessary to accomplish what I have. Adam Summers has shown me a model of daily enthusiasm for his work that I aim to replicate in my career. Finally, I am indebted to Andrea Copping who laid the foundation of this research, gave me my first job out of college, championed me, allowed me to take ownership of this project, and continues to give exceptional and steadying advice. Thanks also to Pedro Arduino, Peter Mackenzie-Helwein, and Laura Lowes for advice along the way.

I would like to thank everyone who aided in procuring and testing marine mammal tissue. Petra Ditsche was the backbone for much of this work, coordinating with the stranding network, completing hundreds of tests, and guiding many of my ideas about this biology portion of this work. Marianne Porter and Adam Summers designed and implemented the first killer whale testing back in 2013, along with Dylan Wainwright. Stephanie Crofts spent many long nights to ensure the freshness of the tissue data. Joe Gaydos, of the SeaDoc Society and Jennifer Olson, from the Whale Museum, provided immeasurable support in collecting tissue. Dyanna Lambourn of Washington Department of Fish and Wildlife aided in procuring the orca calf and one seal. Amanda Witt, Katherine Corn, Jacob Harrison, Chloe Peterschmidt, and Camille Hair all assisted with the biomechanical testing. And to everyone else that was in Lab 8 anytime I was, I apologize for the smell.

This work required many interdisciplinary teammates and I appreciate the patience of all those who helped me wade into new territory. I gained so much from all the biologists, especially Petra and Adam, who often all but demanded that I look at the world in a new

way. Many thanks Jim Thomson and the rest of the Environmental Fluid Mechanics group at UW, who warmly welcomed me into their ranks when there was no other natural fit for me on campus. I appreciate Brian Polagye and my many colleagues at the Pacific Marine Energy Center, who showed me where my work fits into to the larger picture of marine renewable energy. Finally, I am grateful to and greatly admire the mechanical and civil engineering students with whom I traveled the world to conferences, stayed in the office late at night, and learned alongside, particularly Cassie, Ramona, Maddie, Maricarmen, Hannah, Emma, Rob, and Trevor. Thanks also for coming by my office to say hi and eat baked goods.

Special thanks to my number one editor, Ben Hughey, who knows this work better than any public policy wonk should. Also thanks for keeping me fed.

This work was funded primarily by the NSF Graduate Research Fellowship Program, with much of the tissue testing funded by the Department of Energy's Pacific Northwest National Laboratory. Thanks to additional support from University of Washington's Clean Energy Institute, Washington Sea Grant, and Friday Harbor Laboratories.

## DEDICATION

*to my Grandpa Zouri, who was an exceptional tinkerer and engineer, and who believed in tidal energy, composting toilets, and the like way before it was cool.*

November 16, 1931 - May 10, 2018

## Chapter 1

# INTRODUCTION

### **1.1 Motivation**

Alternative energy forms are needed to reduce the negative impacts of greenhouse gas emissions on our climate. While wind and solar energy technologies have grown and matured in the past few decades, the ocean's energy has been largely untapped. As the tide rises, it pushes water from one location to another, creating a current that can be used to generate electricity in a manner similar to that of wind turbines. Generating power from the changing tides has a few promising advantages over its land-based peers. The tide is reliable and predictable, ebbing and flowing every day, twice a day, and it can be forecasted far in advance. The tidal resource is located along the world's coastline, potentially close to the major coastal populations consuming the power.

Alongside these benefits come many unknown environmental impacts of installing tidal energy. These unknowns cause the industry a considerable regulatory burden, as the uncertainty can make financing a difficult task. Finally, it is essential to ensure that installing a promising new renewable energy technology does not harm the environment more than the fossil fuel energy it aims to replace.

### **1.2 Environmental Impacts of Tidal Energy**

Tidal energy has many potential impacts on the ocean environment, just as every method of producing energy for human use has an environmental consequence. By definition, we take energy out of the surrounding environment and move it somewhere else; we put a man-made device in the path of powerful forces of nature. The environmental impacts of tidal energy devices are typically characterized by separating the stressors (the outputs from the

technology causing change) and the receptors (the object being changed) [21].

Though much research and language used focuses on possible negative consequences, the conceivable environmental benefits of ocean energy are vast. Our changing climate has many damaging effects on the ocean ecosystem. Ocean renewable energy can generate power without releasing the carbon dioxide responsible for climate change. In addition to this broad benefit, researchers have posited other advantages. Man-made structures in the ocean, including oil rigs and sunken barges, have been observed to attract marine life, often called “artificial reefs” [46]. Tidal energy platforms could act as artificial reefs. As fishers would want to avoid to avoid gear tangling with a device’s moving parts, a marine protected area may be purposefully or informally created, providing a refuge to allow depleted populations to recover. Wave energy devices have been proposed as a method of shoreline protection [1] and tidal turbines could similarly take energy out of the ocean in a beneficial manner.

The common factor for both positive and negative environmental impacts is a lack of full understanding of the tidal environment. Every site must be individually characterized, as complicated bathymetry poses a challenge for predicting how water will behave even without a tidal device installed. Add in ebbing and flowing nutrients, migrating fish, marine mammals chasing those fish, and a complicated ecosystem is revealed, a site specific and interconnected web. Some of the unknown stressors on this multivariate system are: the moving parts of the device, the static part of the device, noise produced by the device, removal of energy, electromagnetic fields, and chemical leaching.

The stressors place an unquantified burden or benefit on the following receptors: marine mammals, fish, birds, sea turtles, and invertebrates [21]. Though the invertebrate category is vast, the larger more charismatic megafauna have tended to dominate the conversation around environmental impacts of ocean energy, particularly those that are depleted or threatened due to other anthropogenic activities and climate change. Broadening the definition of environmental impact, the installation of tidal turbines may also include socio-economic receptors, like commercial fishing, recreation, and shipping [2]. Retiring risks by demonstrating that they are not a long term problem or positing solutions is a valuable endeavor

toward creating a more environmentally friendly industry.

This work ultimately aims to further the understanding of the risk that tidal turbines pose to marine mammals, focusing on characterizing marine mammal tissue to evaluate likelihood of injury from collision. Though tidal turbines impact can extend to acoustic or behavioral changes, those risks are not addressed here. The Marine Mammal Protection Act of 1972 is strict in its definitions of what constitutes harm, including harassment defined as:

“any act of pursuit, torment, or annoyance which has the potential to injure a marine mammal or marine mammal stock in wild or has the potential to disturb a marine mammal or marine mammal stock in the wild by causing disruption of behavioral patterns, including, but not limited to, migration, breathing, nursing, breeding, feeding, or sheltering.”

This definition certainly encompasses the installation of permanent hazards into marine habitat. The risk of tidal turbines for marine mammals injury can be divided into two general categories that combine to define risk: the probability that an animal will encounter the turbine and the likelihood or consequence of an injury. This dissertation addresses the second category, aiming to provide material properties of marine mammals that could be used to determine the extent and severity of a tidal turbine strike on a marine mammal should it occur and to aid in permitting tidal turbines in compliance with the Marine Mammal Protection Act.

### **1.3 Marine Mammal Behavior in Tidal Channels**

Many marine mammals are present in fast moving tidal channels and could come in contact with spinning blades; the evasive or maneuvering behavior of marine mammals in the presence of tidal turbines has not been characterized. This uncertainty provides the justification for worry about potential collision between marine mammals and blades.

The four marine mammals chosen to examine in this dissertation (harbor porpoise (*Phocoena phocoena*), Southern Resident killer whale (*Orcinus orca*), Dall’s porpoise (*Phocoenoides*

*dalli*), and harbor seal (*Phoca vitulina*) are all present in tidal channels. A study in southwest Wales, UK showed harbor porpoise use of the tidal channels for feeding and traveling [70], but the use of these high velocity regions is not well studied. In the Puget Sound, the recovery of stranded harbor porpoise suggests the population could be moving more into the inland waters of Washington state [45] since the most recent 2002 aerial stock assessment [17] in the regions where tidal energy devices might be installed. Southern Resident killer whales are found throughout the Salish Sea at the same depths where turbines could be deployed. Observations of Dall's porpoise in the north Pacific note that the animals are present particularly in channels with fast moving currents [23]. Harbor seals are often present in tidal channels, using the hydrodynamics of the constricted water flow for feeding [87]. Stretching from Japan throughout the Atlantic and Pacific Oceans in coastal northern latitudes, they have one of the broadest geographic distributions of all pinnipeds [75]. Harbor seals have a wide distribution in potential tidal turbine sites, such as the north coast of Scotland near the first installed commercial scale tidal development [62]. Marine mammal use of tidal channels makes the risk of collision possible. However, with few tidal devices in the water, the marine mammals' long term behavioral response to the turbines are unknown, so the likelihood of a strike occurring has not yet been determined.

The diving behavior of each animal is sporadically documented, and generally these studies apply only to the site that was studied. Animals behave differently in different locations. In general, characterizing if an animal is making a "U-shaped" dive or "V-shaped" dive can be helpful for understanding behavior, as "U-shaped" dives are often associated with foraging at the depth of prey and represent a longer time spent at a potential turbine depth [57]. Harbor porpoises in Funaka Bay, Japan were observed to employ shallow "V-shaped" dives for traveling, and deeper "U-shaped" dives with longer bottom times for feeding [65]. The average depth and length of the dive affects the probability of a collision [19].

Finally, some behavioral research has been conducted to determine behavior changes around operational turbines. Harbor seals in Strangord Narrows still entered the tidal channel in the presence of a SeaGen turbine [74]. Porpoises and dolphins were tracked acoustically

in Ramsey Sound during a 3-month deployment, but researchers concluded they needed more data to understand the small cetaceans' behavior in the turbine presence [60]. Another study using playback to mimic turbine sounds found that harbor seals detected and avoided the turbine, suggesting that the animals would be likely to evade an operating turbine [41]. Understanding the worst case scenario of a tidal turbine collision with a marine mammal could allow permitting to move forward. With devices in the water, more research on the behavioral component can be completed.

#### **1.4 Marine Mammal Potential Injury**

To examine a worst case scenario, understanding how marine mammal's outer layers function and protect them from injury is necessary. In marine mammals, the skin is protective, buoyant, insulative, and structural, all while providing the animal with a streamlined hydrodynamic shape [66]. The skin contains a subcutaneous layer of fat, called blubber, connected to the dermis that aids in these functions. The blubber consists of adipose tissue reinforced with collagen, and is assumed to be less dense, stiff, and strong than its dermal/epidermal counterpart [67, 43]. Blubber may absorb the force of trauma, although its primary function is energy storage and thermoregulation [77]. In aggregate, the skin combined with the blubber layer provides structure and protection while also contributing to buoyancy control, drag reduction, and insulation. One pinniped and three cetaceans are included in this work, but the two orders have different adaptations, causing the difference in the two layers of tissue.

The harbor seal, a pinniped, has fur covering its body, which reduce the drag forces that a seal generates as it swims through the water, much like the scales of a fish or the denticles of a shark, and also provides insulation [27]. The hypodermis is the deepest layer of skin and makes up the blubber in marine mammals. In pinnipeds, like the seal, the skin must be able to support the animal's weight and shed heat on land, while also contributing to swimming through pelvic oscillation. The toothed whales in this study have a similar hydrophobic outer layer covering a fattier blubber layer. These animals employ caudal oscillation, moving their tail fluke up and down to swim, entirely underwater with fast swimming speeds; the animals'



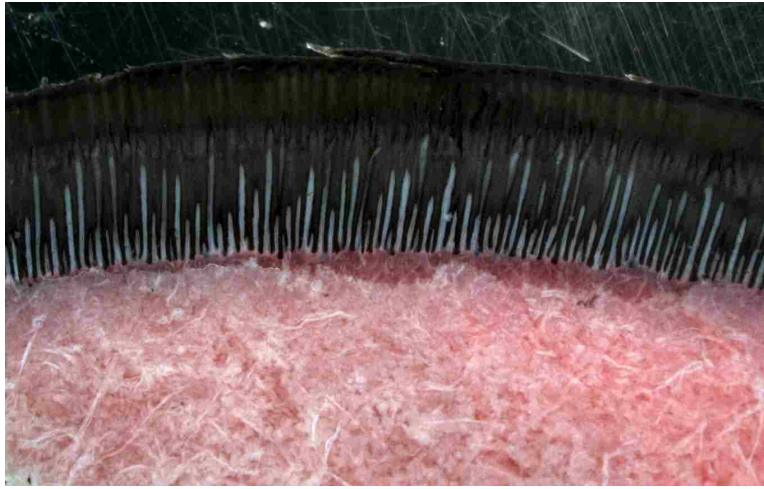


Figure 1.1: Structure of juvenile killer whale skin and blubber.

skin and blubber may be adapted accordingly [29]. The skin and blubber of marine mammals can be visually separated into two distinct parts, with two different structures, as seen in the Southern Resident killer whale (Figure 1.1).

Material properties of marine mammal skin and blubber are needed to quantify what turbine blade speed might cause injury to the animal. Much of what is known about the material properties of how living skin and subcutaneous fat layers behave is based on research on human tissue and its surrogates. Based on other mammal's dermal and hypodermal layers, this work hypothesized that the skin would be a stiffer outer layer, while the blubber would be less stiff and have high extensibility. The skin would act as an elastic membrane, transmitting force, while the blubber absorbs it. Morphological studies of other mammals indicate that skin acts to resist the force of impact by transmitting force in tension in the skin layer, protecting underlying layers of fat, muscles, or organs [25]. Skin fulfills this important function by its ability to endure reversible deformation [69].

It is worth noting here that the two distinct structures seen in Figure 1.1 are functionally both part of the mammal's 'skin', with the integument (or black part of figure) consisting of the epidermis and dermis. The pink part then represents the fatty subcutaneous tissue,

typically referred to as blubber. Though this is perhaps imprecise language, the remainder of this document calls the epidermis and dermis 'skin' and the subcutaneous fat 'blubber'. Skin in many of the surrogate terrestrial mammals does not have this significant of a hypodermal layer of fat and as such is often tested as a whole. This approach is likely valuable in understanding the composite behavior, but in marine mammals, the two layers are visibly different in material properties and large enough to test separately.

Skin behavior in response to trauma has been most thoroughly observed in human skin. In one comparable example for a projectile ten times the skin thickness in radius, the threshold velocity for breaking through the skin was 4.6-5.2 m/s. Based on turbines with relatively slow rotation and much larger geometry, the soft tissue injury needs to be investigated in addition to perhaps the potential of a bone breaking injury. Thus, understanding the skin and blubber composite response is an important goal in order to estimate the resultant injury. Marine mammal skin has some functions that allow it to protect the underlying layers. A similar structure as skin is also seen in sandwich composites; a stiff outer layer allows the force to spread and the internal material to absorb much of the energy [4]. The functionality is readily observable in human skin; often underlying layers bruise while the stiffer outer layer remains undamaged, allowing for less risk of infection or further damage while healing. Human skin research indicates a linear increase of stiffness (elastic modulus) with age as well as increasing anisotropy and decreasing thickness with age [69]. Human, pig, and other mammal skin have long been recognized to be anisotropic; this knowledge is often used in surgery to make incisions in locations which will heal favorably [5]. Anisotropy means that a material has different properties in different directions. Since the skin is pretensioned in a living animal, the direction with higher tension is the stronger axis and incisions made parallel to that axis will heal faster. In the perpendicular direction, the wound tends to pull open based on the skin's natural tension. The abundance of data on terrestrial mammal's skin anisotropy suggests that marine mammal skin would be anisotropic as well. Further, many fish have been documented as anisotropic [42, 59, 64]. Based on this existing work, one might expect marine mammal skin would be generally an anisotropic non-linear elastic

material [55, 28] with strain rate dependence [6].

However, marine mammal tissue's material properties have not been well characterized. Hydrodynamic estimates of dolphin skin suggest that the skin of harbor porpoise (*Phocoena phocoena*) could employ anisotropy to reduce drag [68], as does investigation of the fiber structure of the harbor porpoise caudal keel [40]. The cuvier's beaked whale (*Ziphius cavirostris*) blubber tissues' elastic moduli were tested at low stresses (<50 kPa) to understand the whale's sensitivity to sound and was reported to have an elastic modulus of about 1 MPa [73]. Density of marine mammal skin has been measured in the manatee (*Trichechus manatus latirostris*), harbor porpoise and bottlenose dolphin (*Tursiops truncatus*), with all densities nearly neutrally buoyant [50]. Other biomechanical and descriptive properties of marine mammals' skin and blubber have been measured, such as general thickness of blubber layers and densities [53] or conductivity [26].

Across any marine mammal testing, tissue must be taken from animals that strand dead on the beach. Stranding often occurs in remote locations and at unpredictable time, so an immediate testing of the fresh tissue can be challenging, especially for rare animals like the endangered Southern Resident Killer Whale. Freezing is a common way of preserving the tissue before testing. However, the impact of freezing on the biomechanical properties of the marine mammal tissue is unknown. Evidence suggests that mammalian tissue changes after being frozen. Human arterial tissue reportedly increases in both strength and stiffness compared to fresh tissue [76]. Rabbit skin studies indicate that the precise method of freezing and thawing the tissue contributes to changing the thawed quality [11]. Freezing and other decay of the tissue represents an additional challenge to accurately quantify the response of the material.

### **1.5 Finite Element Method Modeling of Soft Tissue**

Once the material properties of marine mammal soft tissue are understood, a finite element method model can be used. Finite element analysis of soft tissue represents a considerable challenge. Though currently only documented for other mammalian fats [56], marine mam-

mal blubber is likely a nonlinear, anisotropic, viscoelastic, strain-rate dependent, temperature dependent, biological material somewhere between a solid and a fluid. This combination of properties from fluids and solids often requires that simplifications like linearity be made. Further, the subcutaneous fat has attachments to both skin and underlying muscle which add additional complication. There exists no overarching consensus for how to model soft tissue, as this choice often depends on the scale of the question being asked.

A few examples of how mammalian soft tissue has been modeled are included here. Human skin was modeled as isotropic and nonlinear, but given an initial anisotropic stress state, representing the natural tension in skin [12]. Pig skin has been modeled as a hyperelastic strain rate dependent material using the Ogden model of hyperelasticity [72]. To evaluate seat cushion comfort, a seated human skin was modeled as a linear-elastic isotropic material (Poisson's ratio of 0.46, elastic modulus = 0.15 MPa, density = 1100 kg/m<sup>3</sup>), while muscles were modeled with a more complex Mooney-Rivlin hyperelastic isotropic model [38]. (It should be noted this study only designs comfortable seats for male derrières, with no mention of further study.)

A model of human breasts used finite element analysis to predict the location and geometry of a tumor during the compression of a breast for biopsy [7]. The finite element model guides a physician to successfully biopsy the tumor using a non-linear model, which also is computationally efficient to use during a procedure. This study had a course mesh and simple model, prioritizing the efficiency, not necessarily the precise geometry of the tumor.

### ***1.6 Previous Work and Similar Approaches***

Existing research in the area of marine mammal strike is primarily opportunistic and related to vessel strike. Deaths due to blunt force trauma, usually due to vessel collision, are generally characterized by marine veterinarians necropsies and cataloged [14, 47]. Observational reports also cover healing and scarring over the course of years for recovering animals that have undergone strike trauma [82][47]. This empirical data lacks precise information about the forces involved in injuring the animal, so is difficult to apply to new tidal technology.

Impact of a ship strike on a North Atlantic Right Whale (*Eubalaena glacialis*) mandible was investigated through finite element modeling [13][80]. The force required to break the mandible were correlated with vessel speeds. To reduce deaths due to vessel strike, regulation of vessel speed in critical habitat was proposed. The forward velocity of tidal turbine blades is considerably lower than typical vessel speeds and has much less mass behind the blade. Thus, the mechanism of injury likely to occur from tidal turbines is presumed to be dependent on tissue injury as opposed to bone injury.

The most relevant work on this topic comes from the Pacific Northwest National Laboratory (PNNL) and Sandia National Laboratory (SNL), who performed a simplified analysis of a scenario with a Southern Resident Killer Whale and an open-centered horizontal axis tidal turbine [15]. The analysis combined material testing of killer whale tissue with finite element modeling to further understand the potential risk. The analysis was limited by high uncertainty in the quality of tissue data, due to testing only one animal and testing after one year in the freezer.

During the permitting of an OpenHydro turbine in Admiralty inlet of the Puget Sound, PNNL's work was used to determine if this device was safe for marine mammals and weighed in the decision to consent to the permitting of a pilot project. Though the permit was granted and the risk was deemed small, the Orca Conservancy (a conservation group dedicated to protecting the endangered Southern Resident killer whales) campaigned forcefully against this renewable energy project. Working to understand the risk of injury to marine mammals from tidal turbines can be used to appeal to this and other groups of stakeholders, in addition to the regulatory agencies.

### **1.7 Thesis Outline**

The scope of this work covers the characterization of marine mammal skin and blubber, validation of a constitutive model of the tissue, and prototypical parametric studies of the turbine-animal collision. Measurements of marine mammal skin and blubber tested in tension are presented in Chapter 2. Much of the tensile testing work has been published or is under

review and is adapted in this chapter [36, 37].

Chapter 3 covers additional material testing, including indentation testing, bulk modulus, shear modulus, density, and histology work. Some of this work has been adapted from a refereed conference paper [35].

A validation of the finite element model used to numerically represent the marine mammal tissue is presented in Chapter 4. The material from this chapter is in preparation for publication.

Chapter 5 presents a parametric study, determining which factors influence the model results most. This chapter is adapted from another refereed conference paper [34]

Finally, Chapter 6 presents recommendations and best practices for a finite element analysis model and a description of how it could be used at a specific site of interest. It also includes a summary of all results and a discussion of future research directions.

## Chapter 2

### TENSILE TESTING OF MARINE MAMMAL SOFT TISSUE

#### 2.1 Overview

Tensile testing is perhaps the most common engineering test for understanding material properties. In the case of biological materials like marine mammal skin and blubber, it is a useful test that allows a foundational understanding of how the material behaves. The tensile testing program presented here had a few major goals:

1. Determine the elastic modulus, tensile strength, yield strain, and failure strain of the skin and blubber.
2. Characterize the effect of orientation and speed on the material properties.
3. Explore the effect of age and freezing on the tissue material properties.
4. Examine the nonlinearity of the skin and blubber.
5. Relate the material properties of the four animals tested to each other, defining similarities and differences.

Each of these goals informed the testing methodology and statistical analysis used in this chapter.

#### 2.2 Methodology

##### 2.2.1 Tissue Procurement

Marine mammal tissue was obtained post-mortem through the San Juan Island Marine Mammal Stranding Network and the Washington Department of Fish and Wildlife. All material

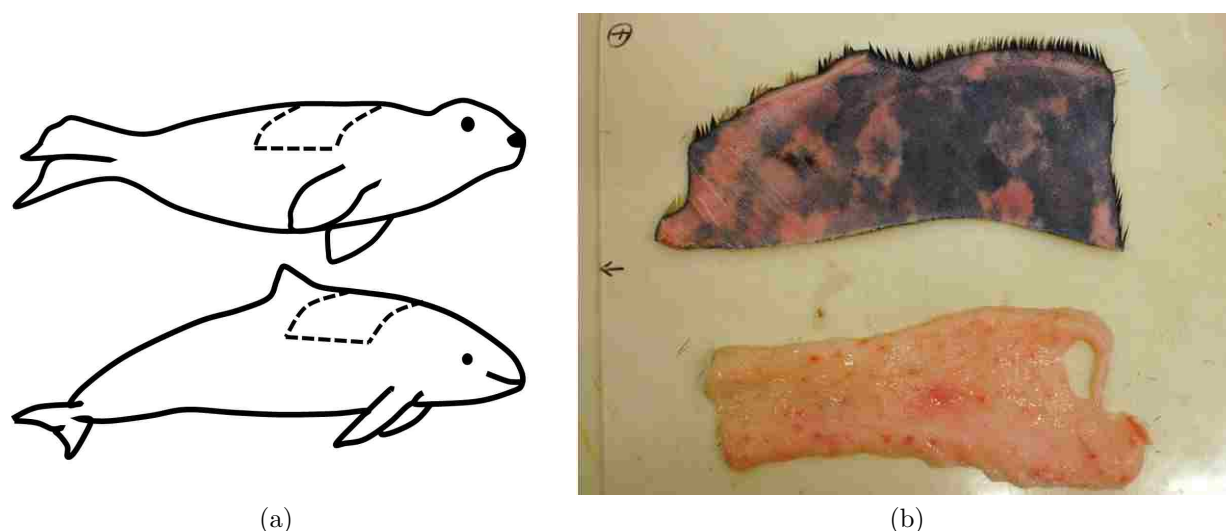


Figure 2.1: Schematic of where tissue is collected on the animal (a) and the seal tissue separated into skin and blubber after removing from animal (b)

testing was completed within 48 hours of stranding to ensure tissue freshness. However, as this research relied on stranded animals, the time of death was not exactly known. Tissue samples were obtained opportunistically from three adult harbor seals (Seal 1, Seal 2, and Seal 3) and two seal pups (Seal Pup 1, Seal Pup 2), each less than four months old. Stranded individuals were not tested, if their blubber layer was extremely thin and they presumably died from malnourishment. All tissue was taken from the thoracic region in the area behind the foreflippers (Figure 2.1). Each piece of tissue consisted epidermis, dermis and hypodermis cut to the muscle.

Each of three harbor porpoises and one Dall's Porpoise samples was procured from an animal that died naturally and then stranded in the San Juan Islands, WA. For each toothed whale, a portion of tissue was removed from the dorsal region of the animal between the two flippers, starting a few inches caudal of the blowhole and extending to a few inches rostral of the dorsal fin. All porpoises were tested within 48 hours of collecting the sample. A portion of the tissue for one harbor porpoise was also reserved for testing after being frozen.

The first orca, L112, was tested prior to the work of this dissertation, but included in



some results. L112 washed up dead in Long Beach, Washington in February 2012 and was somewhat degraded when the tissue was excised. This animal was frozen for approximately one year prior to testing. The calf killer whale was found dead on Dungeness Spit in January 2013 and in fresh condition. This calf was frozen for approximately one month before testing. The adult SRKW used in this study was found in December 2014 on Bates Beach, Vancouver Island, BC. The female orca, named J32, was pregnant at the time of stranding, found freshly dead, with about 4.5 cm of blubber in the region tested. Both animals were frozen before testing to preserve freshness, as testing could not be completed in within the 48 hour freshness limit.

Available morphometric data for all animals can be found in Table A.1.

All individuals were collected with the assistance of the San Juan Island Marine Mammal Stranding Network under authorization from the National Marine Fisheries Service in compliance with marine mammal regulations. (Appendix B)

### *2.2.2 Tensile Tissue Testing*

Once collected, the tissue was separated into two layers, one containing epidermis and dermis (referred to as skin in the following) and the other containing the hypodermis (blubber). The blubber layer was separated into multiple sections, each approximately five millimeters thick. For every individual test, the blubber changed shape as it was cutaway from the skin and cut into smaller samples. Tissue was kept cold and moist during the testing process with paper towels drenched in seawater ( $\approx 11^{\circ}\text{C}$ ). Though the exact temperature was not measured, the seawater temperature range gathered by the Friday Harbor Dock buoy was small ( $< 1^{\circ}\text{C}$ ).

Each subsample was created using a metal punch. Dogbone shaped samples measured the tensile strength and yield strength (defined as where the material begins to become non-linear and begins to exhibit plastic behavior, respectively), while rectangular shaped samples measured the elastic modulus and strain-to-failure. Each sample was forty millimeters in length, with a width of seven millimeters in the center of the specimen (Figure 2.2).

Quasistatic uniaxial tensile testing was conducted on each specimens using an MTS Syn-

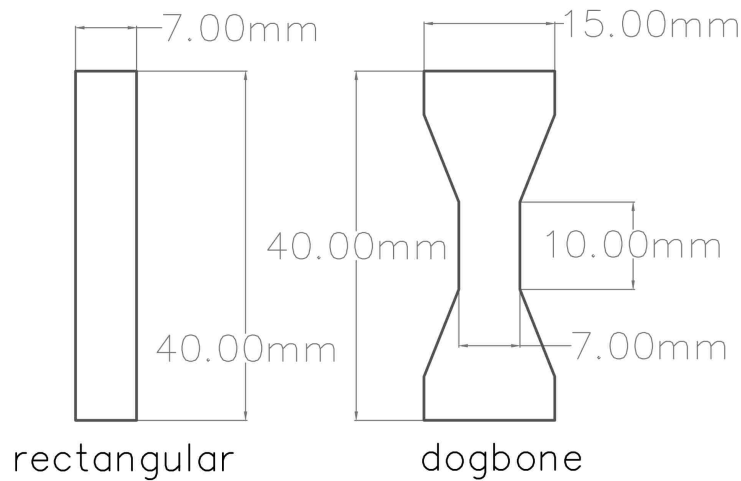


Figure 2.2: Dimensions and geometry of metal punches used for creating material tensile testing specimens, with (left) a rectangular shaped punch for testing modulus of elasticity and (right) a dogbone shaped punch for testing tensile strength.

ergie 100 with a 500 N load cell recording force and length extension during the test. 10 mm of each specimen was clamped into each side of the MTS metal clamps, with a length of 20 mm between the two clamps (Figure 2.3 inset). 60-grit sandpaper was placed around the specimen in the clamps to securely grip the sample and avoid slipping. In a few cases of seal skin testing, the sandpaper alone was not sufficient to avoid slipping and dry ice was placed on the metal MTS Synergie clamps to freeze them to the clamps. Qualitatively, the samples appeared unfrozen for the whole 20 mm gauge length. Similar approaches have been used in mechanical testing of tendons, as higher tensile strength could be reached when the tendons did not slip as they did in ordinary clamps [10, 85]. The cross-section of each sample was determined by measuring the width and thickness of the specimen using a caliper in the center before beginning the test and used to calculate the engineering stress during the test.

Blubber and skin were each tested for anisotropy using three tissue orientations. Relative to the cranial-caudal axis, samples were cut in the longitudinal ( $0^\circ$ ), transverse ( $90^\circ$ ), and diagonal ( $45^\circ$ ) directions. Each of these combinations was also tested at speeds of 1 mm/s and 10 mm/s, representing a strain rate of  $0.05 \text{ s}^{-1}$  and  $0.5 \text{ s}^{-1}$  respectively. A complete series

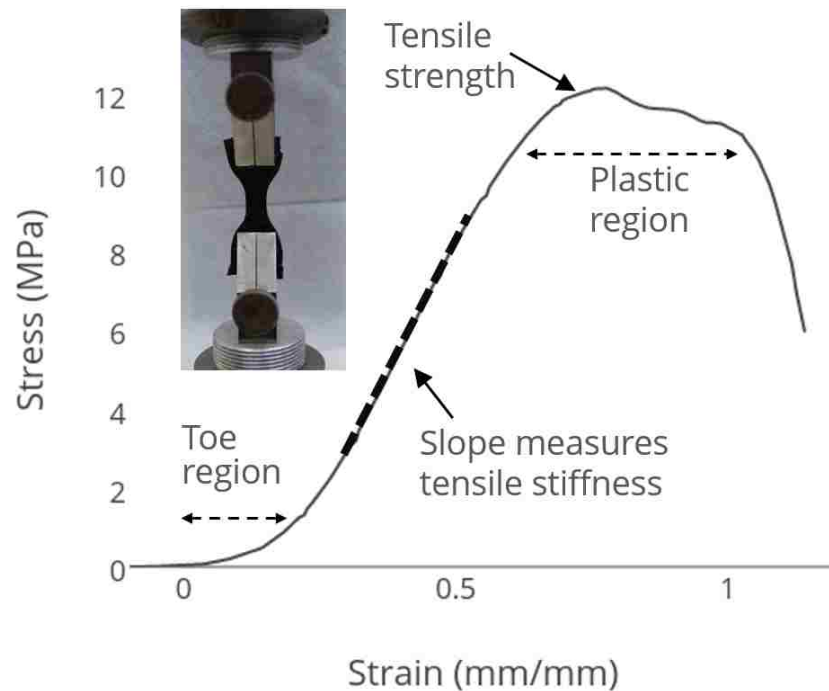


Figure 2.3: Example stress-strain curve shows the test result of a dogbone shaped sample. 'Tensile stiffness' (also called  $E$ , Young's modulus) is measured as the slope of the linear part of this curve. 'Tensile strength' is measured as the maximum strength. The 'plastic region' of the curve is the region where the curve begins to yield, but has not yet failed completely. The inset shows the test setup for this stress strain curve.

of tests then requires 24 cases per animal, using 2 tissues, 2 shapes, 3 orientations, and 2 speeds. Each test case was repeated the test eight times, resulting in 192 subsamples for each animal. Tests where the specimen slipped out of the clamps (due to the oily nature of the material) instead of failing during the test were excluded. Tests in the dogbone shape were excluded from analysis when the subsample did not break near the center of the sample.

For one harbor porpoise and all harbor seals, an additional piece of tissue was separated and frozen at  $-18^{\circ}\text{C}$ , surrounded by saltwater. After four months this material was thawed and the same set of tests were conducted.

### 2.2.3 Data Processing

The force-displacement data were converted to stress-strain data for data analysis; the force was divided by the initial cross-sectional area of the center, resulting in engineering stress. The engineering strain was calculated by dividing the displacement by the initial length ( $L_0$ ) of the sample. In the beginning of each test, the sample did not bear load as it began to stretch; these data were excluded and  $L_0$  was calculated as the length at which the material began to bear load. Using the rectangular samples, the elastic modulus was calculated as the slope of the linear region of the curve (Figure 2.3). The ‘toe region’ was not quantified, as it may not be realistic of behavior in the animal, as the tissue can be pre-stressed in the living animal. Using the dogbone samples, the strength of the material was calculated as the maximum stress reached during the test. The calculation of  $L_0$  does not impact the tensile strength calculations, as the maximum stress remains constant regardless of  $L_0$ . Strain to failure was calculated from rectangular sections as the strain at which the specimen’s ability to bear stress dropped by more than a factor of two.

With a full suite of 192 tests per animal tested, the stress-strain data needed to be converted to a more manageable form. A python script was written to store all of the marine mammal material properties in an SQL database by analyzing each stress strain curve. The elastic modulus in tension was calculated from the linear region of the stress-strain curve. The tensile strength was calculated as the maximum stress recorded. Yield stress was calculated using a 0.2% offset from the linear region of the curve, calculating the stress recorded when this offset line crosses the stress-strain curve. The strain-to-failure is found by finding the region where the curve begins to rapid decrease in stress, showing that the material can no longer hold force. The criteria checked if the change in stress between the next point (i+1) and the current point (i) was twice the value between the current point (i) and the previous point. If this was true for two points in a row, the corresponding strain value was chosen. In all cases, this analysis uses engineering stress, assuming a constant cross-section to calculate stress.

It is worth noting here that each test has a specific naming convention used, allowing quick reference of which test was performed. This naming convention is occasionally referenced elsewhere in the document. An example name is ‘O1\_SK\_R\_1\_45\_1’. The first part of the name has the animal: Harbor Seals (S1, S2, and S3), Harbor Seal Pups (BS1, BS2), Harbor Porpoises (HP1, HP2, HP3), Dall’s Porpoise (DP1), Killer Whales (O1 [referred to also as J32], O2 [referred to also as L112], NO1). The next part is SK or BL for skin or blubber, followed by the shape tested, dogbone (D) or rectangular (R). The next section is the test speed (1 or 10 mm/s), followed by the orientation (0, 45, or 90). Finally, the last number represents the replicates, generally between 7-9.

The SQL database stores the four material properties, as well as the stress strain curves. Summary data and stress strain curves can be queried and reports generated.

#### *2.2.4 Data Analysis*

Data analysis was completed first on the harbor seal data alone using a linear mixed effects regression, then again using multivariate analysis for all animals tested in tension.

##### *2.2.4.1 Linear Mixed Regression*

To look at the seal tissue data, which was the most complete and substantial, a linear mixed regression model was initially used. The model is similar to a linear regression analysis, but each different variable has a different contribution to the linear regression; these are the fixed effects. A mixed regression model contains both fixed effects and random effects. The random effects of the model consists of the animal-to-animal variability, which are not predictable over the whole dataset.

Fresh data were analyzed using a linear mixed effects regression using the R statistical package “lme4” to explain the effects of each variable (orientation, speed, age) on the material properties tested [8]. With this test, all five animals can be used together, with age as an ‘effect’, to raise the otherwise small sample size. A separate linear mixed effects model was created for each of the four material properties studied: skin elastic modulus, skin strength,

blubber elastic modulus, and blubber strength. The fixed effects for the model were the speed of the test (1 or 10 mm/s), orientation (0°, 45°, or 90°) of the test, seal's age (adult or pup), and the interaction between orientation and age of the animal; animal to animal variability was considered a random effect. For each test (e.g. blubber elastic modulus of Seal 1 tested at 1 mm/s and 0°), the eight replicates were averaged before performing statistical analysis. The data was analyzed on a logarithmic scale due to increased variance with higher means that was present throughout the data. On a logarithmic scale, the assumption of constant variability is satisfied.

The linear mixed effects model outputs a t-value for each of the fixed effects. The t-value, also called the t-statistic is the ratio of the difference between the value from its hypothesized value over the standard error, showing how good the model is for predicting the value of the effect (speed, orientation or age). The initial model containing all the fixed effects was simplified by eliminating the fixed effect with the lowest t-value. The updated model was compared with the initial model using the “anova” function in R. The “anova” function, which stands for “ANalysis Of Variance” is a standard R function which when applied to a linear mixed effects model does a Wald test to determine if each of the effects (sometimes called explanatory variables) are significant. If the variables are not significant ( $p > 0.05$ ), the model can be updated to delete this effect. The reported p-value for each test is from a Chi-Square value comparing how well the model predicts the measured tensile test data using the original and simplified model. In the case where multiple fixed effects were significant, p-values for individual factors were calculated by comparing the original model and simplified model using the ‘anova’ function with and without the effect of interest, but containing all other significant effects.

For the frozen data, the same methodology was used, omitting the speed data, as all frozen testing was completed at 10 mm/s. Additionally, the interaction between the age class and the frozen data was examined. One major goal of the separate seal analysis was to see if freezing effects could be predicted in a linear regression model, thereby determining fresh quantities from easier to handle frozen samples.

#### 2.2.4.2 *Multivariate Analysis*

To analyze all animals tested together, a multivariate approach was used. The material behavior was summarized by averaging the approximately eight repetitions taken for each test case. The averaged two material properties from rectangular tests and two material properties from dogbone tests were aggregated to create an object for multivariate analysis. Each object then has four material property variables. In addition to those variables, the objects are assigned groups based on test speed (1 or 10 mm/s), orientation of sample (0, 45, or 90), animal tested (harbor seal, harbor porpoise, Dall's porpoise, killer whale), age class (pup or adult), condition (fresh or frozen), and order (pinniped or cetacean). Blubber and skin were analyzed separately. The statistical analysis was conducted using R version 3.3.1 and the *vegan* statistical package.

A principal component analysis (PCA) was performed to understand how the four material properties are related in skin and blubber. A PCA plots each variable along its own axis in ordinate space. Once plotted, the axes are reoriented such that the first axes explains the largest percent of the variance in the data; the subsequent axes are assigned similarly based on the largest amount of variance. The axes aligned with the most variance are called "components"; the analysis reports how much of the variance is explained by each component. The material properties are highly correlated, making PCA an appropriate technique to explore the relationships between variables. Three out of the four variables have the same units (MPa), were sufficiently normally distributed, and all are continuous, so the data was not transformed before the PCA scales to unit variance. The goal of this analysis was to broadly explore the differences between the species tested. The significance of the PCA was evaluated using a random permutation of the objects, called a Monte Carlo test. The Monte Carlo test switches values in each column, so that the PCA can be compared with a randomly generated set of variables.

To further understand the relationships between the groups (test speed, orientation, and species), a perMANOVA was employed. perMANOVA is a permutational multivariate anal-

ysis of variance. The PCA outputs distances between variables in ordinate space. These distances are compiled into a resemblance matrix, which can be compared to determine statistical differences between objects or the labeled groups in the dataset. Because the variables are continuous, Euclidean distance was used in the resemblance matrix. The perMANOVA was used to understand which groups explained the variance seen in the data. The significance of pairwise differences was compared between species using a permutation test of multivariate dispersions. A p-value of 0.05 was assumed to be significant.

The pinniped dataset is larger than the others, so tends to dominate the data in a way that can blur trends that might otherwise be seen. Because of this, the orientation and speed for the toothed whales alone was also examined to demarcate any additional trends.

Finally, to examine the effect of freezing on the tissues, a Procrustes analysis was conducted using all data which had a fresh and corresponding frozen object. Since these two datasets are not independent, a paired analysis was needed to understand the freezing factor. This dataset contains three adult harbor seals, two pup harbor seals, and one adult harbor porpoise for blubber then one adult harbor seal, two pup harbor seals, and one adult harbor porpoise for skin. These animals each have fresh tests performed in multiple orientations (0 or 90) which are compared with the frozen datasets in the same orientation. The Procrustes analysis allows us to assess the overall agreement in the two matrices, as well as understand if individual observations are more impacted by freezing than others. The skin and blubber were again analyzed separately using a Euclidean distance matrix in both cases. The fresh data was the independent matrix (x) and the frozen was dependent (y).

## **2.3 Results**

### *2.3.1 Observations across all tensile testing*

A complete summary of results is present in Table A.2. One additional orca, L112 was tested, but the results have been eliminated from the statistical analysis due to degradation of the tissue. More exploration of that decision is discussed in Chapter 5.



As a rule, the skin and blubber have markedly different material properties, with skin being an order of magnitude larger in elastic modulus, tensile strength, and yield strength than blubber.

One way of examining the difference between blubber and skin is to examine the shape of the stress-strain curve. The stress-strain curves for the two materials have a different shape across all testing. Examining the harbor seal, the skin specimens tend to have a more defined plateau of plastic deformation; the blubber specimens tend to reach a higher strain before failure (Figure 2.4). In both tissues, a ‘toe region’ was observed, indicating a typical non-linear behavior of soft tissue, but also could be due to tissue not being fully stretched at the beginning of each test.

### *2.3.2 Behavior of Harbor Seal Skin and Blubber*

As the seal data is most complete, a separate analysis was used to further examine the seal material specifically.

The postmortem tested blubber and skin show markedly different results. Skin is stiffer and stronger than blubber regardless of the life history stage, or test speed (Figure A.1). For the elastic modulus, blubber values range from 0.2-3.9 MPa (with a mean of  $1.2 \pm 0.8$  MPa), while skin’s elastic modulus ranges from 3.5-53 MPa (with a mean of  $17.7 \pm 10.1$  MPa). There was a high variability of the elastic modulus between the tested individuals. The tensile strength across all tests was an order of magnitude larger for the skin (range of 2.3-63.2 MPa, mean of  $17.8 \pm 11.7$  MPa) than for the blubber (0.1-2.3 MPa, mean of  $0.8 \pm 0.8$  MPa).

Another way of examining the difference between blubber and skin is to examine the shape of the stress-strain curve. The stress-strain curves for the two materials have a different shape across all testing. The skin specimens tend to have a more defined plateau of plastic deformation; the blubber specimens tend to reach a higher strain before failure (Appendix A and Figure 2.4). In both tissues, a ‘toe region’ was observed.

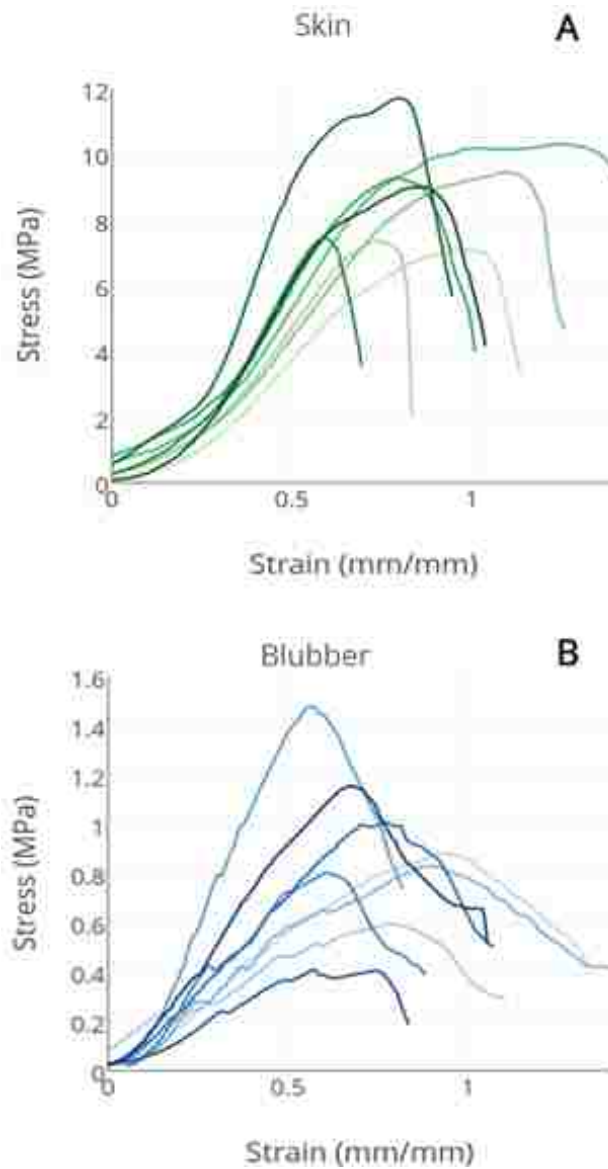


Figure 2.4: Stress-strain curves for rectangular shaped tissue specimens from Seal 1 tested at a 10 mm/s test speed. Note that y-axis scale is different for skin (greens) and blubber (blues). Blubber stress-strain curve shows a larger strain to failure and less defined plastic region.

### 2.3.2.1 Impact of tissue orientation on strength and stiffness

Harbor seal material test results show a small amount of anisotropic behavior across the range of testing in both skin and blubber, elastic modulus (stiffness) and strength (Figure A.1). The null hypothesis was that the orientation of the sample does not affect the stiffness and strength of the skin using the linear mixed effects regression. Two linear mixed effects models were tested, one with orientation and one without, comparing these two tests with an ANOVA. Skin tensile stiffness shows a significant difference between orientations ( $\chi^2 = 10.83$ , p-value = 0.03). This trend was not consistent in the relationship between orientations across all individuals (Figure A.1C). Tensile strength of the seal skin was significantly higher in the hoop orientation ( $90^\circ$ ) than in longitudinal orientation ( $0^\circ$ ) ( $\chi^2 = 8.49$ , p-value = 0.04, Figure A.1D). Though a significant effect was seen for both of these tests, the magnitude of differences is smaller than differences between animals, so is difficult to establish the functional role it plays. Strength and stiffness would be expected to be impacted by the same patterns, but do not see this, so the data is not conclusively anisotropic.

When examining tensile stiffness of the blubber, the orientation affects the elastic modulus ( $\chi^2 = 10.81$ , p-value = 0.03). Further, an interaction effect is seen between the age of the animal and the angle of the tissue ( $\chi^2 = 7.93$ , p-value = 0.02) where there is a more pronounced difference for the seal pups between the hoop ( $90^\circ$ ) and longitudinal ( $0^\circ$ ) orientations, which could be due to the requirements of birthing or changing material properties as they shed their lanugo coat. In the seal pups, the mean tensile stiffness of the  $90^\circ$  specimens is 50% higher than those in the  $0^\circ$  orientation (0.472 MPa and 0.314 MPa for the pup at  $90^\circ$  and  $0^\circ$  respectively). In two out of the three seals tested at a  $45^\circ$  body orientation, the highest stiffness was at the  $45^\circ$  body orientation. However, this orientation was not tested for every animal. The tensile strength of the blubber did not vary in regard to its body orientation ( $\chi^2 = 7.18$ , p-value = 0.07).

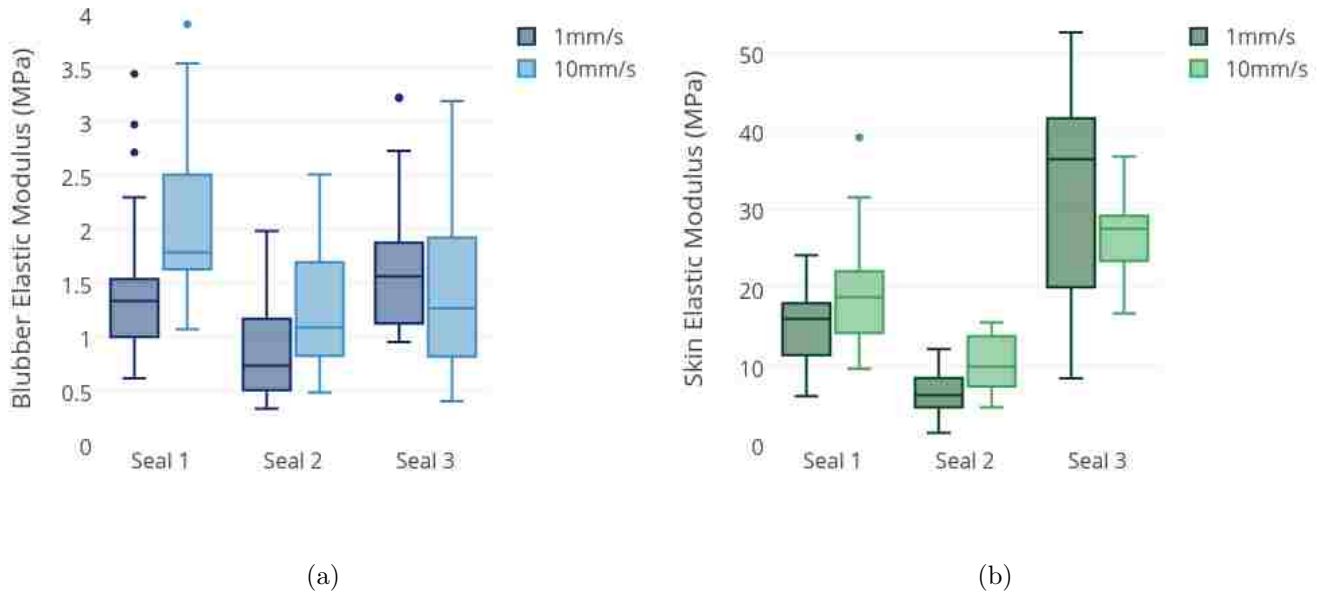


Figure 2.5: Tensile stiffness of blubber (blues) and skin (greens) in three adult Harbor Seals (data averaged over orientation). As an overall trend, skin and blubber show a stiffening effect with higher test speeds.

### 2.3.2.2 Test speed effects on the measured strength and stiffness

The test speed has a small impact on the results measured for stiffness and strength in adult harbor seals. Looking at tensile stiffness, both blubber and skin do not show a significant effect for the test speed using an ANOVA comparing a linear mixed effects regression with and without the test speed factor ( $\chi^2 = 3.04$ , p-value = 0.08 and  $\chi^2 = 3.07$ , p-value = 0.08, respectively). In both cases, however, a higher test speed results in higher stiffness. The adult seal blubber increases 28% on average (from 1.30 MPa at 1 mm/s to 1.67 MPa at 10 mm/s). Adult seal skin increases from a mean of 16.32 MPa at 1 mm/s to 18.86 MPa at 10 mm/s (Figure 2.5).

The strength tests show a different trend in the impact of test speed. Blubber strength

is impacted by test speed ( $\chi^2 = 5.53$ , p-value = 0.02), but the higher test speed leads to lower blubber strength (overall average of 0.86 MPa at 10 mm/s compared to 1.81 MPa at 1 mm/s). Skin strength did not show a significant difference for the measured test speeds ( $\chi^2 = 3.61$ , p-value = 0.06).

### 2.3.2.3 Biomechanical properties of adult seals and pup tissue

There is a large difference between biomechanical properties in adult and pup harbor seals (Figure A.1). The stiffness of the blubber as well as the strength of blubber and skin were all considerably lower for the pups compared to the adult seals. The pup samples tended to be less variable; their distributions were tighter across all tests. When examining only the pup tests for anisotropy, a pattern in skin strength, skin stiffness, and blubber stiffness is present where the 90° direction is stiffer and stronger (Figure A.1B-D).

Comparing skin stiffness between adult and pup found no significant difference between the two age classes ( $\chi^2 = 1.08$ , p-value = 0.78), while the other three material metrics showed large differences between the two age classes. Blubber stiffness ( $\chi^2 = 19.05$ , p-value = 0.0003), blubber strength ( $\chi^2 = 10.91$ , p-value = 0.004), and skin strength ( $\chi^2 = 9.47$ , p-value = 0.009) were significantly lower for the pups compared to the adults. When averaged across all other factors (orientation, animal) for blubber stiffness, the pup material properties are much smaller (0.499 MPa) compared to the adult blubber stiffness (1.669 MPa).

### 2.3.2.4 Impact of freezing on the biomechanical properties of the skin tissue

Freezing affected the material properties of the tissues, though the changes varied between skin and blubber, as well as between the two age classes. No consistent trend is seen regarding the orientation of the tissue in the adult harbor seals, but the pup shows a tendency for the 90° frozen tissue to be stiffer and stronger than the 0° frozen tissue. This trend is consistent with the results of the fresh tissue. The freezing does not appear to change the anisotropic behavior of the tissue. Further, like the fresh data, the differences between individuals are generally larger than the differences found between orientations. Seal 1 was tested at three

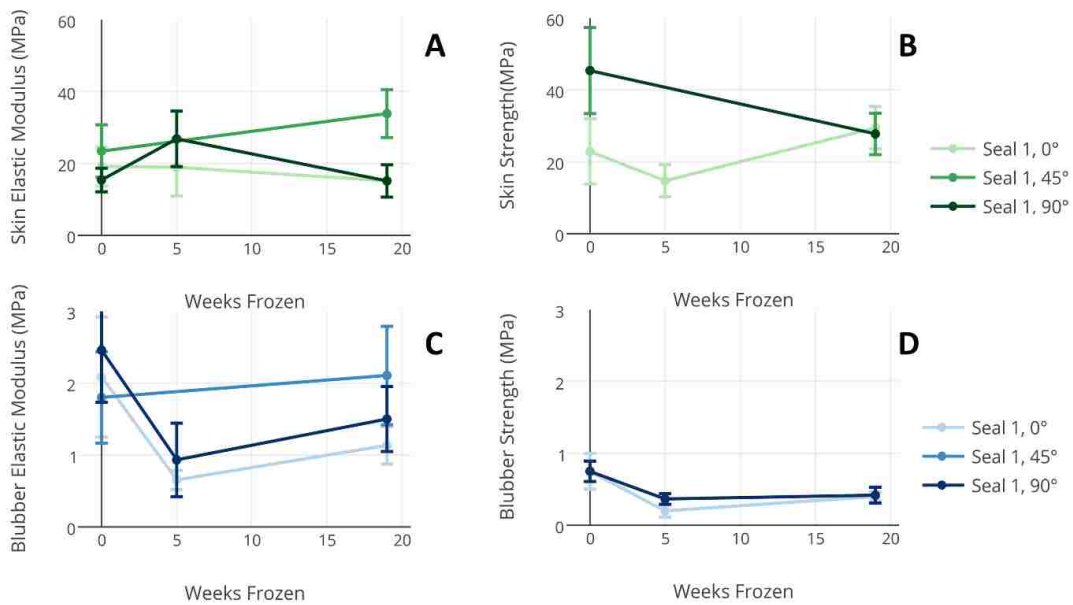


Figure 2.6: Elastic modulus and tensile strength shown for fresh and frozen adult harbor seal samples at a test speed of 10 mm/s. Within each animal, the data remains isotropic, as in the fresh samples.

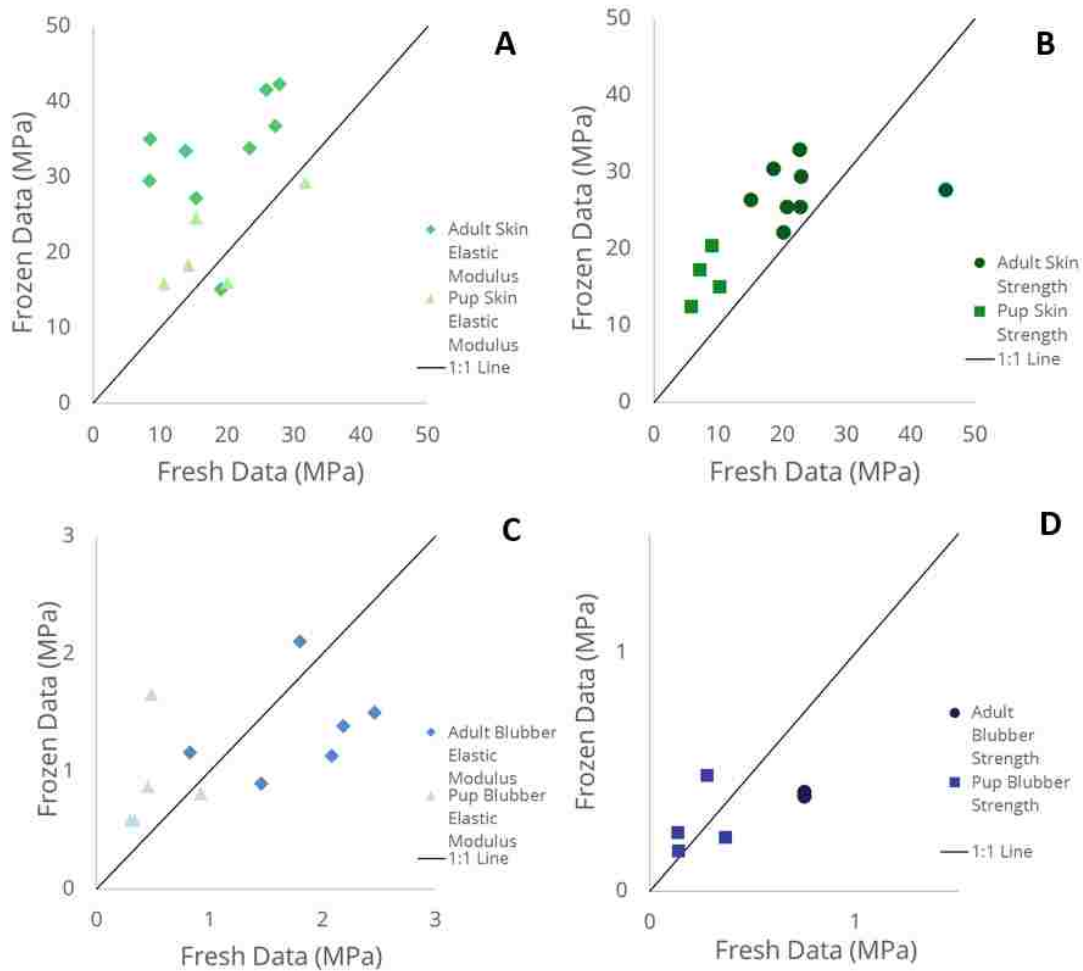


Figure 2.7: For every test repeated both on both fresh and frozen data, the data are paired to compare the same angle and animal. For harbor seal skin (A,B), the freezing generally results in larger values for both strength and elastic modulus. For harbor seal blubber (C,D), freezing adult blubber results in a decreased strength and elastic modulus. However, freezing pup blubber overpredicted the fresh pup blubber material properties (C,D).

times (fresh, frozen 1 month, frozen 4 months, Figure 2.6). Using a paired t-test, the material properties tested were not significantly different between the two frozen times for skin and blubber (skin:  $t(2) = -0.67$ , p-value = 0.57, blubber:  $t(3) = -2.93$ , p-value = 0.06), though the sample size for comparison is small. Skin thickness with the frozen and fresh samples was not significantly different.

To understand if freezing impacted the pup and adult tissue differently, a linear mixed effects regression was used, including the interaction of age and condition of the tissue (fresh or frozen). In general, the freezing impacted the pup and adult tissues differently. Freezing the skin of harbor seals generally leads to an overprediction of the material properties of strength and elastic modulus compared with freshly tested materials. For the elastic modulus of skin, an interaction is seen between the age class and the frozen data ( $\chi^2 = 493$ , p-value = 0.03). A significant effect of freezing is seen ( $\chi^2 = 17.78$ , p-value = 0.0001) for this metric, with the frozen tissue being stiffer than the fresh tissue; this freezing effect is more present in the adult animal (Figure 2.7A). In skin strength, a significant increase in strength is present ( $\chi^2 = 25.34$ , p-value =  $3.1 \times 10^{-6}$ ) in the frozen adult and pup tissues. Skin strength showed a significant interaction between the age class and freshness ( $\chi^2 = 8.92$ , p-value=0.003), where the pups' skin is more impacted by the freezing than the adults' (Figure 2.7B). Averaged over all other factors, the adult frozen skin was 20% stronger than the fresh tissue (28.233 MPa compared to 23.518 MPa), while the pup frozen skin was 100% stronger after being frozen (16.006 MPa compared to 8.005 MPa).

The tensile stiffness of the blubber shows a significant effect of freezing ( $\chi^2 = 13.18$ , p-value = 0.001) and an interaction between the two age classes. For the pups, the blubber is stiffer after being frozen; for the adult seals, the blubber tissue decreases in stiffness (Figure 2.7C). The strength of the blubber was significantly different after freezing ( $\chi^2 = 9.65$ , p-value = 0.008), and impacted the pup and adult tissues differently. For the pups, the strength of the blubber increased after freezing, but for the adult seals freezing decreased blubber strength (Figure 2.7D).



### 2.3.2.5 Discussion

In much of the data analysis, there existed a larger difference between individual animals than between the different test variables that were examined. Still, when comparing these animals with the San Juan Island's Marine Mammal Stranding Network, it can be concluded that the adult animals were representative of the general population in length, girth, and weight. The analysis would benefit from larger numbers of animals, but was restricted by opportunistic seal strandings. The large difference between animals is not unexpected. Human tissue testing has continually reported a wide range of material properties across multiple subjects [61].

Because of that larger difference across the population of animals than seen between different angles of testing, both tissues of the harbor seal are recommended to be modeled as an isotropic solid. There is no evidence that the trends of an isotropic material would hold across marine mammals, especially outside of the pinniped family. Further, the isotropic or anisotropic trends could be localized to the anatomical region tested. The anisotropy of human skin is well documented [5], but is still often modeled isotropically. The assumption of an isotropic model has considerable simplifying implications in material modeling. In the absence of more compelling proof of anisotropy, this is an assumption worth making.

The isotropic trend seen in harbor seal tissue may have root in their swimming mechanism and physiology. Shark skin anisotropy is shown to aid in locomotion [83] while dolphin is purported to reduce drag through anisotropy [68]. Seals have a different locomotion mechanism than the caudal oscillators of the cetaceans or undulation of sharks; harbor seals may not be employing the same strategies as these other aquatic mammals. Their semi-aquatic nature requires land-based locomotion as, so their skin must also be stronger to carry their body weight out of the water.

A difference in age class of the animal was seen for three out of four material properties tested. Age has been shown in humans to impact the material properties of skin [24]. The two age classes had significantly different material properties; the pup has more elastic blubber

and less strong blubber and skin. Greater elasticity allows for growth in these young animals and is consistent with other mammals. The two age classes of tissue did not respond the same to freezing. The fatty acid content of harbor porpoises changes with age [54], which could freeze differently than its adult counterpart.

Freezing has an impact on the material properties of harbor seals, with a more pronounced difference in the skin. The frozen and fresh data were highly correlated, so a freezing coefficient could potentially be developed with further study to calculate the fresh properties from only frozen testing. Blubber's higher fat content could potentially decrease the impact of freezing compared to skin. The method of freezing could impact the frozen tissue results as well, as the temperature and speed of freezing impacts the formation of ice crystals. Freezing protocol was shown to impact dog vocal fold tissues [16].

### *2.3.3 Multivariate Analysis across Species*

#### *2.3.3.1 Comparison with previous analysis*

After intensively examining the seal data, multivariate analysis illustrates whether or not the patterns seen in the seal data are present across all marine mammals tested. Just as in the linear mixed regression analysis, the skin and blubber have markedly different material properties, with skin being an order of magnitude larger in elastic modulus, tensile strength, and yield strength than blubber, just as seen with the seal data alone. Similarly to the linear mixed regression, this analysis does not show a strong effect of orientation. This multivariate result can be compared with analyzing the effect of speed, condition, orientation, and age on each material property separately, as shown in the previous section. The linear mixed effect analysis indicated mixed results on the significance of the material properties. For example, seal skin's elastic modulus was found to be significantly impacted by orientation, but in the opposite trend that seal skin's tensile strength was found to be. Since these two variables are highly correlated, the evidence does not give us a meaningful understanding of the effect of orientation. The two analyses disagreed that speed was a significant factor, as

the multivariate approach showed a significant difference for skin. Both analyses found that freezing the tissue changes the material properties with a high correlation to the fresh data. The current multivariate approach allows a more robust understanding of the materials in concert, as well as the broader context of species differences in the materials.

### *2.3.3.2 Properties of skin and blubber across all species*

One difference in the seal and the toothed whales is the relationship between elastic modulus and tensile strength. For the seal, every test of both skin and blubber show that the elastic modulus and tensile strength are nearly the same value. However, the toothed whales (porpoises and orca) have a different trend, where the strength is consistently of lower magnitude. This observation shows a different functional role for these two tissues between the two classes of marine mammals.

The difference in the seal and the toothed whales is readily observable in a principle component analysis (Figure 2.8). The highly correlated nature of elastic modulus and tensile strength seen in the skin PCA is largely driven by the seal data. Using a principal component analysis, the material properties are expectedly highly correlated. For the skin PCA, 69% of the variance is explained using the first component, and a cumulative 94% is explained using the first two (Figure 2.8). The first component is the only significant component using a Monte Carlo test because it explains so much of the variance (69%). Still, the first two components are used for visualization and presentation of the data. The skin PCA tells us that the variables, especially elastic modulus, tensile strength, and yield strength, are highly positively correlated (Table 2.1). All the material properties are highly loaded on one component, indicated by the axes of Figure 3, with the exact structure coefficients available in Table 2.1. A stiffer (high elastic modulus) skin material will tend to also be stronger (high tensile strength) and endure more stress before yielding (high yield strength).

When this PCA analysis is repeated with only toothed whales, there is confirmation that the three toothed whales are still quite similar to each other, but there is also a fundamentally different relationship, where elastic modulus, tensile strength, and yield are no longer as

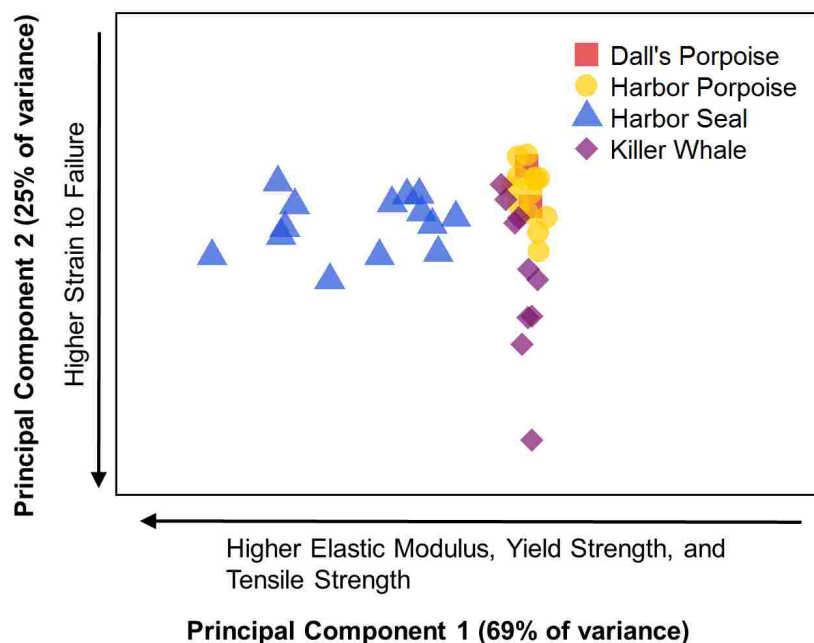


Figure 2.8: Biplot of PCA ordination of all skin material properties with species (Dall's Porpoise, Harbor Porpoise, Harbor Seal, or Killer Whale) denoted. The toothed whales (Dall's Porpoise, Harbor Seal, and Killer Whale) show a clustering separate from the pinniped (Harbor seal) in the ordinate space. The material properties were highly loaded on the first two principal components, with the exact loadings (structure coefficients) in Table 2.1

correlated (Figure 2.10). These trends are also present in boxplots of skin strength (TS) and elastic modulus (E) in Appendix A (Figures A.1-A.3).

Examining boxplots of the blubber material properties, the killer whale data varies the most from the patterns seen in the other animals (Figure 2.9); this observation is reflected in the blubber PCA, with the killer whale clustering separately from the other species (Figure 2.8). The blubber PCA also has a significant first component, which explains 63% of the variance, and a cumulative 87% of variance over the first two components (Figure 2.11). A negative correlation for elastic modulus and strain to failure is seen strongly in the second component of blubber, and is present in the skin analysis shows a predicted relationship that

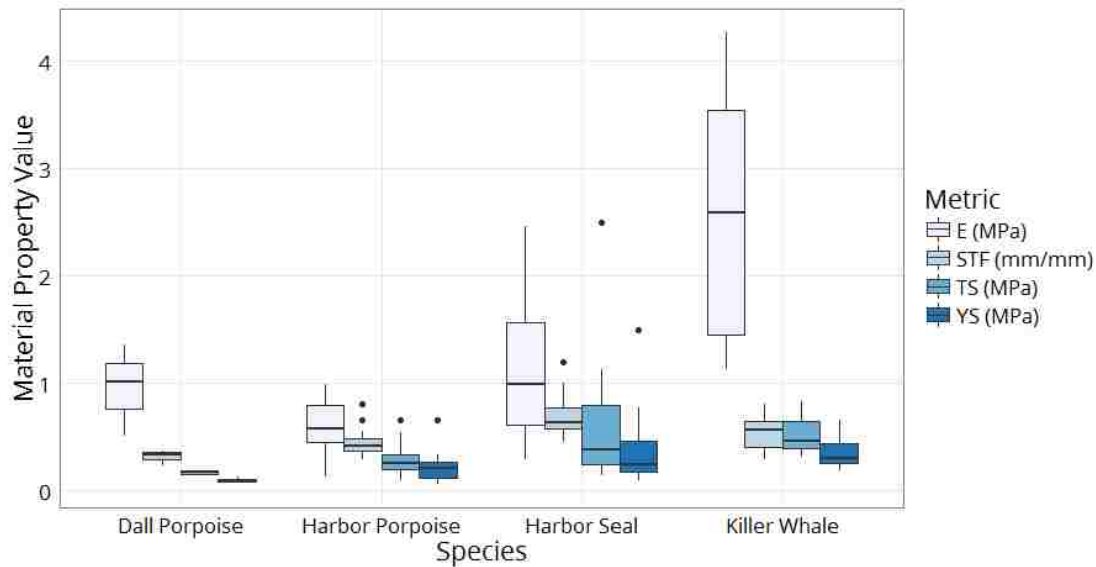


Figure 2.9: Boxplots of each of the four material properties over all tests for each species blubber, including both juvenile and adult animals. All marine mammals show the same general trends in the relationship between the relationships between the material properties captured in tensile testing.

Table 2.1: Mean and range of each material property variable for both skin and blubber. The structure coefficients (Pearson product-moment correlations) between the material properties variables and the first two principle components, with skin and blubber in separate principal component analyses.

Variable	Skin		Blubber			
	Mean (range)	Structure coefficients	Mean (range)	Structure coefficients	PC1	PC2
Elastic Modulus (MPa)	10.35 (1.35-41.85)	PC1 -0.550 PC2 0.096	1.35 (0.13-4.27)	0.290	0.846	
Yield Strength (MPa)	4.33 (0.37-21.99)	-0.585 -0.013	0.33 (0.06-1.50)	0.600	0.007	
Tensile Strength (MPa)	5.46 (0.53-22.63)	-0.595 -0.001	0.51 (0.1-2.49)	0.612	-0.040	
Strain to failure (mm/mm)	0.63 (0.26-1.71)	-0.044 -0.995	0.56 (0.24-1.20)	0.425	-0.531	

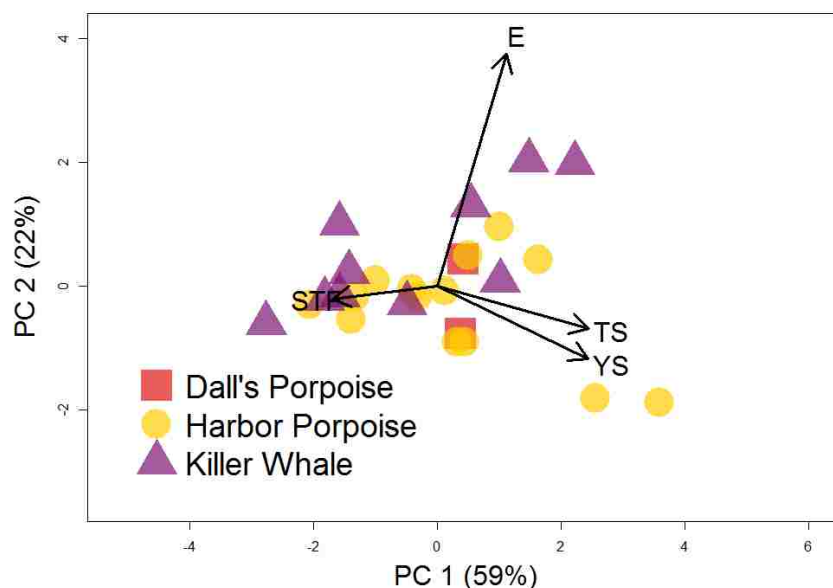


Figure 2.10: Biplot of PCA ordination of all skin material properties with species (Dall's Porpoise, Harbor Porpoise, or Killer Whale) denoted. The toothed whales still cluster together and overlap even when the seal data is removed.

less stiff (low elastic modulus) materials can endure more strain before failing (high strain to failure).

### 2.3.3.3 Effect of Species, Speed and Orientation on Tissue Material Properties

Species of animal is the largest driver of the differences observed between the materials across blubber and skin tissues. In the skin tissue, a significant difference was also seen in the groups of both speed and species (Table 2.2). In a pairwise comparison of the skin tissue between species, all other species are significantly different from harbor seal (perMANOVA, killer whale  $p = 0.0004$ , Dall's porpoise  $p = 0.0445$ , harbor porpoise  $p < 0.0001$ ), but none of the other pairs were significantly different, meaning that harbor porpoise, killer whale, and dall's porpoise skin are not significantly different from each other across the four material property metrics. No effect of the orientation was seen in the tissue for skin or blubber. Blubber did

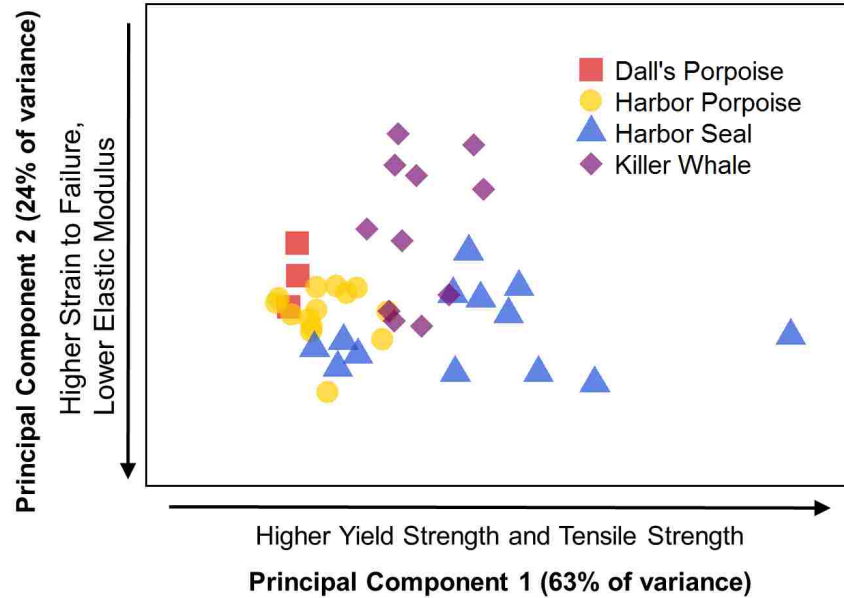


Figure 2.11: Biplot of PCA ordination of all skin material properties with species (Dall's Porpoise, Harbor Porpoise, Harbor Seal, or Killer Whale) denoted. The toothed whales (Dall's Porpoise, Harbor Seal, and Killer Whale) show a clustering separate from the pinniped (Harbor seal) in the ordinate space. The material properties were highly loaded on the first two principal components, with the exact loadings (structure coefficients) in Table 2.1

not exhibit significantly different material behavior at the two speeds tested. Once again for blubber, the species had the most significant impact on the material properties. In a pairwise comparison for blubber, all Dall's porpoise and harbor porpoise were significantly different from harbor seal (perMANOVA, Dall's porpoise  $p = 0.0054$ , harbor porpoise  $p < 0.0001$ ). Harbor porpoise and Dall's porpoise were not significantly different.

#### 2.3.3.4 Impact of Freezing on Skin and Blubber Biomechanics

The Procrustes of harbor seal and harbor porpoise (the only animals tested both fresh and frozen) analysis found a significant relationship between the fresh and frozen data for

Table 2.2: Results comparing the material properties across groups of orientation, speed, and species. P-values  $<0.05$  are assumed to be significant.

<b>Skin</b>			
<b>Group</b>	<b>F</b>	$R^2$	<b>P(&gt;F)</b>
Orientation	0.304	0.003	0.616
Speed	10.343	0.900	0.002*
Species	23.44	0.612	0.001*
<b>Blubber</b>			
<b>Group</b>	<b>F</b>	$R^2$	<b>P(&gt;F)</b>
Orientation	0.359	0.005	0.684
Speed	0.423	0.006	0.626
Species	12.219	0.506	0.001*

skin ( $m^2=0.48$ ,  $p=0.003$ ), but not for blubber ( $m^2=0.80$ ,  $p=0.164$ ). The skin and blubber residuals were examined to see if any observations had lower residuals. The harbor porpoise has the lowest average residual, though the two lowest residuals are both found in a single animal of a different species, one harbor seal pup. While the residuals are highest in the skin for the adult harbor seal, the blubber residuals are the lowest in this animal.

## 2.4 Summary

Material testing outside the living animal will naturally result in different conditions than in vivo. This effect has not been quantified for marine mammals. Further, the biological material will likely have different material properties in compression, much like human skin [61]. A rigorous material constitutive model would also require further testing of the bulk modulus and shear modulus. Finally, it remains possible that untested factors, like the gender of the animal, is a larger factor than the ones that were examined.

Using material properties across four species, adaptations can be compared in the composite behavior of the material, showing the diversity in aquatic tissue structure. This approach also lends itself to examining similarities between species. All three toothed whales had similar mechanical properties. This may be a result of similar adaptations in the structure and therefore function across these species, even with a large variation in size. This sim-



plifying observation is valuable, as a much more common animal, like the harbor porpoise, could act as a surrogate for understanding the morphology and material properties of more rare and difficult to obtain tissue, like the Southern Resident killer whale, but cannot be generalized to the blubber of the toothed whales, as the killer whale blubber was stiffer and stronger than the porpoises. Testing an additional seal, other pinniped, or marine mammals from an additional evolutionary line like the manatee and dugong would be the natural next steps to determine if skin similarities exist among each clade. The simplifications possible from generalizing across multiple species of marine mammal soft tissue can be used in the modeling explored later in this dissertation.

Looking at the tensile testing results of skin and blubber, it is obvious that this material is not linear elastic. Tensile testing alone is limited in that it cannot predict the full range of behavior of the material. Tensile testing cannot predict how the material will behave in compression. Like many other biological materials, both skin and blubber could be expected to behave differently in compression, as examined in Chapter 3.

## Chapter 3

# INDENTATION, SHEAR MODULUS, BULK MODULUS, DENSITY, AND HISTOLOGY EXPERIMENTS

### 3.1 Overview

Tensile testing alone cannot give a complete picture of a material. In biological materials, this is particularly pronounced, as the material typically behaves differently in tension and compression, with significantly less stiffness under compressive load. Human cartilage has been shown to be much stiffer in tension than in compression [44]; the same pattern is seen in pig skin [72]. The compressive behavior of the material can be tested in a variety of methods, including confined compression and unconfined compression on a variety of shapes. Indentation testing is another method from which compressive mechanical properties can be determined; it is typically a non-destructive method. Spherical indentation uses a rigid indenter and measures force and displacement as the indenter moves into the test material. The force and displacement can be reduced to a uniaxial stress strain curve for the material in compression. This method does not test to failure, so the compressive strength of the material is unknown. The first goal of additional material testing was to determine the blubber's elastic modulus in compression using this method.

A second goal was to determine the level of complexity in material modeling of the tissue. With tensile testing of skin and blubber not showing convincing trends of anisotropy, perhaps a relatively simple material model is appropriate for the tissue. A readily observable linear region is seen in each material, and a linear elastic approach greatly simplifies the model, as well as future testing of additional animals. Adding further testing allows a more comprehensive description of the material behavior. To that end, the shear modulus and bulk modulus were tested.

The elastic modulus ( $E$ ), shear modulus ( $G$ ), and bulk modulus ( $K$ ) are three interrelated material properties. In an isotropic linear elastic material, these properties are all interrelated by a simple constitutive equation:

$$E = 2G(1 + \nu) = 3K(1 - 2\nu) \quad (3.1)$$

A more complicated material constitutive equation is likely needed for the large deformation in marine mammal tissues during a tidal turbine strike, but a linear elastic model has been used to approximate other mammalian skin [67]. Measurement of all three moduli allows for creation of a more complex constitutive equation. Marine mammal blubber is likely near incompressible, with the Poisson's ratio  $\nu = 0.5$ . Using the isotropic constitutive relations, the ways in which this material differs from the typical assumptions made about living tissue can begin to be understood.

Describing the individual animal's response to shear forces that the blade could impart will aid in more fully understanding the potential for injury. Understanding marine mammal's bulk modulus will allow a understanding of compressibility in the animal, potentially also illustrating how the material may be compressed at deeper water depths as the animal swims to the turbine depths. Finally, with every additional material test performed, the similarities or differences between different coastal marine mammals are confirmed, allowing generalizations to be made in modeling collisions.

## **3.2 Indentation Testing**

### *3.2.1 Overview*

Preliminary finite element models have indicated that during a collision, the skin has the highest forces in tension, while the blubber experienced more stress in compression. For this reason, it was a priority to understand the blubber's behavior in compression.

However, skin and blubber are connected tissue and as such behave as a composite material. All previous testing had separated the two layers, which could impact the result. The

composite behavior of the skin and blubber was tested by using an indentation test on the two layers together. The primary goal of the compressive material study is get appropriate material properties that are then used to validated a finite element model. Chapter 4 evaluates material models to accurately capture the response seen in the composite material testing. This constitutive model can ultimately be used as a basis for evaluating injury from a tidal turbine blade. Linear elastic material models have occasionally been used to simulate soft tissue, though are likely inappropriate for the large deformations seen during a blade strike. Pig skin has been modeled as a hyperelastic strain rate dependent material using the Ogden model of hyperelasticity [72]. This testing and analysis has presently been completed for harbor porpoise, killer whale, and harbor seal.

Finally, compression testing, like the tension testing, aims to identify how similar the animals material properties are. This analysis could also limit the development of constitutive material models for toothed whales, perhaps even large mysticete whales with further study. The seal is assumed to be significantly different due to their use of both terrestrial and aquatic locomotion, as well as from the analysis performed in Chapter 2.

### *3.2.2 Methodology*

#### *3.2.2.1 Tissue Procurement*

The compression testing was performed on animals also used for tensile testing. Harbor porpoise 2, the same animal tested in tension, was tested fresh in July 2015. The orca for this testing was the J32 Orca, also tested in July 2015 after being frozen since the animal stranded in December 2014. Seal pup 2 was tested in December 2015 after being frozen for 15 weeks. The seal data was notable because the blubber most visibly expanded after the skin was removed.

### 3.2.2.2 Indentation Tissue Testing

To perform indentation testing, a spherical indenter was displaced into a piece of tissue using the MTS Synergie 100 and a 500 N load cell. The indentation test was performed on a composite piece of tissue, using both blubber and skin still connected as well as blubber alone. For each animal tested, the tissue was approximately 8 cm by 9 cm, cut to be smaller than the plate supporting the sample below (Figure 3.1). A 12.7 mm plastic ball was pushed into the sample; force and displacement was recorded for the duration of the test. At approximately 20% of the depth of the sample, it is likely that the plate begins to contribute to the stiffness of the recorded force. For each test, the indenter was pushed a few millimeters past the 20% depth. Repetitions were performed by moving the location of the ball on the block of tissue. All repetitions were conducted with a buffer zone away from the edge of the tissue of approximately 2 cm.

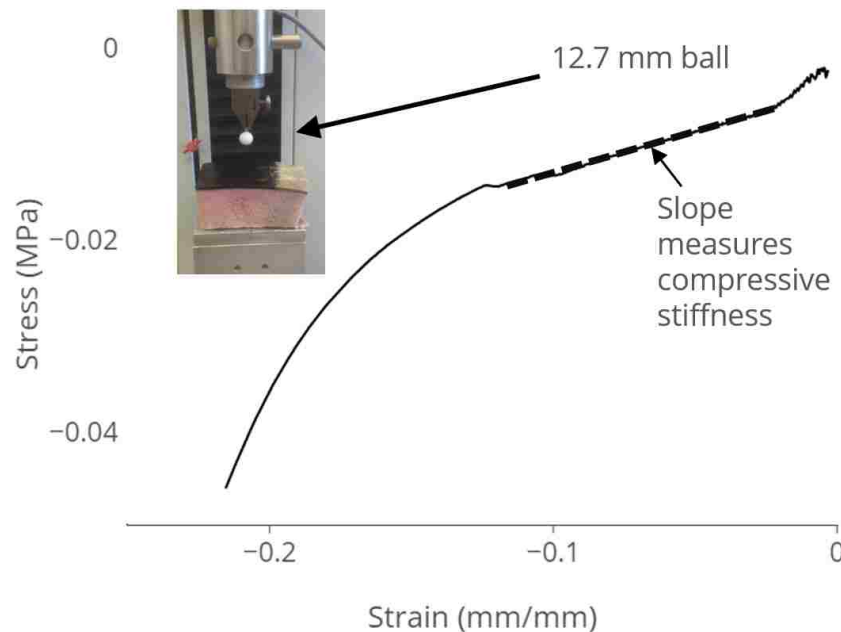


Figure 3.1: Example stress-strain curve of compression testing. Inset shows testing setup.

Spherical indentation was conducted in the elastic region of the material. It is assumed

that the indenter does not deform during the testing. The material contact is assumed to have no adhesion and therefore Hertz's theory can be used to convert the indentation test to a compressive stress strain curve.

Elastic modulus of the material was calculated as a function of the penetration depth, assuming a blubber Poisson's ratio of  $\nu = 0.5$ , a value often used for human fatty tissue. Hertz method assumes the total depth penetration,  $h$ , can be related to the the radius of contact,  $a$ , using the radius,  $R$  of the indenter (3.2).

$$h = \frac{a^2}{R} \quad (3.2)$$

The reduced or indentation modulus is then calculated,  $E_r$ , using the Hertz relationship between the recorded load,  $P$ , and the contact radius,  $a$  (3.3).

$$E_r = \frac{3P}{4h^{3/2}\sqrt{R}} \quad (3.3)$$

If the indenter is assumed to be rigid compared to the blubber, the blubber's elastic modulus in compression  $E$  is then calculated using the Poission's ratio  $\nu$  and  $E_r$  (3.4)

$$E = \frac{E_r}{1 - \nu^2} \quad (3.4)$$

The maximum stress is calculated under the indenter using the a relationship between recorded load and the contact area for contact between a sphere and elastic half space (3.5).

$$\sigma = \frac{3P}{2\pi a^2} \quad (3.5)$$

To fully reduce the spherical indentation to a uniaxial compression value, this same method can be used to calculate the strain, using the elastic modulus at each depth (3.6)

$$\epsilon = \frac{\sigma}{E} \quad (3.6)$$

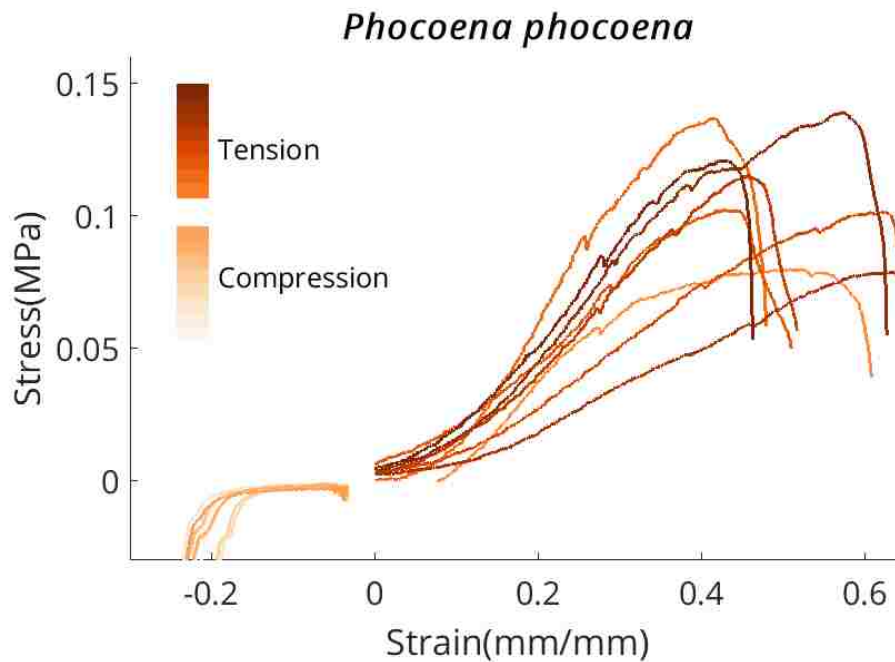


Figure 3.2: Harbor porpoise (*Phocoena phocoena*) blubber measurements. Lighter orange in the negative direction represents compression tests, while darker orange in the positive direction represents tension testing. Each line represents an individual test, which can be averaged to find the results in Table 3.1. When measured in compression harbor porpoise has an order of magnitude smaller elastic modulus.

### 3.2.3 Results

#### 3.2.3.1 Comparison of blubber in tension and compression

Compressive tests show a blubber elastic modulus that is an order of magnitude different than that measured in tensile testing for the toothed whales. This is not seen in the seal. The full stress-strain curve can be assembled using results from both tests, although the values near zero stress are difficult to pinpoint (Figures 3.2-3.3). As the experiment reaches greater than 20% strain, the impact of the rigid blade beneath the plate begins to have a large impact on the test, so this part of the experiment is not included in the analysis.

In addition to examining the stress strain curves, the compression values elastic modulus was calculated by evaluated Equation 3.4 where the strain is equal to 0.1 (Table 3.1).

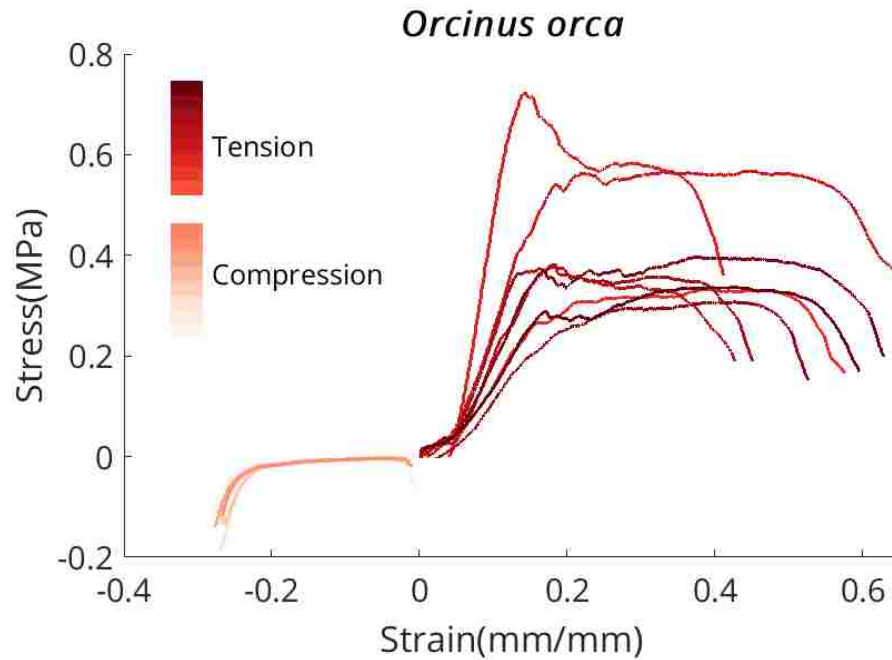


Figure 3.3: Killer Whale (*Orcinus orca*) blubber measurements. Lighter red in the negative direction represents compression tests, while darker red in the positive direction represents tension testing. Each line represents an individual test, which can be averaged to find the results in Table 3.1. When measured in compression orca has an order of magnitude smaller elastic modulus. As a further difference with harbor porpoise (Figure 3.2), the orca blubber in tension has a much more defined plastic region and overall stiffer values.

Table 3.1: Comparison of values of elastic modulus in tension and compression. For tension values, the value represents an average across all tissue orientations. Elastic modulus in compression is calculated as the value of E where the strain was 0.1

	Orca J32	Harbor Porpoise 2	Baby Seal 2
Tension E (MPa)	3.03	0.430	0.837
Compression E (MPa)	0.084	0.042	0.283



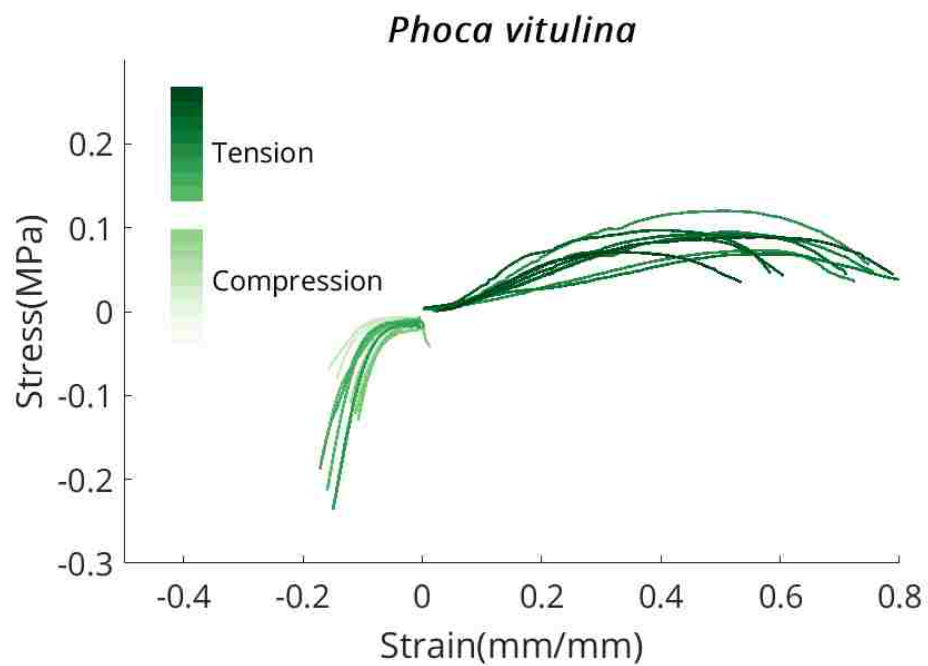


Figure 3.4: Harbor Seal (*Phocoena vitulina*) blubber measurements. Lighter green in the negative direction represents compression tests, while darker green in the positive direction represents tension testing. Each line represents an individual test, which can be averaged to find the results in Table 3.1. When measured in compression seal has a similar elastic modulus.

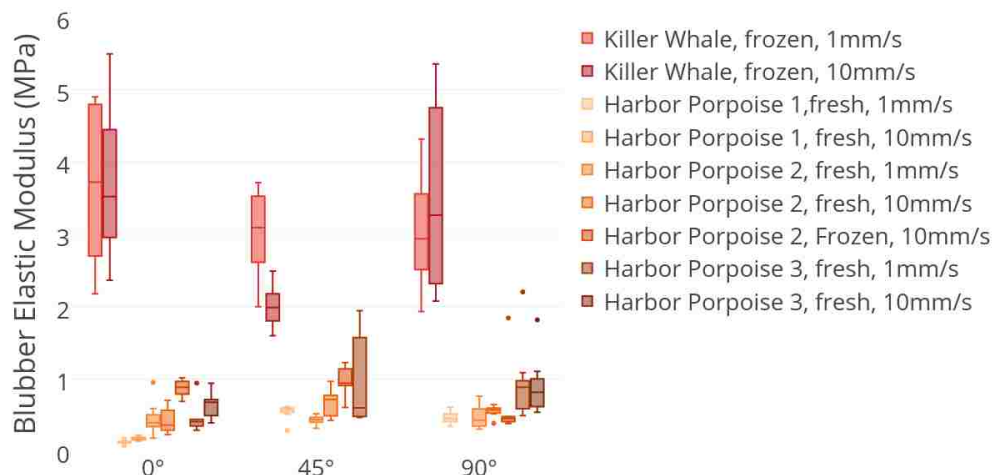


Figure 3.5: Across all adult orca and harbor porpoise tensile testing, the orca has much stiffer blubber. This trend is also present in compression testing (Figures 3.2-3.3)

### 3.2.3.2 Compression Testing Differences Between Species

Compression testing highlights how harbor porpoise and orca blubber may not be similar enough to model similarly. During the tensile testing, the blubber of these two animals was quite different (Figure 3.5). However, it further enforces the fact that the seal is in a class of its own.

## 3.3 Conclusions

The important conclusion of compression testing is that blubber must be modeled as different in tension and compression, especially for the toothed whales. To successfully determine how the material reacts to a blade strike, the compressive values must be included. This spherical testing still cannot show the maximum compressive strength, which also may be important in evaluating the consequence of a tidal turbine strike.

With just one Southern Resident Killer Whale, conclusions cannot be drawn about the

whole population. The material properties unique to the whale that was tested may be based on the gender and age of the whale and not representative of the animal. A more degraded whale, three-year old female L112, of the same small subpopulation in the Salish Sea was tested in 2013; the material properties that were reported for only the  $0^\circ$  and  $90^\circ$  directions and showed more variability than J32 [15]. Further, this work found that the blubber had a higher elastic modulus than skin in all test cases. Carlson et al. tested a more fresh neonate and found skin stiffer and stronger than blubber, matching the results presented here for both killer whale and porpoise [?]. The comparison with L112 will be further discussed in Chapter 5.

### 3.4 Bulk Modulus

#### 3.4.1 Overview

Expanding on compression testing using a spherical indenter, bulk modulus measures how the material changes in volume under uniform confined compression. As a blade moves into a marine mammal, it is essential to understand how that material compresses under the confined conditions inside the living animal. If the material is assumed to be ideal, isotropic and homogeneous, there exist simplified methods and assumptions of the bulk modulus value, but blubber especially is likely more complicated in its reaction to impact. Bulk modulus is sometimes called volumetric compression and can be defined as:

$$K = -V \frac{dP}{dV} \quad (3.7)$$

where  $K$  represents bulk modulus,  $dP$  is a change in pressure,  $dV$  is a change in volume, and  $V$  is the original volume. In an isotropic material, it can be simply related to the elastic modulus. Evaluating this material property can allow understanding of how the impact propagates through the material, as well as how close both skin and blubber behave to a simplified linear elastic isotropic model. Bulk modulus has a more conventional test method across different materials, with a confined compression test, but can also be tested by prop-

agating a wave through the material, which has been executed in both soils [39] and tissues [32]. The bulk modulus is related to the speed of sound in a material by the formula:

$$c = \sqrt{\frac{K}{\rho}} \quad (3.8)$$

where  $c$  is the speed of sound and  $\rho$  is the density of material.

Both skin and blubber are likely nearing incompressible, with much higher magnitude values for bulk modulus than the shear and elastic moduli [11].

### 3.4.2 Methods

The bulk modulus testing needed to be completed on a existing machine on both skin and blubber separated from one another, as in the tension testing. The MTS Synergie 100 with a 500 N load cell has clamps that can accomodate a variety of shapes. Due to the high forces necessary to test a nearly incompressible material, a series of calculations were performed to ensure the machine was not overloaded and accurate results were collected. The following analysis also allows for an understanding of the accuracy in the measurement of bulk modulus. Finally, the test set up was printed on a Formlabs Form 2 3D printer, so the stiffness of 3D printed resin material was compared against the forces during the test to ensure the plastic was sufficiently stiff for testing accurately.

The bulk modulus test, as designed, is a volumetric test. Thus, it can be modeled as a thick-walled cylinder to define a reasonable test setup with accurate and precise results. A generic confined test has a cylindrical test sample inserted into a thick walled cylinder. A force is then applied from the top using a plate of the same size as the sample and inner diameter of the thick walled cylinder (Figure 3.6)

A thick walled cylinder solution in plane strain can be used to approximate how tall the sample should ideally be, though in reality this was determined by the sample thickness. With the same load, a taller sample will have a higher change in height. Because the material is nearly incompressible, the change in height is small and must be larger than the error in

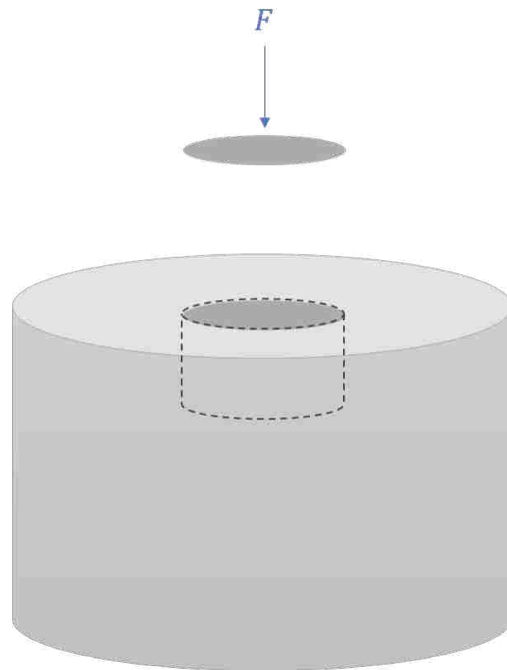


Figure 3.6: Bulk modulus test setup where a downward force is applied to a plate to volumetrically compress a sample

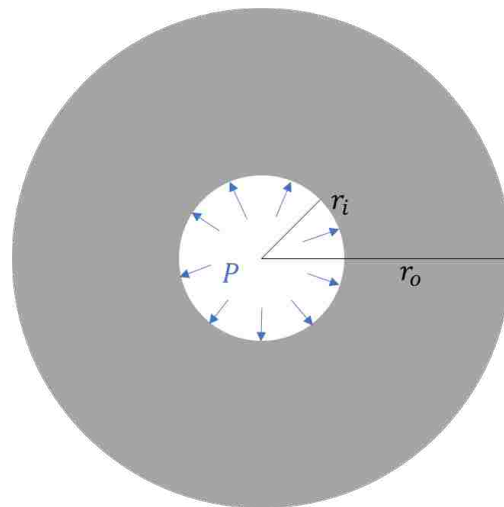


Figure 3.7: Top view of the forces inside the bulk modulus setup once force is applied to sample. Inner ( $r_i$ ) and outer ( $r_o$ ) radius is labeled.

the MTS Synergie's displacement sensor to be accurate. Using a thick walled solution, the outer radius pressure is defined as zero and the inner radius pressure as the force on the plate divided by the area of the plate (Figure 3.7).

$$P = \frac{F}{r_i^2 \pi} \quad (3.9)$$

Literature values from water and other similar substances were used to determine the force required to displace by at least 0.1 mm using the 500 N load cell.

Finally, the material to construct the bulk modulus test rig must be evaluated. The material must be stiff enough that there is a negligible displacement in the inner radius during the volumetric compression test. With the case of internal pressure only, the inner displacement change can be defined as:

$$\Delta r_i = \frac{r_i^3 P}{E(r_o^2 - r_i^2)} \left[ (1 - \nu) + (1 + \nu) \frac{r_o^2}{r_i^2} \right] \quad (3.10)$$

where  $E$  is the elastic modulus of the device surrounding the tissue and  $\nu$  is the Poisson's ratio of that material.

The volumetric change in strain can be related to Equation 3.10 to find a suitable material and its dimensions for this test setup.

$$\epsilon_{vol} = \epsilon_x + \epsilon_y + \epsilon_z \quad (3.11)$$

$\epsilon_z$  can be approximated as the change in height ( $\Delta H$ ) over the original height ( $H$ ), while  $\epsilon_x$  and  $\epsilon_y$  can be approximated as the change in the inner radius over the original radius.

$$\Delta \epsilon_{vol} = 2 \frac{\Delta r_i}{r_i} - \frac{\Delta H}{H} \quad (3.12)$$

A change in pressure can be related the bulk modulus multiplied by a change in the volumetric

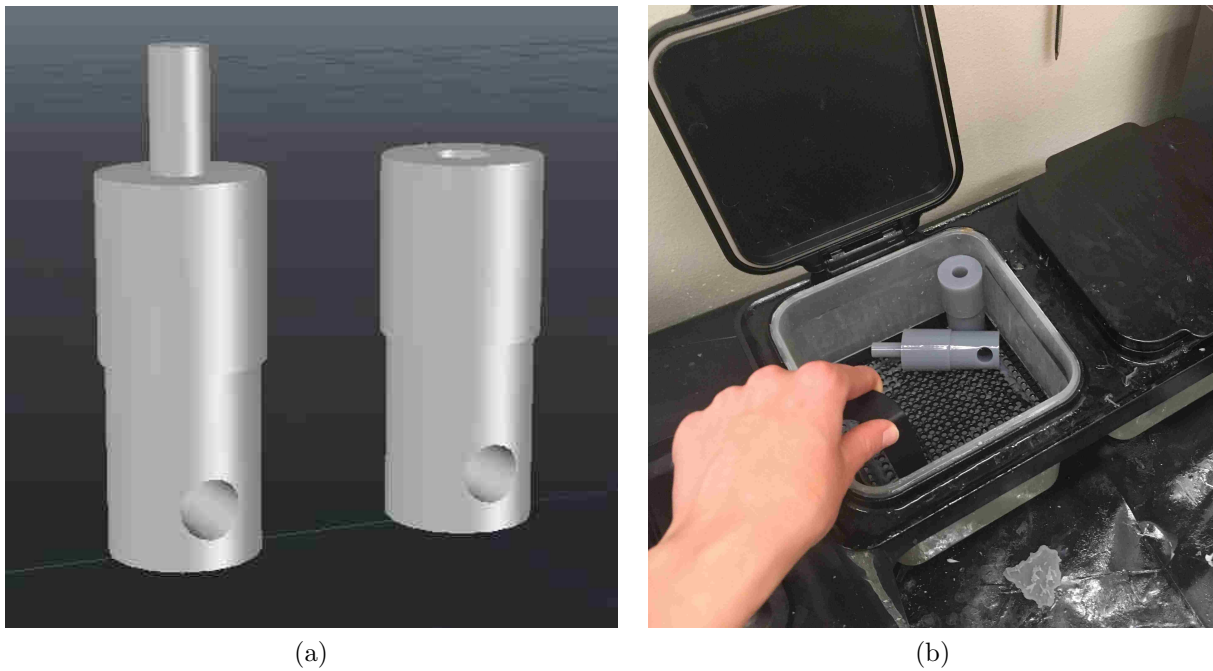


Figure 3.8: Clamp design in AutoCAD (a) and after printing on the Formlab Form 2 printer, clamps are rinsed in an alcohol bath (b)

strain:

$$\Delta P = k\Delta\epsilon_{vol} \quad (3.13)$$

Thus, to accurately measure bulk modulus, the material in the testing device must have an elastic modulus and Poisson's ratio such that the material is stiff enough to satisfy the relationship:

$$2\frac{\Delta r_i}{r_i} \ll \frac{\Delta H}{H} \quad (3.14)$$

Using this derivation, the bulk modulus clamps were designed in AutoCAD and printed on a Formlabs Form 2 printer using the grey standard resin (Figure 3.8). Based on the calculations, sample heights of 5 mm or greater were assumed to be sufficiently accurate and the samples of skin were taken with the largest height the specimen would allow. All final variables used in the derivation are summed in Table 3.2

Three animals were tested in bulk modulus testing, the J32 killer whale, Harbor Porpoise

Table 3.2: Parameters used for bulk modulus accuracy calculations.  $F$  is set to 450 N to encourage not overloading the MTS Synergie load cell with bulk modulus testing.

Variable	
$r_i$	12.7 mm
$r_o$	38.1 mm
$F$	450 N
$E$ (resin)	1.4 GPa
$\nu$ (resin)	0.35
$2\frac{\Delta r_i}{r_i}$	0.0127 mm

Table 3.3: Power and speed used to cut different individual's tissues with laser cutter.

Animal	Tissue Type	Power	Speed (mm/s)
Killer Whale	Blubber	28	1
	Skin	40	2
Harbor Porpoise	Blubber	100	3.75
	Skin	100	10
Harbor Seal	Blubber	50	1
	Skin	100	2.75

2, and Seal 4. Pieces of tissue from the three individuals were thawed after being frozen for over a year. Blubber and skin were separated from each other using a Chef'sChoice Premium Electric Food Slicer 615. Due to the thickness of the killer whale blubber, the blubber layer was cut in half, but for all others the full thickness of the blubber layer was used.

Once separated, the blubber and skin was cut into half inch cylindrical subsections using a HurricaneLasers laser cutter. Depending on the thickness, tissue type, and animal, different laser cutting settings were needed to ensure the laser cutter cut through the thickness of the material without charring the edges (Table 3.3). This was accomplished using a trial and error method until decent samples were achieved. It was during this initial trial and error that the killer whale blubber was determined to be too thick to cut accurately with the laser cutter.

Once cut into cylinders, each specimen height and diameter was measured before loading into the bottom printed clamp. The top clamp was manually adjusted downward until the



sample began to bear load, then the MTS was zeroed. The test was then started and the top clamp proceeded downward at 1 mm/s until the load cell registered 450 N. After the test, blubber samples generally looked crushed, with the exception of the killer whale samples which were much more intact. The skin samples generally looked intact.

Once tested, the force-displacement data recorded was analyzed and compiled using Matlab. Volume of the sample was calculated at every time step as the height of the sample changed, allowing for calculation of Equation 3.7.

### 3.4.3 Results

The bulk modulus results are summarized in Figure 3.9. The most evident result is that harbor seal blubber behaves differently than the other two, which is consistent with qualitative observations of the individuals' blubber tissue.

An additional interesting method of understanding these results is to compare them to expected results if the material were isotropic. If isotropic, simple constitutive models can relate previous calculation of elastic modulus with these bulk modulus calculations, like those shown in Equation 3.15.

$$E = 3K(1 - 2\nu) \quad (3.15)$$

By using an approximate value for Poisson's ratio,  $\nu$ , the measured bulk modulus can be compared to a calculated version of the quantity. These measured and calculated results have the same order of magnitude for bulk modulus, but are highly sensitive to the value of  $\nu$  (Table 3.4).

## 3.5 Shear Modulus

### 3.5.1 Overview

Shear modulus is a measure of how the material responds to shear force, typically denoted as  $G$ . This is an important value, as the blade can impart shear forces on the animal, especially

Table 3.4: Summary of averaged bulk modulus results compared to bulk modulus results calculated from estimated poisson's ratio,  $\nu$ , and elastic modulus. Numbers are presented as average plus or minus the standard deviation.

		Bulk Modulus (MPa)		$\nu$
		Measured	Calculated	
Killer Whale	Skin	$56.85 \pm 18.57$	$33.67 \pm 21.23$	0.47
	Blubber	$38.58 \pm 12.45$	$55.88 \pm 12.86$	0.49
Harbor Porpoise	Skin	$30.98 \pm 2.93$	$18.09 \pm 9.85$	0.47
	Blubber	$29.74 \pm 9.13$	$9.12 \pm 4.14$	0.49
Harbor Seal	Skin	$49.98 \pm 3.81$	$98.16 \pm 53.53$	0.47
	Blubber	$8.34 \pm 1.13$	$24.71 \pm 8.45$	0.49

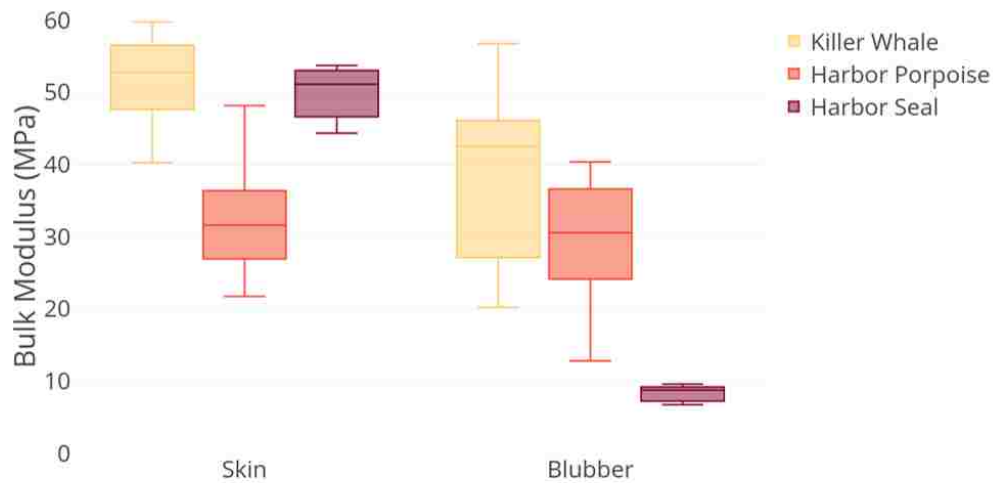


Figure 3.9: Bulk modulus testing results across three animals and two tissues. Middle line of the box plots represent the median of the data, with the box representing the middle 50% of the data.

as it penetrates deeper into the skin. A ratio of the shear stress ( $\tau_{xy}$ ) to shear strain ( $\gamma_{xy}$ ), shear modulus can be defined as:

$$G = \frac{\tau_{xy}}{\gamma_{xy}} \quad (3.16)$$

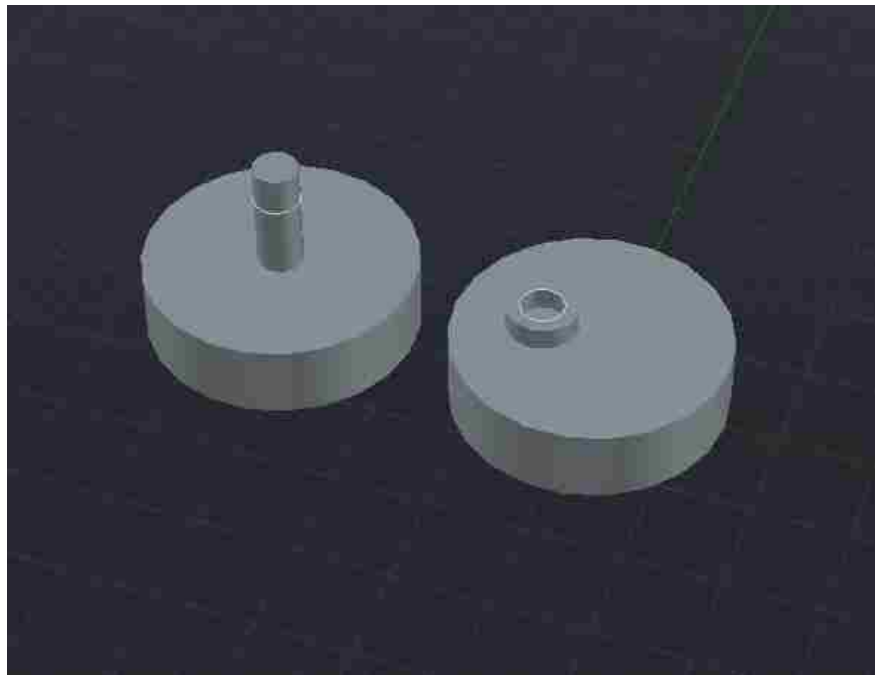
Testing shear modulus can be accomplished using a variety of methods. Even for a material such as wood, there is not a definite way of testing the material, as the ASTM standards (ASTM D 198) allow testing in torsion or a three-point bending test to determine shear modulus, potentially yielding different results [86].

Shear modulus is an especially significant material property in marine mammal blubber. A solid material and a fluid material respond to shear force in different ways, but vertebrate fat is generally characterized as somewhere between a solid and fluid, with viscoelastic qualities. As such, quantifying the tissues' response to shear force is a challenge. In the absence of consensus on how best to test this property for a fatty soft tissue, many fields' methodologies were examined, from soil science to biotechnology.

In viscoelastic materials, the shear modulus is divided into two parts, the storage modulus ( $G'$  which represents the elastic properties) and the loss modulus ( $G''$  which represents the viscous properties). To measure the viscous properties, especially in more fluid materials like human blood or gels, a rotational rheometer is a common tool. Using this tool, the shear stress relationship to the rate of shear can be measured. A rotational rheometer was used to measure the dynamics shear properties of three species: humpback whale (*Megaptera novaeangliae*), gray whale (*Eschrichtius robustus*), and sperm whale (*Physeter macrocephalus*) [78].

### 3.5.2 Methods

A rotational test using two plates was devised. The first plate is connected to a servo motor to rotate the plate. The second plate is fixed to a load cell, recording the force at the outer radius of the plate. The tissue sample is placed between the two plates. The motor attaches to the bottom plate off center, such that a shear force is applied (Figure 3.11). With this



(a)

Figure 3.10: Shear modulus plate design in AutoCAD. Left plate is top plate and right is bottom plate compared to Figure 3.11

setup, the shear force applied to the tissue sample can be determined.

Both plates were designed in AutoCAD and printed on a Formlabs Form 2 printer. The bottom plate (right in Figure 3.10) has a hole where the motor gear fits. This hole was designed to be too small for the motor gear. After the print finished, the motor gear was inserted in the uncured material and formed to fit, thus making a snug fit. After this process, the material was cured under UV light.

Because the shear modulus is much lower in magnitude than the bulk modulus, this test can function at a variety of sizes given the limits of the testing equipment. With the goal of creating only one tissue sample size, the values derived for bulk modulus geometry were used to evaluate and design the shear modulus test setup.

The shear modulus test setup was made from a Tower Pro MG005R high torque metal gear servo motor controlled by an Arduino Uno R3. The top plate was fixed to a Sper

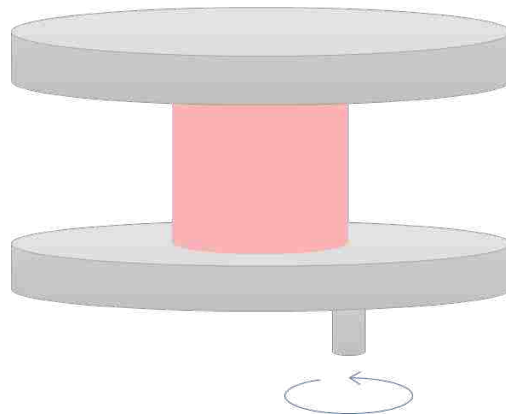


Figure 3.11: Shear modulus test setup where motor turns a tissue sample while the force at the outer radius of the top plate is measured.

Scientific Torque Meter, registering the torque incurred by turning the motor on the bottom plate. The two plates were rigged to be fixed in the x and y direction, but moveable in the z direction so that different height samples could be tested.

Samples were cut in the same method as for bulk modulus testing. The samples were loaded into the test rig by moving the two plates together to the height of the material, with the material perhaps slightly in compression, and held in place by sand paper fixed to the clamps. Height and diameter of the sample were measured with calipers.

To begin each test, the torque meter was zeroed, then the motor Arduino code was started. The motor was programmed to rotate  $30^\circ$  over 3 seconds, hold for 3 seconds, then return to the original position, then rotate  $30^\circ$  over 12 seconds, hold for 3 seconds, then return to the original position. For some harbor porpoise skin samples, especially those with the thinnest skin, the  $30^\circ$  rotation was too large, so a  $20^\circ$  rotation was used.

Data was recorded as torque over time. An average of the torque during the hold period was taken, which was generally level during the test. The two time periods did not have significantly different maximum torques, so only one result was calculated.

To calculate the shear modulus, a relationship between torque and shear modulus is need:

$$G = \frac{LT}{\theta} J \quad (3.17)$$

where  $G$  is shear modulus,  $L$  is the height of the sample,  $T$  is the torque registered from the torque meter, and  $J$  is the torsion constant for the section. For a circular solid shaft, the polar moment of inertia or torsion constant can be expressed as:

$$J = \frac{\pi r^4}{2} \quad (3.18)$$

where  $r$  is the radius of the cylindrical piece of tissue.

### 3.5.3 Results

The shear modulus tests show a more complicated picture than the bulk modulus. The seal skin is the most different from the other skins (Figure 3.12).

Shear modulus results can be compared with expected results of an isotropic material using the following equation:

$$E = 2G(1 + \nu) \quad (3.19)$$

The seal skin differs the most from the expected isotropic behavior (Table 3.5). It is possible that the seal's fur allowed the material to slip, but this was not visibly obvious during the test. All of the shear tests show an order of magnitude lower value than the predicated value for shear. One possible explanation is that the material behaves unexpectedly in shear because of its fluid properties, and another is that the test setup was not an accurate measure of this quantity.

## 3.6 Density

Density of marine mammal skin has been measured in the manatee (*Trichechus manatus latirostris*), harbor porpoise and bottlenose dolphin (*Tursiops truncatus*), with all densities

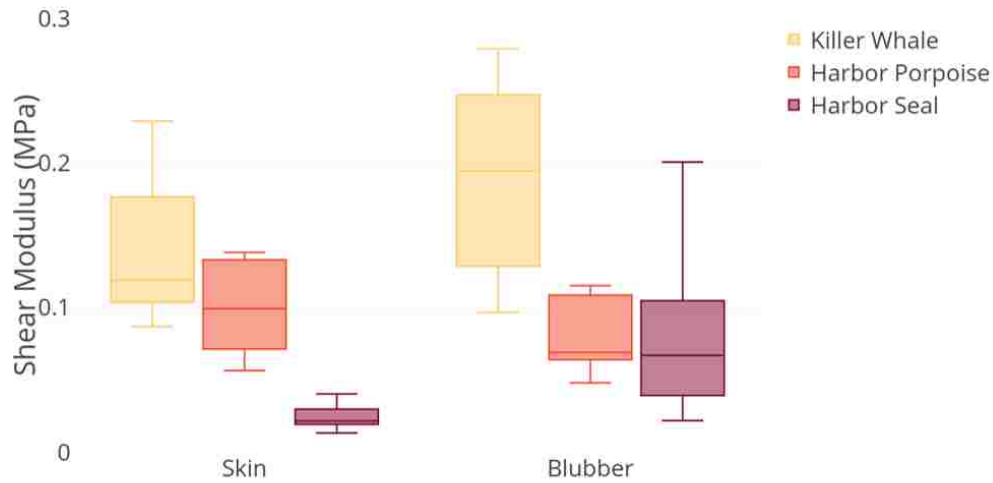


Figure 3.12: Shear modulus testing results across three animals and two tissues. Middle line of the box plots represent the median of the data, with the box representing the middle 50% of the data.

Table 3.5: Summary of averaged shear modulus results compared to shear modulus results calculated from estimated poisson's ratio,  $\nu$ , and elastic modulus. Numbers are presented as average plus or minus the standard deviation.

		Shear Modulus (MPa)		$\nu$
		Measured	Calculated	
Killer Whale	Skin	$0.14 \pm 0.05$	$2.06 \pm 1.30$	0.47
	Blubber	$0.18 \pm 0.07$	$1.13 \pm 0.26$	0.49
Harbor Porpoise	Skin	$0.10 \pm 0.03$	$1.11 \pm 0.60$	0.47
	Blubber	$0.08 \pm 0.02$	$0.18 \pm 0.08$	0.49
Harbor Seal	Skin	$0.02 \pm 0.01$	$6.01 \pm 3.28$	0.47
	Blubber	$0.08 \pm 0.06$	$0.50 \pm 0.17$	0.49



Figure 3.13: Density of skin (pictured above) measured through displacing water in a graduated cylinder, measuring the liquid displacement and change in mass.

near to being neutrally buoyant [50].

### 3.6.1 Methods

Density of each tissue was determined by measuring volume by means of liquid displacement and mass. Each piece of tissue measured was an irregular size, collected from leftover tissue during tensile testing. Samples were cut small enough to fit easily inside the 10 mL graduated cylinder. Using a graduated cylinder and a ScoutPro 400g scale, the scale was first zeroed with 6 mL of water in the cylinder (Figure 3.13). The tissue was then dropped into the graduated cylinder and the changes in volume and mass were recorded. For every density measurement, approximately 8 repetitions of the density measurement were collected.

Density data was analyzed using a two-way analysis of variance (with the R function `aov`), looking at the age class and type of tissue compared to measured density.



Table 3.6: Density measurement for four seals, porpoises, and orca exhibits the expected trend of blubber being less dense than skin.

Density	Seal 1	Seal 3	Seal Pup 1	Seal Pup 2	Harbor Porpoise 1	Dall's Porpoise 1	Orca J32
Blubber (g/ML)	0.93	0.904	0.875	0.917	0.849	0.733	–
Skin (g/ML)	1.103	1.032	1.069	1.056	1.138	1.13	1.06

### 3.6.2 Results

Blubber was significantly less dense than skin (Two-Way ANOVA,  $p$ -value  $< 2e-16$ ), but a significant difference was not seen between the adult and pup seal samples (Table 3.6); Seal 2, two harbor seals, and orca blubber were not measured. All measurements were near the average density of sea water, 1.025 g/mL, as expected for an animal aiming to remain neutrally buoyant. The tissue density, as with other ex vivo measurements, could be different inside the animal.

## 3.7 Histology

### 3.7.1 Overview

To confirm and inform material testing results from all other tests, a small histology study was performed. Polarized light microscopy is a useful method for examining the orientation of collagen fibers in skin and blubber as they are birefringent, meaning that the fibers refract light differently based on the direction of the light. This method can be used for more quantitative analysis, like quantifying the amount of collagen in certain tissues [52], studying the structure of collagen [84], or analyzing anisotropy in a material [81].

### 3.7.2 Methods

A small subsection of tissue, measuring approximately 5 mm on each side, was cut from a killer whale (J32), harbor porpoise (Harbor Porpoise 2), and harbor seal (Harbor Seal 4) using a scalpel. The seal's fur was removed using tweezers to pull out. Post freezing, the hairs

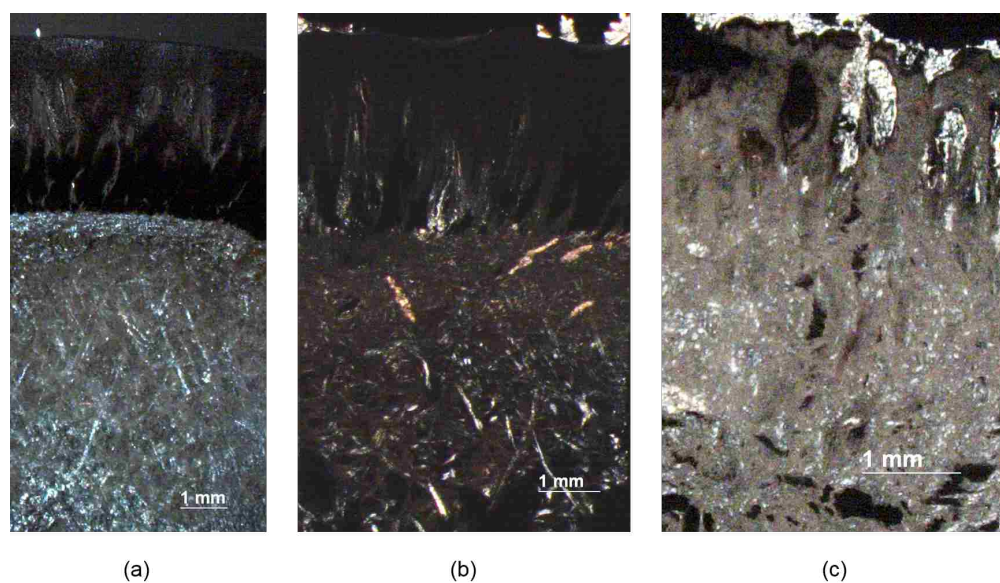


Figure 3.14: Microscope photographs of harbor porpoise (a), killer whale (b), and harbor seal (c) skin and blubber layers under polarized light after being preserved in Paraffin wax.

come out easily. The three samples were put together in a 500 mL beaker of formaldehyde for 24 hours.

The samples were placed together in a 50 mL Falcon tube of 30% ethanol for 20 minutes, then transferred to 50%, 70%, 80%, 95%, and 100% ethanol, each concentration for 20 minutes. Simultaneously, paraffin wax and a 1-to-1 solution of ethanol and paraffin wax was placed in a oven at 42°C until liquid. The samples were put in the 1-to-1 solution of ethanol and paraffin wax, then 100% paraffin wax for 1 hour each. The samples were then embedded in paraffin wax and allowed to cool.

Each sample was sectioned into approximately 10 micron sections on a microtome. Sections were placed on gelatin-coated microscope slides, then one drop of distilled water was added, allowing the sections to unroll and adhere to the slides. Sections were examined under a Zeiss V20 dissecting microscope.

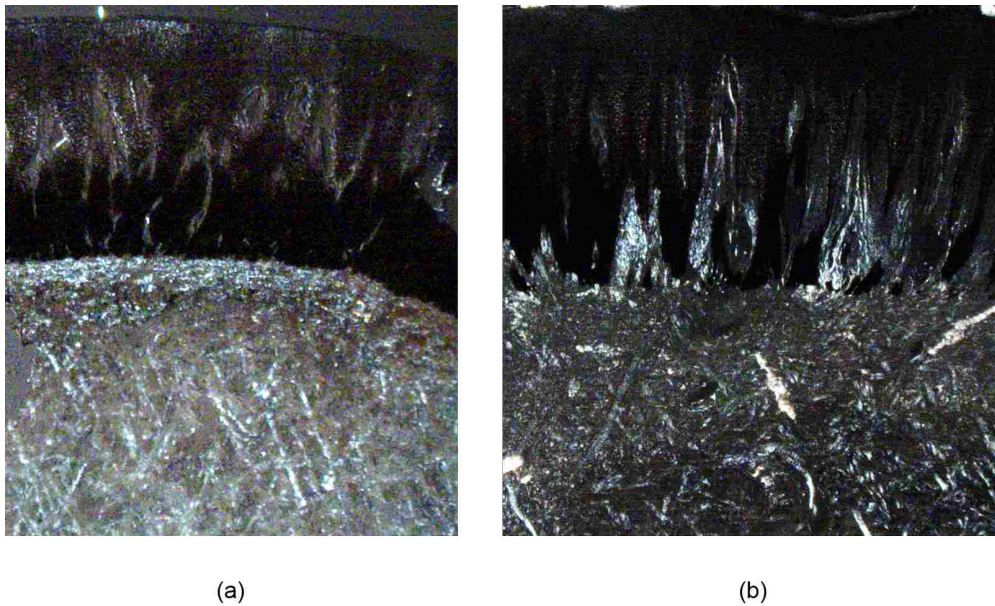


Figure 3.15: Microscope photographs of harbor porpoise (a), killer whale (b) skin and blubber layers under polarized light after being preserved in Paraffin wax, highlighting the difference in connection between skin and blubber layers of the two species.

### 3.7.3 Results

The collagen fibers of harbor porpoise and killer whale are easily visible in the blubber layer (Figure 3.14), but the seal sections did not fix in the paraffin wax as well and fell apart somewhat during sectioning. Though the harbor seal and killer whale have some similarities, the most striking difference is the connection between the skin and blubber (Figure 3.15), where the killer whale blubber layer appears to penetrate into the skin layer. This structure in the killer whale skin is visible without a microscope; another view of the structure without polarized light is presented in Figure 3.16.

## 3.8 Discussion

Additional material testing and examining the material using histology allows a fuller picture of the two tissues. Across this material testing, the comparison between harbor porpoise and

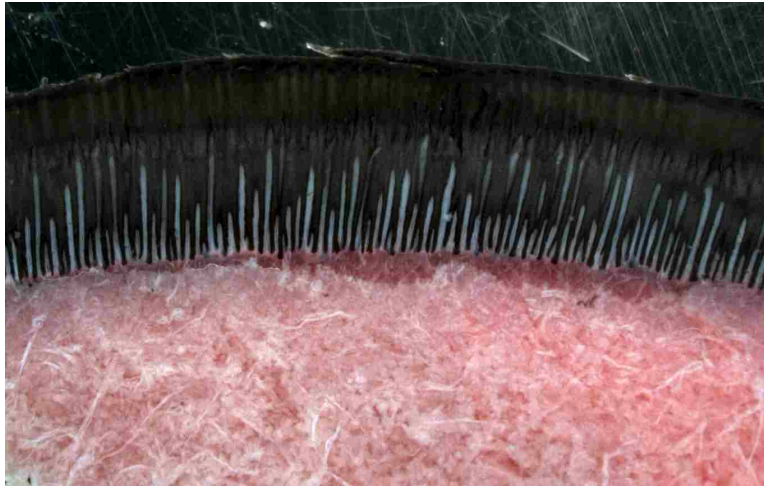


Figure 3.16: Structure of juvenile killer whale skin and blubber.

killer whale was more muddled than in tensile testing. While multivariate statistics from tensile testing indicated that harbor porpoise and killer whale skin were not significantly different, the bulk modulus results do not agree. The shear modulus results comparing these two species are similar, but the shear modulus testing may be less reliable. Still, rubber is often quite compliant in shear and strongly resistant to volume changes, so the high bulk modulus compared to shear modulus is not unreasonable. Reports of the ratio of bulk modulus to shear modulus in rubber can be similar to what was captured in this experiment, of about 500 times [33]. An additional limiting factor is that hyperelastic models, as are likely appropriate for blubber and perhaps skin, vary shear modulus as the material experiences more shear [63], which is a possible untested behavior present in marine mammal tissue.

Using a combination of material properties, the full behavior of the material can be recreated as a constitutive model. Comparing between toothed whale species will continue in the validation in Chapter 4, as the ultimate goal of relating species is creating few models and using a more common species to represent the material properties of a more rare one. With more material tests, it seems increasingly unlikely that harbor porpoise blubber is a potential surrogate material for killer whale blubber, where both compressive (Figure 3.2)

and tension (Figure 3.5) testing.

## Chapter 4

### VALIDATION OF MATERIAL MODEL

#### 4.1 Overview

Moving from material testing to creating a realistic computational material model required validating the computer model based on laboratory testing. Since the model cannot be validated using an actual collision between a turbine and marine mammal, another method was devised to confirm the model's effectiveness prior to modeling the tidal turbine strike.

To validate the model, a complex stress state is needed to ensure that the turbine strike injury will be well represented. Unlike the simpler tensile testing with each piece of tissue separated from the intact structure, testing the material using a spherical indentation test allowed a complex stress state with the composite structure undamaged. Similar methods have been used to validate a material model or testing method in hyperelastic synthetic gels and cartilage [58], nanoindentation of viscoplastic metals [51], as well as a method to understand analytical constitutive modeling [88].

The material validation was completed on harbor porpoise and killer whale, comparing these two toothed whale species to understand how similar the materials constitutive model can be to accurately represent each tissue. Though harbor porpoise blubber is not a likely analog for killer whale blubber, the skin is shown to be more similar. Harbor porpoise are a common species a potentially a good surrogate model for killer whales. Marine mammal research often use surrogate animals, including terrestrial animals like minks [31], captive animals, or representative species for different groups of marine mammals.

All modeling was completed in Abaqus 6.12, a commercial finite element analysis software, using Standard/Explicit models.

## 4.2 Methodology

### 4.2.1 Material Models

Material models were created based on the results of the blubber alone spherical indentation testing, as well as using input from the other material tests. Since a very different behavior was found in the tension and compression data, material models were created using both stress-strain curves. Examining a variety of material models allows an understanding of which models most accurately represent the laboratory result in a numerical model.

The most likely analog for these materials, aside from other biological materials, is rubber. Rubber is generally thought of as nearly incompressible, much like the tissues of the marine mammals discussed in this chapter, and many hyperelastic constitutive models have been developed to model rubber. With just a small load, the material can deform significantly then return to its original shape unchanged. Characterizing this large deformation without damage region is thus very important for characterizing injury in biological materials. While linear elastic material has stress that responds linearly with strain, the hyperelastic model can have more complex behavior. Hyperelastic models use the strain energy density to create a relationship between stress and strain.

Constitutive models were compared to these developed model using the hyperelastic constitutive laws and the test data derived in Chapter 3. In many cases, matching a constitutive law to test data resulted in an unstable material model. In other cases (like the Neo-Hookean model), the model did not match the input test data curve used to generate a hyperelastic constitutive model, so thus was not used. The models evaluated were the Polynomial, Reduced Polynomial, and Ogden Models. Comparing of hyperelastic models with test data was completed in Abaqus, using the “Evaluate material” module after entering in the test data. Evaluating the material fits each type of model to the test data, also detailing if the model could become unstable.

#### 4.2.1.1 Polynomial Hyperelastic Model

The full polynomial model defines the strain energy function,  $W$  as:

$$W = \sum_{i,j=0}^N C_{ij} (\bar{I}_1 - 3)^i (\bar{I}_2 - 3)^j + \sum_{i=1}^N \frac{1}{D_i} (J - 1)^{2i} \quad (4.1)$$

where  $C_{ij}$  are the material constants that can be determined from laboratory testing.  $D$  controls the compressibility of the material and can be zero if the material is fully incompressible.  $J$  is the elastic volume ratio and  $N$  is the number of terms in the energy function.

When  $N = 1$ , the polynomial hyperelastic model becomes the Mooney-Rivlin Model:

$$W = C_{01} (\bar{I}_2 - 3) + C_{10} (\bar{I}_1 - 3) + \frac{1}{D_i} (J - 1)^2 \quad (4.2)$$

It is interesting to note here that the initial shear modulus can be compared to the material constants. ‘Initial’ means that in this formulation, the shear modulus is not constant. For the Mooney-Rivlin Example, initial shear modulus  $G_0$  can be calculated as:

$$G_0 = 2(C_{10} + C_{01}) \quad (4.3)$$

After Abaqus fits this formulation to the spherical indentation test data, the shear modulus computed can be compared to the laboratory test for further confirmation of the validation.

#### 4.2.1.2 Reduced Polynomial Hyperelastic Model

The reduced polynomial is based on the full polynomial, but removes  $I_2$ .

$$W = \sum_{i,j=0}^N C_{ij} (\bar{I}_1 - 3)^i + \sum_{i=1}^N \frac{1}{D_i} (J - 1)^{2i} \quad (4.4)$$

When  $N = 1$ , the reduced polynomial hyperelastic model becomes the Neo-Hookean



Model, which is the simplest of the suite of typical hyperelastic models.

$$W = C_{10}(\bar{I}_1 - 3) + \frac{1}{D_i}(J - 1)^2 \quad (4.5)$$

In the Neo-Hookean model, the initial shear and bulk modulus can also be calculated, with shear modulus as:

$$G_0 = 2C_{10} \quad (4.6)$$

The initial bulk modulus can be computed as:

$$K_0 = \frac{2}{D_1} \quad (4.7)$$

This again lends an opportunity to use the shear and bulk modulus values tested in the laboratory to validate and inform the hyperelastic validation models.

#### 4.2.1.3 Ogden Hyperelastic Model

The Ogden model is based on principal stretches as opposed to the invariants that the other models have been based. This model defines strain energy as:

$$W = \sum_{i=1}^N \frac{\mu_i}{\alpha_i^2} (\lambda_1^{\alpha_i} + \lambda_2^{\alpha_i} + \lambda_3^{\alpha_i} - 3) + \sum_{i=1}^N \frac{1}{D_i} (J - 1)^{2i} \quad (4.8)$$

Where the principal stretches are  $\lambda_1$ ,  $\lambda_2$  and  $\lambda_3$ . If the material is assumed to be incompressible, the  $D_I$  term can be removed, as that term represents the volumetric change in strain energy.

#### 4.2.2 Blubber Linear Elastic Models

An assumption of linear elastic behavior is the simplest choice for modeling. Values from both spherical indentation and tensile testing were used. With the spherical indentation test,

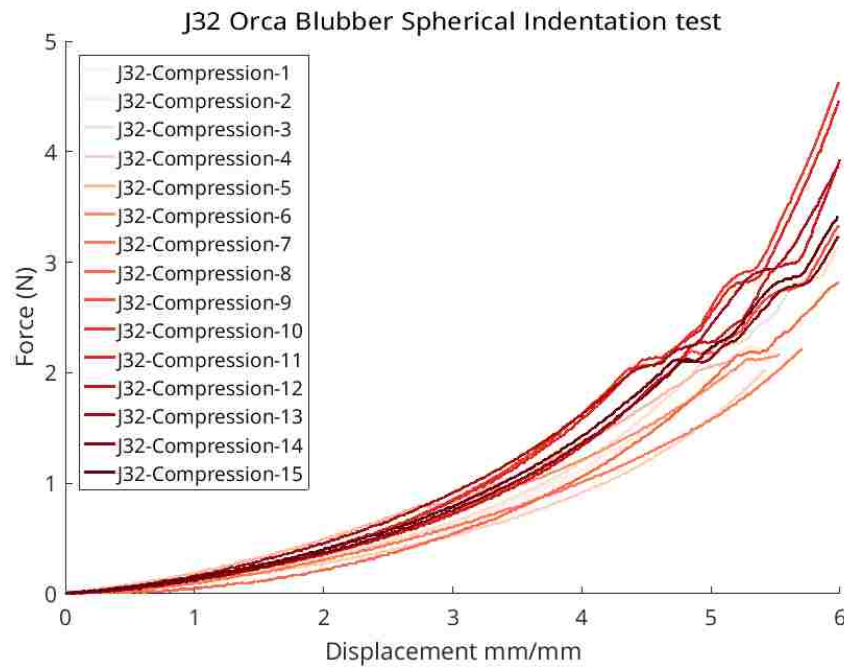


Figure 4.1: Force–displacement curve for all blubber only spherical indentation tests

a single elastic modulus value can be determined, as shown in Table 3.1. Since the blubber was not as variable as skin under uniaxial tensile testing (and the tensile values were likely incorrect), an average tensile elastic modulus was used to test this material model.

#### 4.2.3 Blubber Hyperelastic Models

To model blubber as a hyperelastic material, an iterative process was used to determine the best model. After processing the raw blubber only spherical indentation testing as described in Chapter 3, representative stress strain curves were chosen. For the killer whale, the raw force-displacement curves can be seen in Figure 4.1. The first curve chosen to represent the data was an average choice, which was Trial 9. On this curve, a cubic equation was fit using 20 points and that curve was input to Abaqus (Figure 4.2).

Using that input, the Abaqus material evaluation software was used to create multiple hyperelastic models. Though all the models mentioned above were evaluated for Trial 9, the

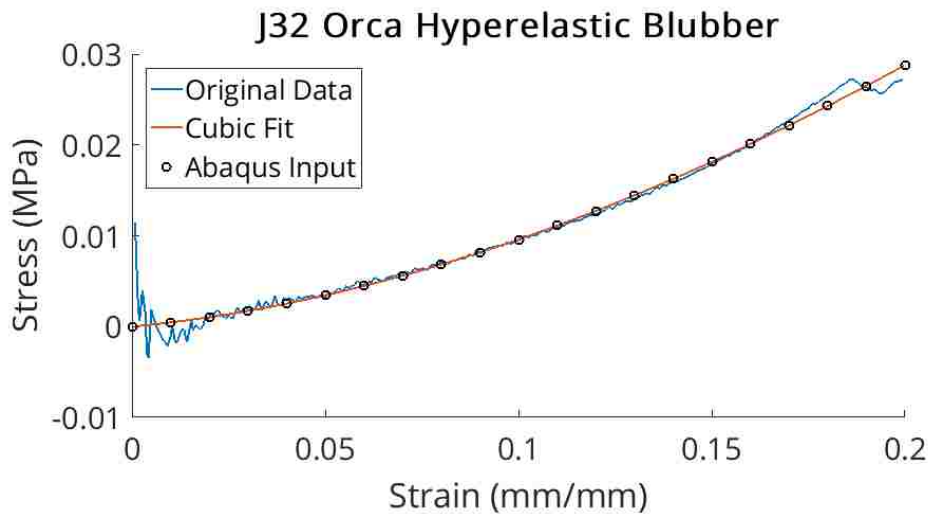


Figure 4.2: A typical compression curve for blubber is shown in blue. A cubic fit was fit to this data, then a few points were taken on this curve as an input to the Abaqus hyperelastic models. Note that this was modeled in Abaqus as compressive data and thus as negative stress and strain. The oscillations at the beginning come from an artifact of dividing by zero (or very close to zero) in converting the data from force-displacement to stress-strain.

reduced polynomial with  $N = 1$ , reduced polynomial with  $N = 2$ , and the Ogden model with  $N = 3$  were chosen based on their stability over the necessary strains.

These models were tested using the blubber only model of the spherical indentation test, as described further in the Abaqus setup portion of these methods. When Trial 9 did not provide adequate results, other methods were chosen. The reduced polynomial with  $N = 2$  model seemed to be the most effective at capture the same curve in the force-displacement data and also had the benefit of being very stable. Another method attempted was averaging all the curves to create ABAQUS input data, but this method tended to provide less stable input data and choosing an individual trial gave better results. It is also possible that averaging the data gave unrealistic data as input.

Based on the killer whale hyperelastic blubber modeling, the harbor porpoise methods were refined. A middle trial was chosen, as opposed to looking at average material properties for the indentation test. Linear elastic and tension testing models were not evaluated for

this species.

#### 4.2.4 *Skin Linear Elastic Models*

Again for skin, modeling the material as linear elastic was desirable as it is the simplest choice. Due to the large variation in skin tensile testing for killer whale, a range of tensile testing values was used to model the skin. The skin was parameterized into high, middle, and low values, corresponding to those found in Table 4.1. This model assumed an isotropic skin and blubber model since there was not a definitive trend in orientation. When modeling the blubber as linear elastic with compression values, I used an average elastic modulus from Table 3.1.

#### 4.2.5 *Skin Hyperelastic Models*

Skin was modeled using a hyperelastic model of its tensile behaviors. To ensure reasonable behavior near zero, a fifth-order polynomial was fit to the curve, forcing a (0,0) intercept to a typical stress strain curve for orca skin. Points on this curve were chosen as input to the Abaqus hyperelastic model evaluation software. The best model for skin was the Ogden formulation.

Finally, the chosen killer whale skin was modeled over the harbor porpoise blubber and compared to the harbor porpoise skin and blubber spherical indentation raw data, allowing comparison across species.

#### 4.2.6 *Abaqus Setup*

The blubber material models were first tested on a blubber-only model of the spherical indentation test. As in the actual laboratory test, the block of blubber was 2.6 cm tall, with a width of 9.5 cm and length of 8 cm. The block of blubber, resting on a rigid plate, was subjected to a gravity load initially and then the indentation test began with a 12.7 mm (0.5 inch) ball pushing into the block. The block had mesh concentrated in the center of the

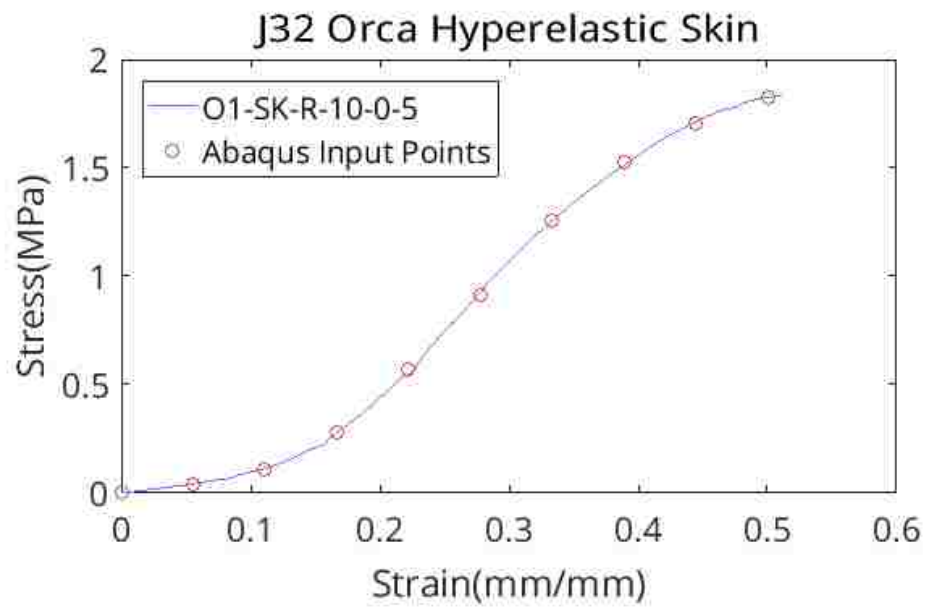


Figure 4.3: A typical tensile curve for skin is shown in purple. A fifth order polynomial was fit to this tension testing data (Rectangular sections, tested at 10 mm/s, cut at 0°, per the convention highlighted in Chapter 2), then a few points were taken on this curve as an input to the Abaqus hyperelastic models.

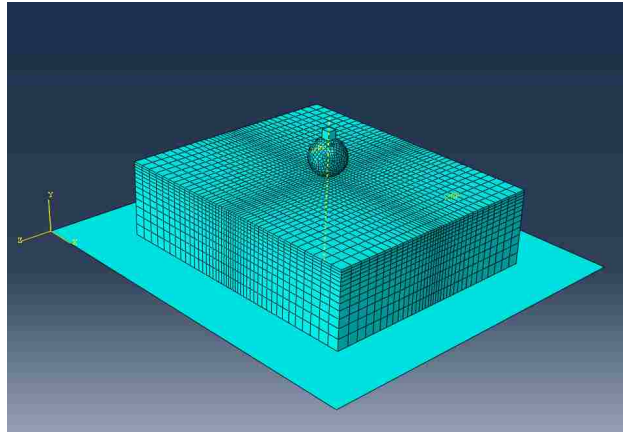


Figure 4.4: Abaqus model of the killer whale compressive test for blubber only tests. Mesh is concentrated in center of block, with a rigid plate and sphere to represent the rest of the test. A block with mass is place on top of the sphere to determine the reaction force on the sphere.

tissue and the top of the tissue, with seeds applied to the edges of the block. For the sides of the tissue, the seeds were double biased with a minimum size of 0.001 and maximum size of 0.004 (units in meters).

This block of tissue has C3D8R elements, an 8-node linear brick with reduced integration. After the gravity load is applied, a rigid shell sphere pushes down on the tissue, mimicking the laboratory test. Since the sphere is rigid, a cube on top of the sphere was used to compute the reaction force from the tissue applied to the sphere. The cube is tied to the location on the sphere where the MTS Synergie records force (Figure 4.4). Between the sphere and top of tissue, there is surface-to-surface contact with a frictional coefficient of 0.15.

In addition to the blubber only testing, the output of the composite indentation testing was used as a validation tool. For the killer whale, a skin thickness of 4 mm was used for a total thickness of 45.05 mm. The blubber and skin are tied together and do not have any other contact properties between them. The spherical indenter was modeled as a rigid shell. Similar to the the blubber only model, fixed to the top of the sphere was a single element where the displacement is applied; the reaction force from the composite material

is computed here as well. The entire system rests upon a rigid fixed plate (Figure 4.5).

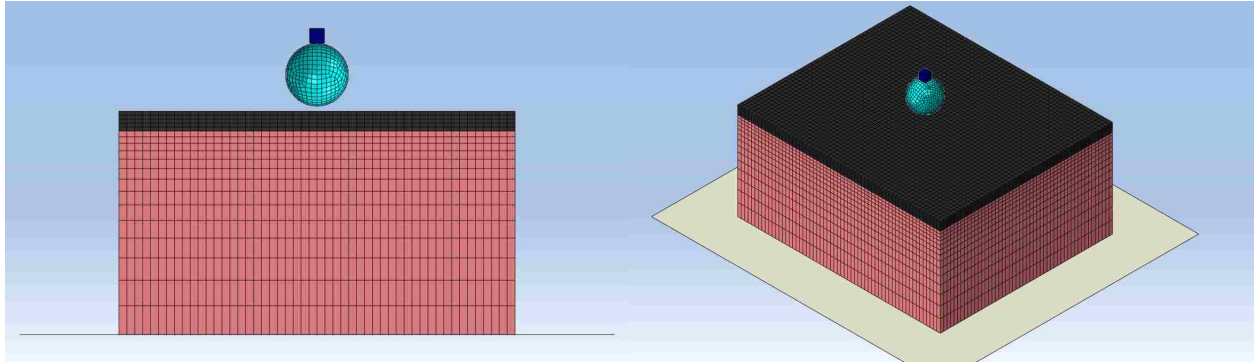


Figure 4.5: Abaqus model of the killer whale compressive test in two views. Black is skin, pink is blubber, teal is the indentation ball. The indenting ball is modeled as a rigid sphere.

#### 4.2.7 Material Models Tested

A complete description of the material models created and tested can be found in Table 4.1 and Table 4.2.

### 4.3 Results

#### 4.3.1 Blubber Only Material Modeling

The first blubber material tested was based on the blubber-only laboratory test, Trial 9. This test was chosen as the middle of all killer whale spherical indentation tests completed. Using Abaqus's material evaluation software, multiple hyperelastic models were chosen to represent this curve's data numerically (Figure 4.6), with the exact coefficients in Table 4.1.

Trial 9 testing revealed that this specimen did not give the expected behavior. Trial 2 was chosen to represent a lower bound of the data. The range of the data set, including Trial 2 can be seen in Figure 4.1, but the processed stress-strain curve was used to determine the Abaqus input, as shown in the example in Figure 4.2. The average tests generally did not give good results either, perhaps because averaging led to unrealistic input data.

Table 4.1: For the killer whale skin and blubber, many hyperelastic models were evaluated to determine which best matched the spherical indentation test. In addition, the coefficients calculated here can be compared to shear and bulk modulus testing to further validate the models.

<b>Blubber</b>		
Material model	Input Data	Coefficients
Linear Elastic	Tension Data Average	$E = 3.03$ MPa
Linear Elastic	Indentation Data Average	$E = 0.084$ MPa
Neo-Hookean	Indentation Trial 9	$C_{10} = 12087.384, D_1 = 5.065 \times 10^{-6}$
Reduced Polynomial N=2	Indentation Trial 9	$C_{10} = 9616.939, C_{20} = 43912.476, D_1 = 6.366 \times 10^{-6}$
Ogden N=1	Indentation Trial 9	$\mu_1 = 18224.592, \alpha_1 = -8.287, D_1 = 6.719 \times 10^{-6}$
Reduced Polynomial N=2	Indentation Data Average	$C_{10} = 18189.817, C_{20} = -1436.637, D_1 = 3.366 \times 10^{-6}$
Ogden N=1	Indentation Data Average	$\mu_1 = 39254.070, \alpha_1 = 9.476, D_1 = 3.119 \times 10^{-6}$
Mooney-Rivlin	Indentation Data Average	$C_{10} = 14450.388, C_{01} = 2972.902, D_1 = 3.514 \times 10^{-6}$
Neo-Hookean	Indentation Data Average	$C_{10} = 18049.190, D_1 = 3.392 \times 10^{-6}$
Reduced Polynomial N=2	Indentation Trial 2	$C_{10} = 9608.15, C_{20} = 43968.5, D_1 = 6.372 \times 10^{-6}$
Ogden N=1	Indentation Trial 3	$\mu_1 = 7856.279, \alpha_1 = -14.125, D_1 = 1.559 \times 10^{-5}$
Reduced Polynomial N=2	Indentation Trial 3	$C_{10} = 3852.552, C_{20} = 59482.216, D_1 = 1.589 \times 10^{-5}$
<b>Skin</b>		
Material Model	Input Data	
Ogden N=1	Tensile J32.R.10.0.5	$\mu_1 = 2842243.64, \alpha_1 = 10.407, D_1 = 4.308 \times 10^{-8}$
Ogden N=1	Tensile J32.R.10.0.3	$\mu_1 = 2435.745, \alpha_1 = 20.005, D_1 = 5.024 \times 10^{-5}$
Linear Elastic	Low Tension Data	$E = 3$
Linear Elastic	Middle Tension Data Value	$E = 5$ MPa
Linear Elastic	High Tension Data Value	$E = 9$ MPa



Table 4.2: For the harbor porpoise blubber, hyperelastic models were evaluated to determine which best matched the spherical indentation test. In addition, the coefficients calculated here can be compared to shear and bulk modulus testing to further validate the models.

<b>Blubber</b>		
Material model	Input Data	Coefficients
Ogden N=1	Indentation Trial 2	$\mu_1 = 3212.278, \alpha_1 = -16.040, D_1 = 3.812 \times 10^{-5}$
Ogden N=2	Indentation Trial 2	$\mu_1 = 5021.276, \mu_2 = 557.703, \alpha_1 = -14.2450, \alpha_2 = -25, D_1 = 2.195 \times 10^{-5}$
Reduced Polynomial N=2	Indentation Trial 2	$C_{10} = 215.604, C_{20} = 20768.392, D_1 = 2.840 \times 10^{-5}$

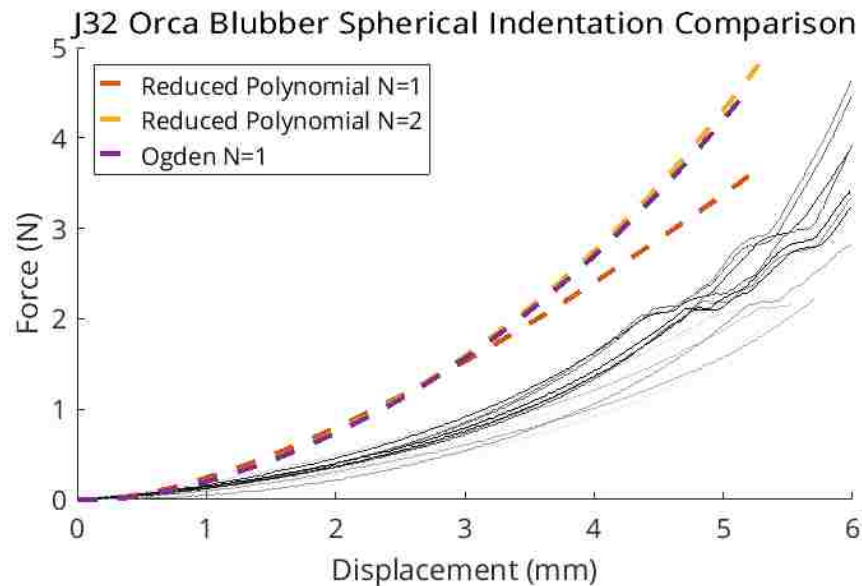


Figure 4.6: Spherical indentation raw data tests are shown in gray, with material model results in dotted line for Trial 9 of the J32 killer whale data.

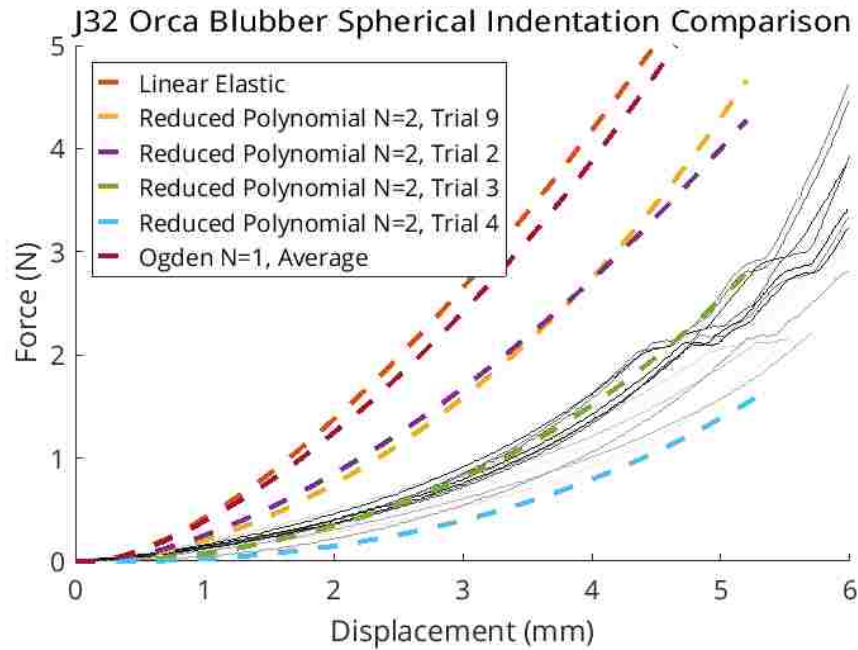


Figure 4.7: Spherical indentation raw data tests are shown in gray, with material model results in dotted line for multiple material models tested for the J32 killer whale data. Exact material coefficients can be found in Table 4.1.

Trial 2 expectedly gave a lower than appropriate force-displacement curve. The Trial 4 Reduced Polynomial with  $N=2$  gave a reasonable result and that model was carried into validating the complete skin with blubber model (Figure 4.7).

Using what was learned from the killer whale testing, the harbor porpoise validation converged much quicker (Figure 4.8). This model does not, however, successfully represent any of the killer whale data, even the lower values, suggesting that blubber cannot be modeled similarly across these two species, as expected from the multivariate testing in Chapter 2.

#### 4.3.2 Skin and Blubber Material Modeling

By completing blubber-only analysis first, the skin could be focused on more fully in the composite material validation, but the blubber material was still parametrized to see if the same tests were the preferred modeling choice across both validations.

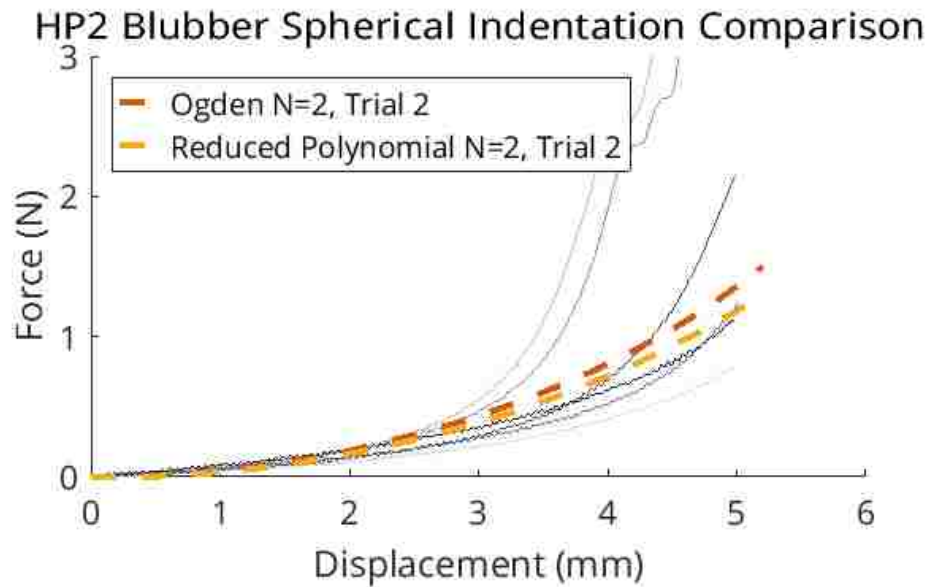


Figure 4.8: Spherical indentation raw data tests are shown in gray, with material model results in dotted line for multiple material models tested for the HP2 Harbor Porpoise data. Exact material coefficients can be found in Table 4.2.

In modeling the spherical indentation test, one important observation is the regions of the material in tension and in compression. As the sphere pushes into the material, the skin acts as a membrane and is primarily in tension. The blubber however is shown to be in compression. Similar to the blubber only results, when simple linear elastic models of the blubber in tension are used, no agreement is seen between the numerical and experimental results (Figure 4.9). This is an important finding, as this is how the material was modeled in the original PNNL report. However, a simple linear elastic model of blubber using the compressive elastic modulus begins to match the laboratory results (Figure 4.10). A hyperelastic model of the blubber further matches the compression test, as the force-displacement curve has a more distinct curved shape.

The skin models impacted the model fit as well as the blubber. Using the determined blubber material model from the blubber-only testing, a more targeted approach was used to determine the best skin behavior. Untangling whether a lower modulus or hyperelastic

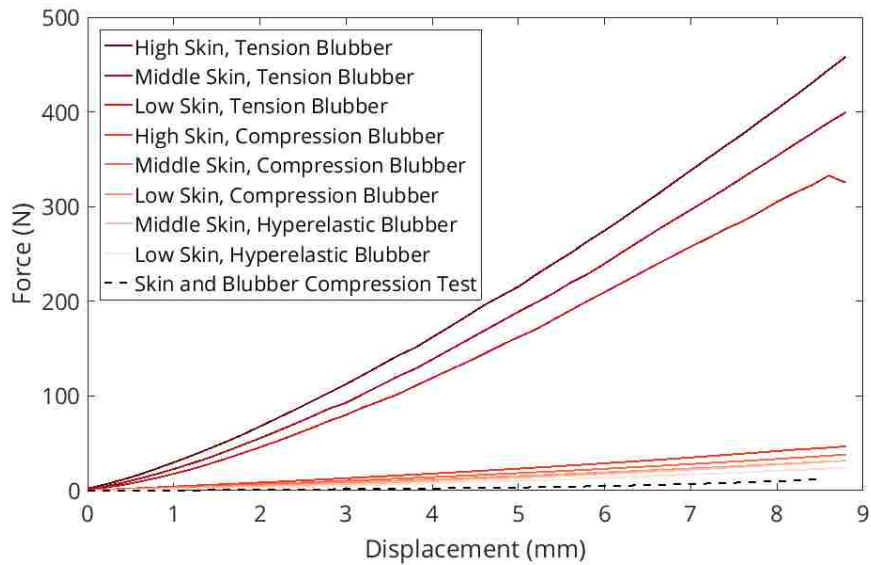


Figure 4.9: Compilation of material models to validate composite behavior of materials. Laboratory data shown in black dashed line. In this case, tension blubber refers to a linear elastic model of the blubber with tension data, compression blubber refers to a linear elastic model applying spherical indentation data, and hyperelastic blubber refers to a hyperelastic model determined from the compression data Trial 9

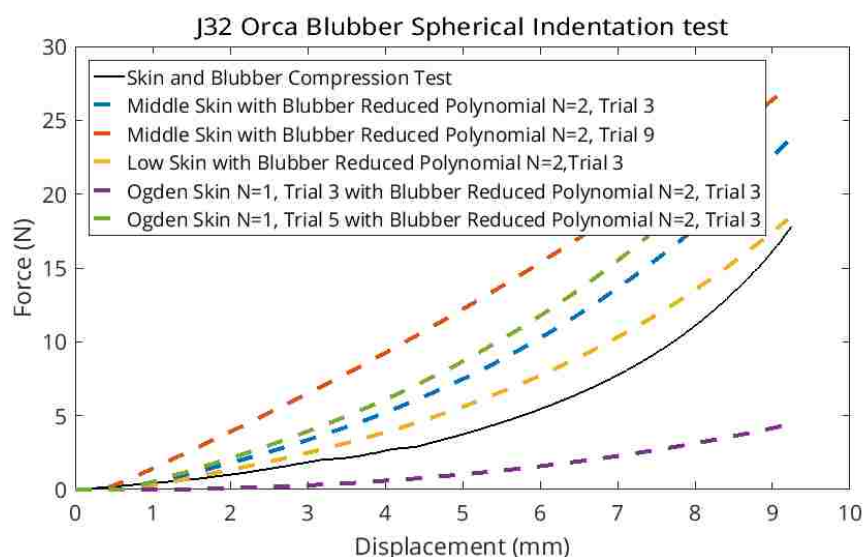


Figure 4.10: Compilation of material models highlighting only those using compressive values for blubber. Force displacement curve from laboratory data shown in black line.

material was a better approach for matching the data was difficult. Averaging all trials for the J32 Orca in tension gives an average elastic modulus of 6.06 MPa. Trial 3 (O1-SK-R-10-0-3,  $E = 5.14$  MPa) and Trial 5 (O1-SK-R-10-0-5  $E=6.43$ ) are well representative of that data.

#### 4.3.3 Shear and Bulk Modulus Comparison

The testing of shear and bulk modulus completed in Chapter 3 can aid in better understanding the validated model. With the skin data, where the model was hard to decide if a linear elastic or hyperelastic was more appropriate, adding these additional parameters could be helpful. As described in Equation 4.6 and 4.7, the measured quantities can be used to evaluate the model fit. Alternatively, models generated by the shear and bulk modulus values could be compared to the results generated from other skin or blubber testing.

For skin, the linear elastic models were compared to the hyperelastic models. The bulk

Table 4.3: For each model created, a bulk modulus and shear modulus can be calculated. In the case of the Ogden model, these are the appropriate values for small strains and the values change as strain increases.

Model	Trial	Bulk Equation	Calculated Bulk Modulus (MPa)	Shear Equation	Calculated Shear Modulus (MPa)
Ogden	3	$K = \frac{2}{D_1}$	0.04	$G = \mu_1$	0.0024
Ogden	5	$K = \frac{2}{D_1}$	46.43	$G = \mu_1$	2.84
Linear Elastic	Low	$K = \frac{E}{3(1-2\nu)}$	16.67	$G = \frac{E}{2(1+\nu)}$	1.02
Linear Elastic	Middle	$K = \frac{E}{3(1-2\nu)}$	27.78	$G = \frac{E}{2(1+\nu)}$	1.70

modulus for a linear elastic material can be computed from the equation:

$$K = \frac{E}{3(1 - 2\nu)} \quad (4.9)$$

where  $\nu$  is the Poisson's ratio,  $K$  is bulk modulus, and  $E$  is elastic modulus.

The shear modulus ( $G$ ) can be calculated from the equation:

$$G = \frac{E}{2(1 + \nu)} \text{ or } G = \frac{3KE}{9K - E} \quad (4.10)$$

The Poisson's ratio is somewhat unknown, but was measured for L112 killer whale skin as 0.47 in the PNNL report, which is used to calculate the bulk and shear modulus assumed in each model (Table 4.3). For killer whale skin, a bulk modulus of 56.85 MPa was measured and a shear modulus of 0.14 MPa. As discussed in Chapter 3, the shear modulus measured seems to be an anomaly, where perhaps the test set up did not successfully capture the behavior of the material. Rubber is reported as having a shear modulus of 0.3 MPa, a value that is repeated and used throughout the literature and even textbooks, so this value is not implausible.

A final skin model was created using the values for bulk modulus and shear modulus. Using a bulk modulus of 56.85 MPa and a shear modulus value of 0.14 MPa gives  $\mu_1 =$

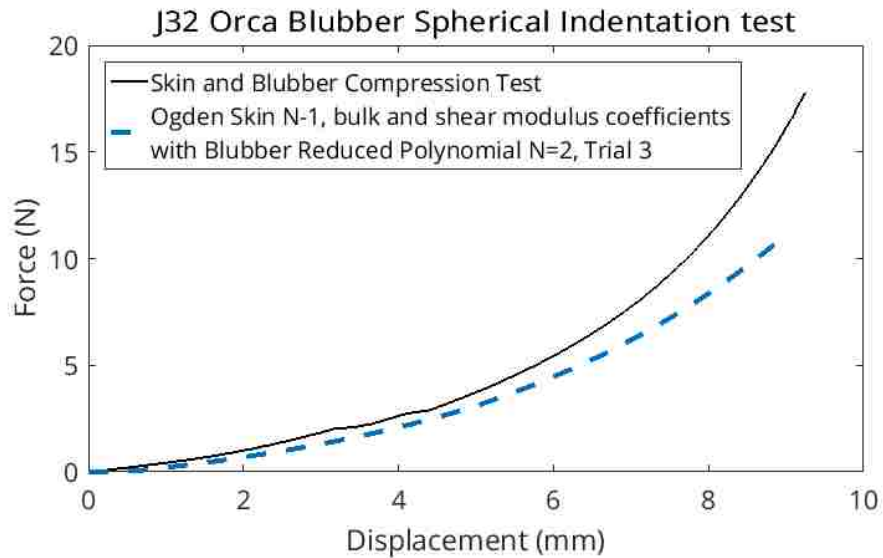


Figure 4.11: Compilation of bulk and shear modulus generated skin model to validate composite behavior of killer whale tissue. Laboratory data shown in black line.

140000 (units in Abaqus are in Pascals) and  $D_1 = 3.57 \times 10^{-8}$ . This model gives a fairly accurate representation of the laboratory data (Figure 4.11), better than any other model generated.

## Chapter 5

# PARAMETERIZATION OF MATERIAL PROPERTIES FOR FINITE ELEMENT ANALYSIS

### 5.1 Overview

This section focuses on the large natural variability of the tissue that was tested. An important question to answer before delving into a very specific and rigorous material model is determining how much the variation of this material model impacts the result. How much does the potential injured tissue change with different sets of material properties?

This variability is seen particularly in the adult killer whale tested in tension (Chapter 2). Material properties for the following analysis were taken from two orca samples, L112 and J32, with the neonate orca providing additional context. L112, a three-year old juvenile orca, was notoriously degraded when it stranded, and was frozen for more than a year before testing (Figure 5.1). This analysis aided in evaluating whether L112 was too degraded to use. Both killer whales were tested exclusively after being frozen.



Figure 5.1: L112 orca washed up in Long Beach, WA. February 12th, 2012. Photo by Cascadia Research.



The three datasets of SRKW skin and blubber (an eighteen year old adult, a three year old juvenile specimen and a neonate) showed different patterns. It is unknown whether the differences in patterns are based on the development of the animal or the degraded nature of the juvenile tissue, but Chapter 2 did show that there exists considerable variation in harbor seal and harbor porpoise data amongst the freshest of specimens. The 2014 PNNL report that this work primarily builds off of noted the high variability in the L112 data, which was the only data available at that time [15].

Each set of tensile testing data contained a small number of samples; the original size of the material obtained for testing was the limiting factor. Limited sample sizes produced a wide variability in each set. For example, with just 8 samples of blubber and skin for L112, the skin and blubber elastic modulus results are not statistically different (Welch's t-test, p-value = 0.19, Figure 5.2-5.3), even though the properties observed under the microscope (Figure 1.1) seemed to be different. Further samples were more limited by the amount of tests that can be completed while the tissue is still 'fresh' (within 48 hours of retrieval). Every other marine mammal had a significant difference between skin and blubber, making L112 perhaps an outlier. When comparing the two sets of stress strain curves for the blubber and skin, the two sets of data have a similar peak stress, but the blubber has a less defined plastic region of the curve (Figure 5.4). In the case of the J32 and L112 data, the skin shows a higher strain to failure than the blubber, unlike what was predicted based on other mammals. In the case of L112, the blubber has a higher variability than the skin (Figure 5.3). For each set of data, the statistical power was low; thus, many material properties were considered to bound the results of this chapter.

A second focus is once again understanding how each animal's specific adaptations change the possibility of injury. Using average results across the four species tests, while keeping geometry constant allows exploration of how the combined material properties interact to protect the animal. The composite nature of marine mammal skin adds complexity to understanding the function of skin, but the collective behavior can be modeled with a finite element method approach based on material properties of each layer. Marine mammals

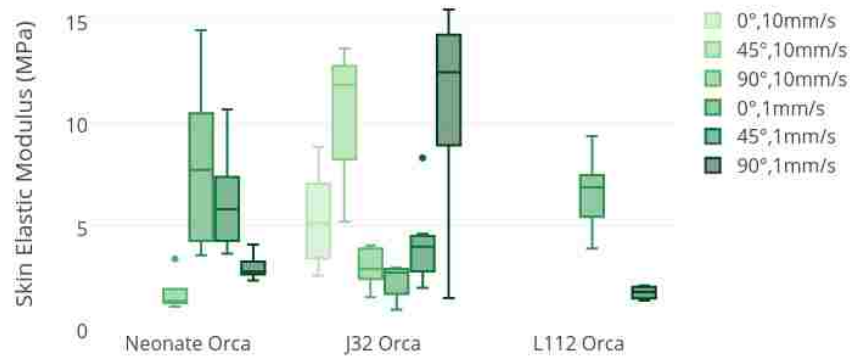


Figure 5.2: Three orca specimens have a similar range in their elastic modulus skin values.

experience many physical stresses on their body. One such stress is the natural tension in the body, which changes dynamically with movement, like swimming. A penetrating load is another common encounter, through predation or hitting with manmade objects. These normal events can be modeled and compared across species. Though individual layers of tissue may be similar between species, the combination or geometry particular to each species can be examined using individualized models.

## 5.2 Parameterization of L112 and J32

### 5.2.1 Methodology

#### 5.2.1.1 Tissue Material Properties

The material properties used in this setup are based on tensile testing completed in 2013 on L112 and 2015 on J32 (Table 5.1). Because 1 mm/s data 0° and 90° was used for L112, the same data is used on J32, though examining all speeds for J32 shows that this data, especially the 90° was higher than the total average used for validation in Chapter 4. The material properties used allow comparison of how parameterizing the materials impact the

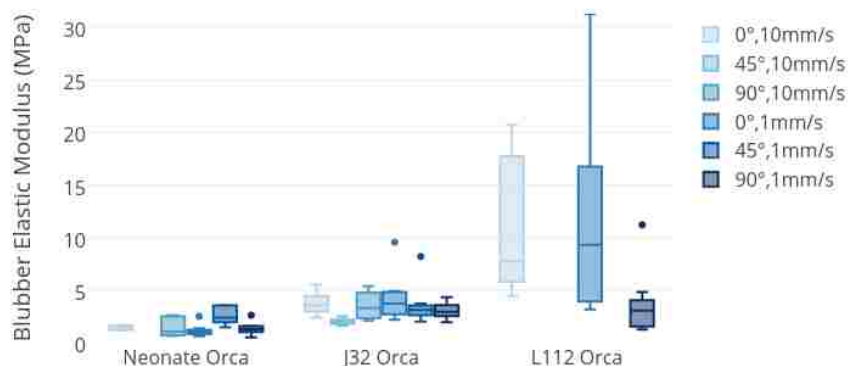


Figure 5.3: Elastic modulus values of orca blubber in tension. L112, a whale observed to be more degraded than other sections, shows a much different blubber pattern.

results.

#### 5.2.1.2 Finite Element Model Setup

A finite element model was created using the commercial solver Abaqus. A series of finite element analyses using the range of L112 and J32 material properties was developed. Both animal's data were used to model the variability in impact response due to skin and blubber material parameter uncertainty. A parametric study was set up, where 9 runs were tested using high, low, and average values for the skin and blubber elastic modulus (Table 5.1). For the blubber, there was one very high outlier (Figure 5.3), and in that case the second highest value was used.

A NACA 0015 airfoil geometry was used to model the blade as a general stand-in for a typical turbine blade. The blade is based on a 6 meter diameter turbine, similar to that modeled in the PNNL report [15]. The width of the blade is modeled as 10% of the blade's length. The blade's material properties were modeled as steel for simplicity (Table 5.2), with

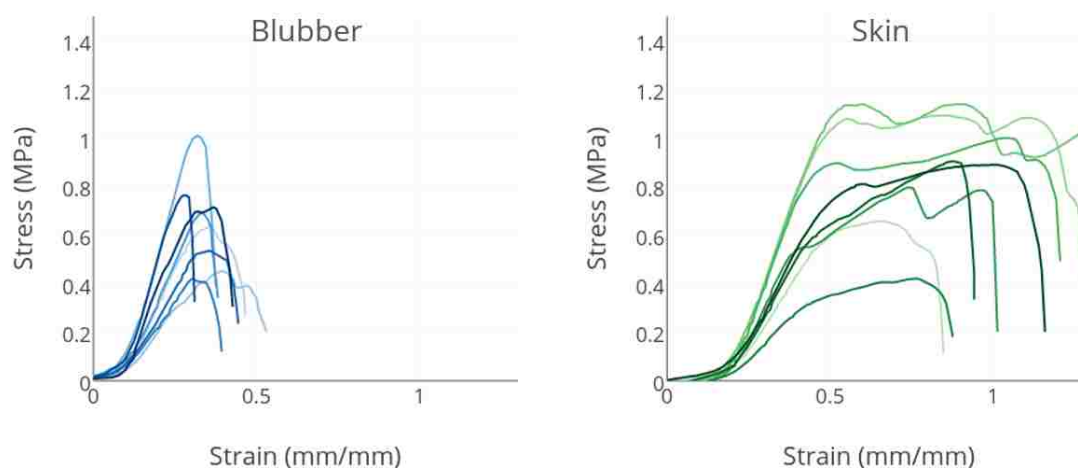


Figure 5.4: Stress-strain curves for rectangular shaped tissue specimens from the J32 Orca tested at a 10 mm/s test speed. Blubber stress-strain curve shows a lower strain to failure and less defined plastic region.

linear elastic material properties.

A cylinder was used as a simplified model of the animal (Figure 5.5), based on the girth of an average-sized SRKW, at 90 cm in diameter. The skin thickness in the circular model is the average of the juvenile SRKW skin sample thicknesses. The density of the whale was modeled as  $1000 \text{ kg/m}^3$  for simplicity. Literature data shows that other marine mammals' skin and blubber have a similar range, with harp seal blubber at  $920 \pm 10 \text{ kg/m}^3$  [9], skin for a bottlenose dolphin at  $969 \pm 25 \text{ kg/m}^3$  [50], and skin for a manatee at  $1,121 \pm 42 \text{ kg/m}^3$  [50]. Poisson's ratio was input as 0.47 for both blubber and skin based on extensometer testing on the neonate skin.

For both parts, the whale and the blade, the finite element model was created with C3D8R elements. Mesh was concentrated in the center and top of the cylinder where the blade hits (Figure 5.5).

Table 5.1: SRKW Juvenile (L112) and Adult (J32) skin and blubber elastic modulus properties used in ABAQUS modeling. These values were based on the 1 mm/s data because that is what was used in the PNNL modeling. L112's degraded tissue make it's material properties less credible, but the 90°, 1 mm/s test for J32 is also the most variable of any test (Figure 5.2)

	L112			J32			
	Tensile Stiffness (MPa)			Tensile Stiffness (MPa)			
	Low	Average	High	Low	Average	High	
Skin	3.9	6.6	9.36	Skin	10.51	13.26	15.53
Blubber	3.16	11.8	17.94	Blubber	1.93	3.03	4.32

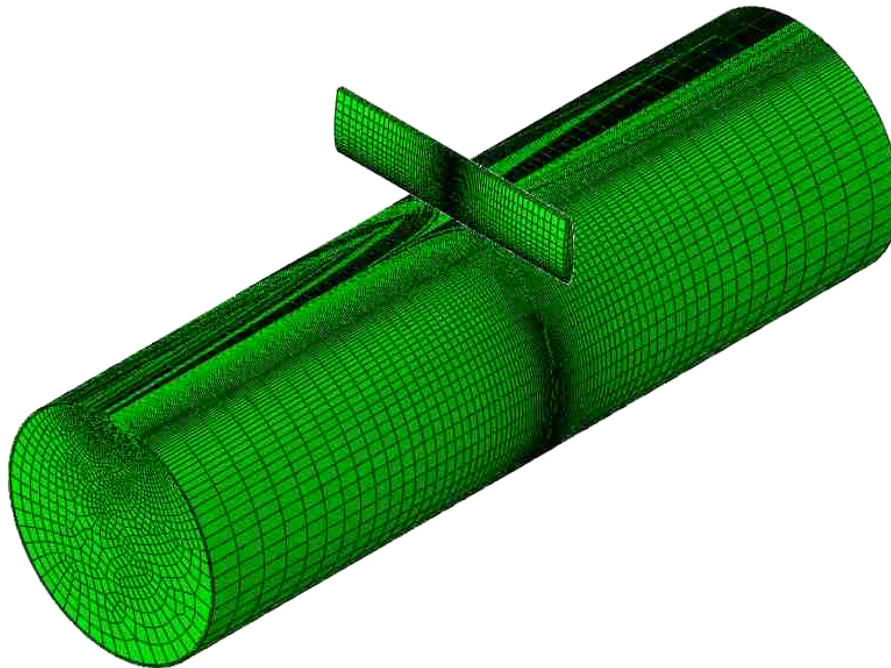


Figure 5.5: Geometry of each model run.

Table 5.2: Skin, Blubber, and Steel material properties used in ABAQUS modeling.

	Density (kg/m <sup>3</sup> )	Poisson's Ratio	Elastic Modulus
Blubber	1000	0.47	<i>see Table 5.1</i>
Skin	1000	0.47	<i>see Table 5.1</i>
Blade	7750	0.3	200 GPa

### 5.2.1.3 Model Evaluation

To understand the results of the model, the areas of the geometry where the skin and blubber had exceeded their tensile strength were evaluated, as measured by the tensile testing described in Chapter 2. The parametric study was run for each of the 9 cases, for both L112 and J32. The average skin-average blubber was the baseline for this study. Von Mises Stress was calculated on the top center element of the whale skin model, directly under the blade; displacement was calculated on the corresponding node. The node and element represent the maximum stress and displacement present in the whale model in the center of the model, directly under the center of the blade.

### 5.2.2 Finite Element Model Results

The parameterization and data from two different whales have a large impact on the results of the model run. The average skin, average blubber run for L112 shows a potential for damage to the skin. As shown in Figure 5.6a, the maximum stress in the skin exceeds the average tensile strength of 2.23 MPa. In Figure 5.6b, the gradual increase in displacement seen after the initial impact results from the whale translating downward after the blade impact. The mass of the whale then slows the motion of the blade, as the blade has only initial velocity forces on it. Thus, the critical displacement and corresponding stress corresponds to the peak values shown at approximately time  $t = 0.025$  seconds.

When the blubber is kept at the lowest value, but the skin is varied, much more variable results for L112 are found. The lowest elastic modulus value for L112 blubber is twice as high, while the L112 skin is generally half as stiff as its J32 counterpart. Due to a lower ratio between the skin and blubber, L112's blubber is forced to bear a larger part of the force (Figure 5.7)

The idea of how the difference in material properties impacts the results of the model can be explored further by examining the extent of the injury potentially incurred by the animal. For L112, the maximum stress of skin is 2.23 MPa, the experimentally observed

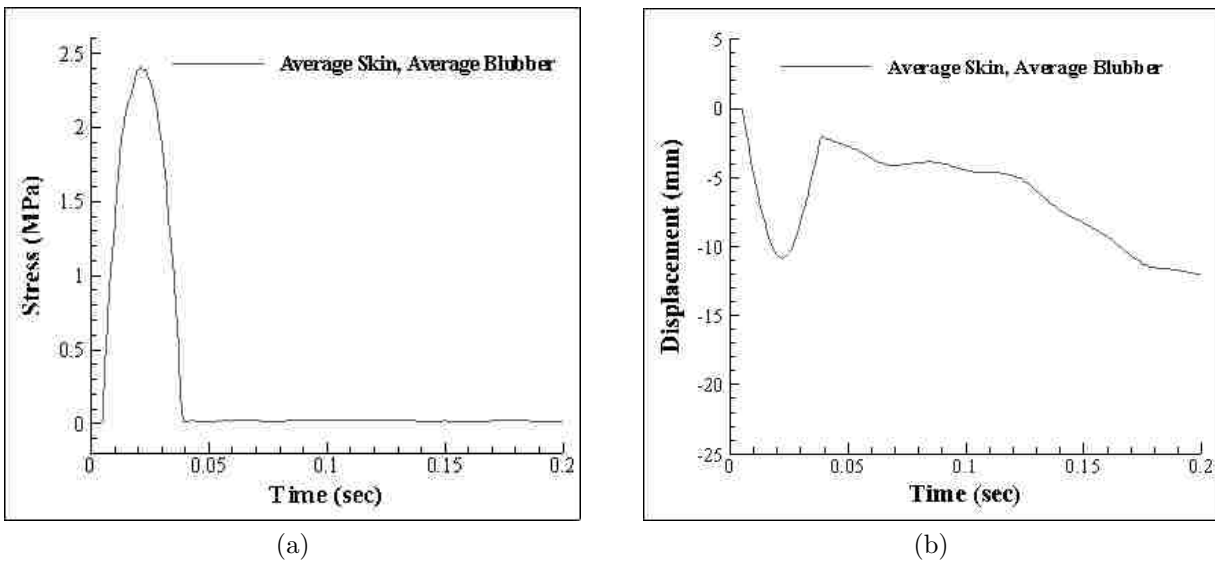


Figure 5.6: Stress (a) and displacement (b) in juvenile orca skin directly under the blade is shown for a model run using average skin elastic modulus values and average blubber values.

tensile strength of the skin. With low blubber, this suggests that in these scenarios, the animal not only incur damage to the skin. For J32, the maximum tensile strength is 2.79 MPa, leading us to observe potential damage across all tests with low blubber. However, the location of the maximum stress is at the interface between the blubber and skin, indicating the skin would likely not fail at the surface.

For L112, the skin and blubber are much closer together, which means that the skin does not act as a protective mechanism in the predicted way. Further, when the skin does not act as a protective layer, a very high stress in both skin and blubber is present, as is seen in the L112 case of high skin (9.36 MPa) and high blubber (17.94 MPa) (Figure 5.8b and Figure 5.8d). In this case, the skin no longer acts in tension above the stretchier layers below. It is more likely to be injured before the blubber, unlike what is typically expected where the blubber is more likely to break before the skin, causing a bruise.

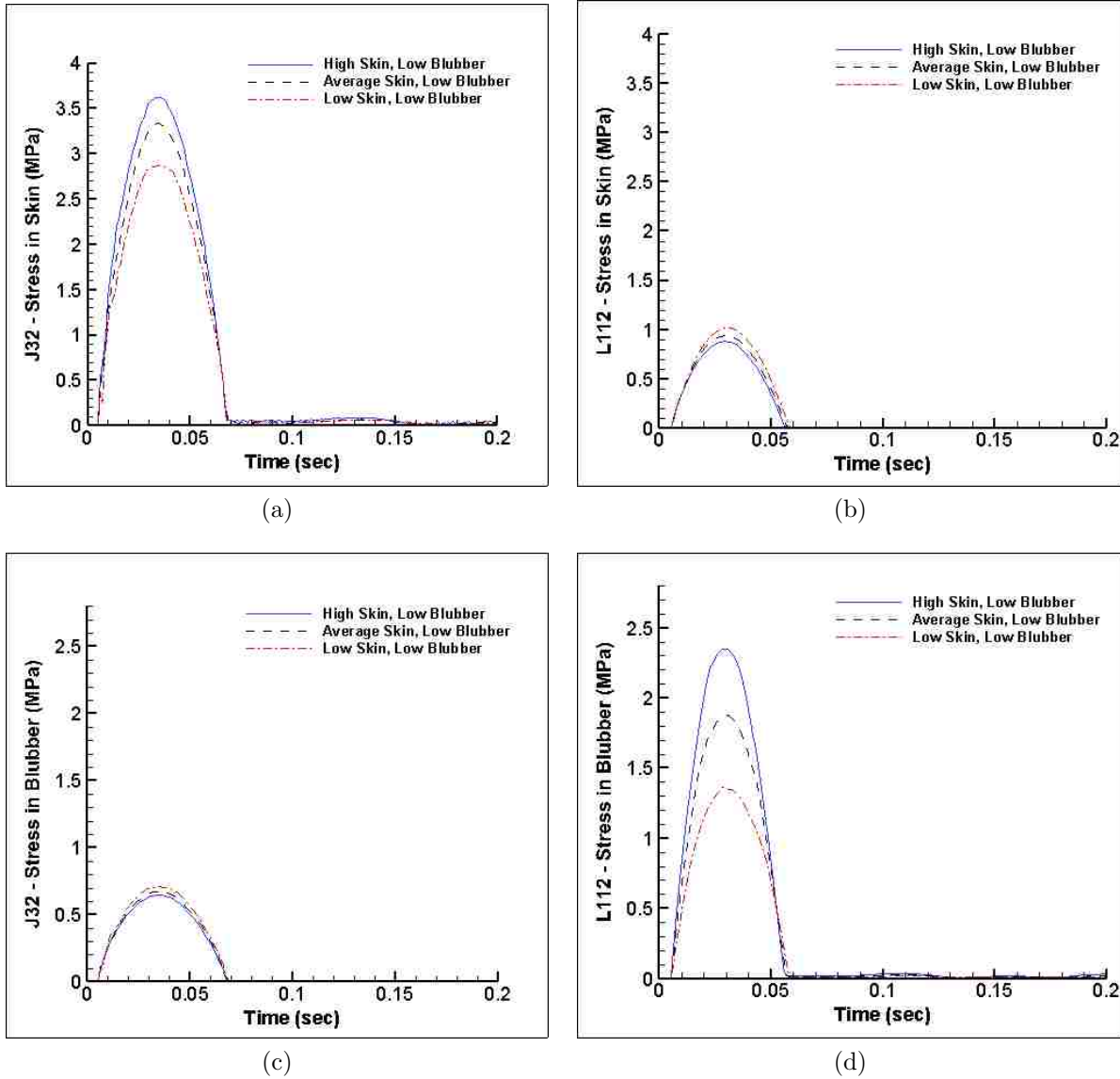


Figure 5.7: Stress over the course of the model run using high, average, and low orca skin data with low orca blubber data, as prescribed by Table 5.1. In J32, varying the skin doesn't show a strong impact on the results, while the full range of skin values for L112 shows a large amount of variability.



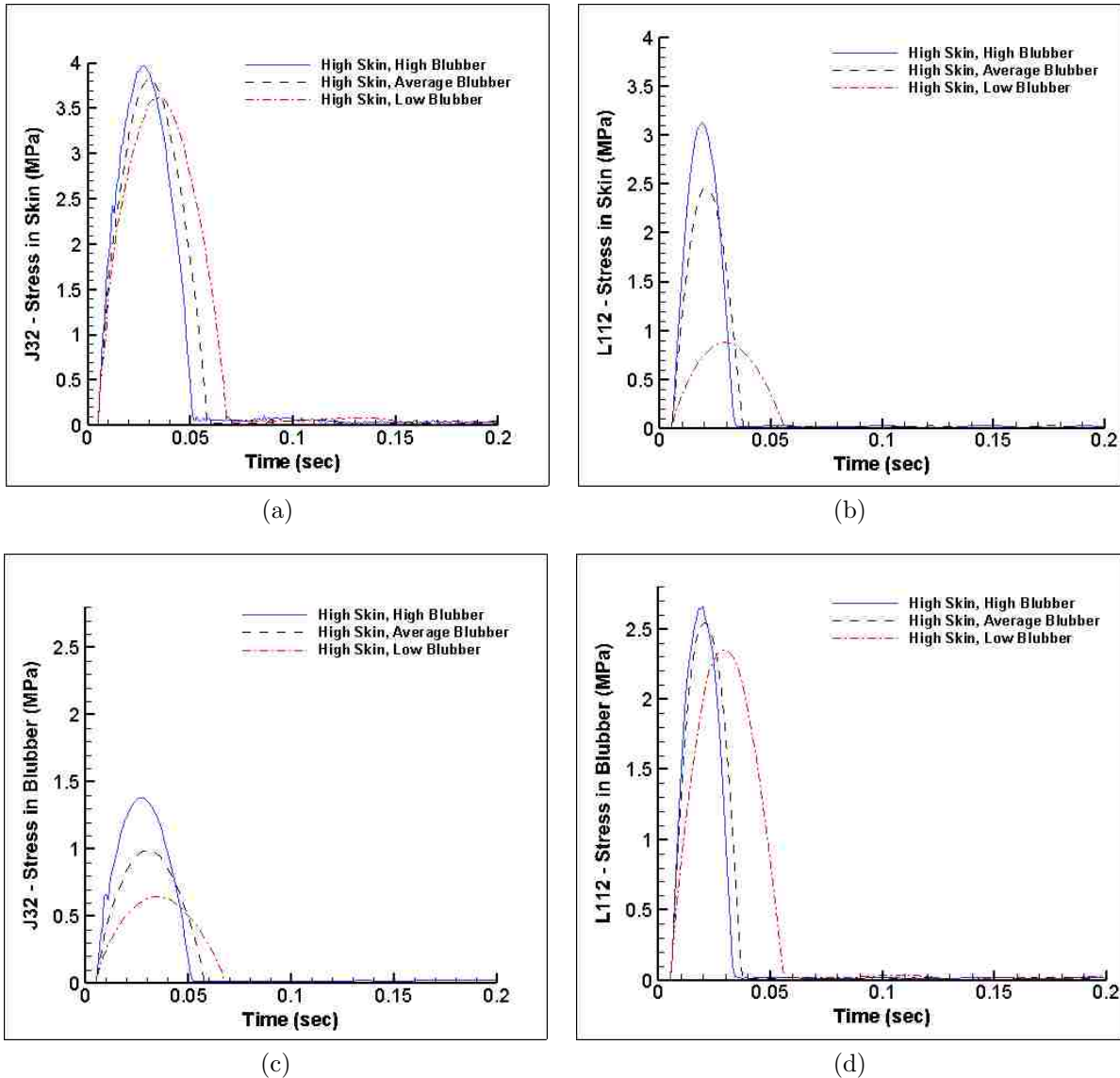


Figure 5.8: J32 (a) and L112 (b) skin stress using high, average, and low orca blubber data with high orca skin data, as prescribed by Table 5.1, (c) and (d) show the same for the stress in blubber. The stress in the highest stressed element is reported over the time series of the simulation. In J32, varying the blubber doesn't show a large impact on the results, while the full range of blubber values for L112 shows a large amount of variability especially in skin stress.

### 5.2.3 Discussion

The L112 blubber data are incongruent with anything seen across all other testing. Further, this incongruency has a large impact on the model results, suggesting that this data should be eliminated from the overall pool of marine mammal data. The original PNNL report faced a similar quandary, observing that the blubber was much stiffer than its overlying skin. To solve this problem, that report used the stiffer neonatal skin. When observing the suite of marine mammal data collected since that original setup in 2013, it is clear that the blubber was a larger contributor to the error and uncertainty in that report.

The variations seen during testing are large enough to cause significantly different results in this simplistic model. Varying the magnitude of maximum stress by 1 MPa can lead to a large difference in whether or not that element of tissue is compromised. Further, the extent or volume of tissue varies further. The most important factor is the relationship between the blubber and skin. When the blubber is higher or close to the value of elastic modulus for skin, very different results are found than when skin is much greater than blubber. Though J32 performs much better than L112, this parametric study leads to the conclusion that dialing in the material properties more precisely is essential to finding an accurate portrait of the risk posed from tidal turbine collision.

## 5.3 Comparative Finite Element Method Study

### 5.3.1 Methods

A finite element model was created in the commercial finite element software Abaqus to compare the role of skin and blubber material properties between the four marine mammals regarding swimming and potential injury. For each animal, two materials, skin and blubber, were modeled by averaging the elastic modulus measured across all tests for any adult animals (Table 5.3). For blubber, the density of all animals blubber was set to 0.904 g/ML and a poisson's ratio of 0.49. For skin, the density of all tissue was set to 1.060 g/ML and the poisson's ratio was 0.47. The material model for both materials was modeled as linear

Table 5.3: Elastic modulus used to compare skin and blubber across four marine mammal species.

	Elastic Modulus (MPa)	
	Skin	Blubber
Dall's Porpoise	3.865	0.965
Harbor Porpoise	3.316	0.567
Harbor Seal	22.513	1.670
Killer Whale	6.130	3.353

elastic and isotropic. At the interface of skin and blubber, the two materials were modeled as continuous and tied together, but with different materials on each side of the boundary. The finite element analysis was performed on a block of tissue measuring 100 mm by 100 mm with a total height of 50 mm (5 mm skin layer and 45 mm blubber layer) under two loading conditions. The first loading condition was a uniaxial tension load, where an equal pressure of 0.2 MPa was applied in a static analysis on the two opposite sides of the block in the direction normal to the tissue. A uniform mesh of C3D8 elements was used across the block, with an approximate global size of 2 mm. This scenario illustrates the loads that might be present during typical swimming or maneuvering. In the second scenario, a rigid spherical indenter (10 mm diameter) pushes 50 N into the tissue from the top center of the block in a dynamic explicit analysis. This scenario represents the skin's protective abilities, against predation or other punctures. In this analysis, the mesh of C3D8 elements was concentrated in the center of the block, with a minimum seeding size of 1.7 mm and maximum size of 3.4 mm across the top of the block. In the z direction on the block, the mesh was concentrated at the top, near the indenter, with a mesh size of 1.25 mm through the skin layer, then a minimum size of 1.3 mm to 4 mm in the blubber layer. The block of tissue for this scenario had a concentrated mesh in the center under the indenter and used one plane of symmetry to reduce computation time.

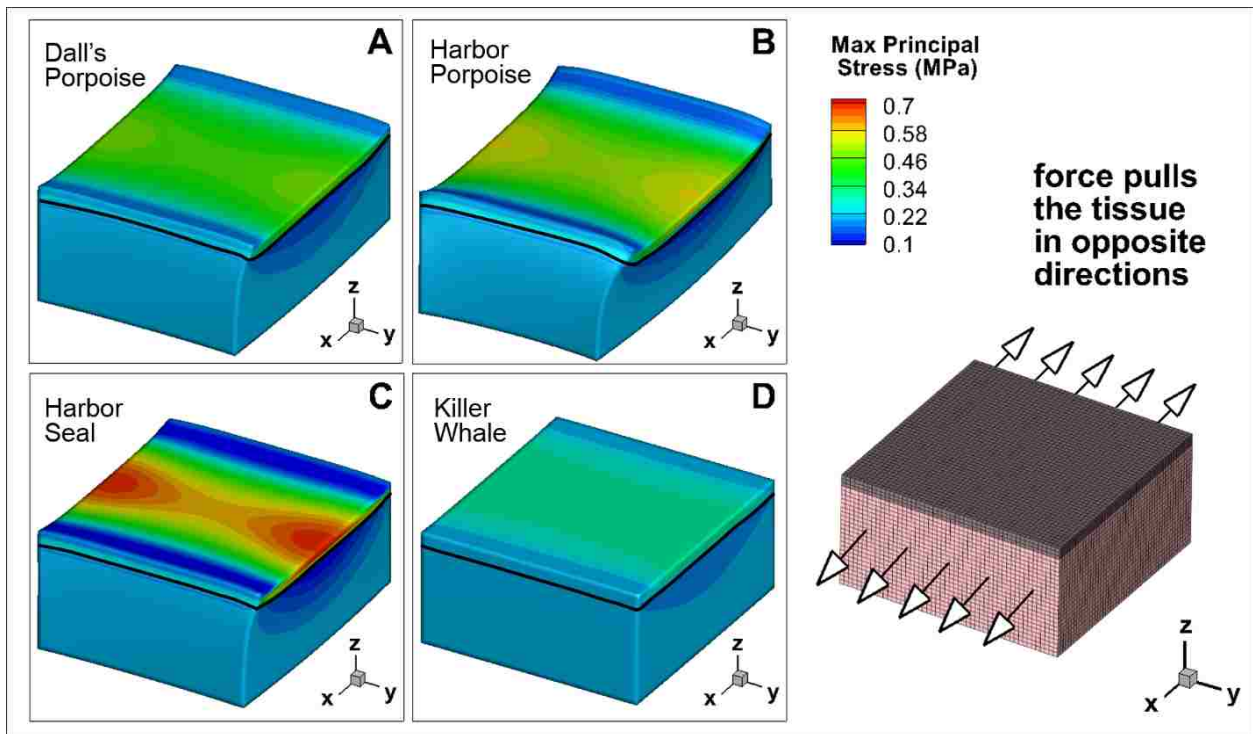


Figure 5.9: Maximum principal stress under a tensile load of 0.2 MPa on a representative block of layered skin and blubber across four species. Inset describes the finite element method setup for the block of tissue. Black line in A-D denotes interface of skin and blubber.

### 5.3.2 Comparative effect of load on deformation

In a block of tissue under tension, which represents deformation under normal locomotor movements, if the two layers are identical a constant stress would be seen throughout. The killer whale tissue, with moduli of 6.1 MPa (skin) and 3.4 MPa (blubber) is the closest to a uniform material, thus the differences between the two layer's deformation is very small (Figure 5.9D). The greatest stress in the composite material, seen in the harbor seal (Figure 5.9C), results from the largest difference between two material properties. Even in the composite formulation, Dall's porpoise and Harbor porpoise are similar, though the harbor porpoise tissue stretches further under the same tensile load (Table 5.3).

In the finite element model of impact, an indenter is pressed with 50N of force into the

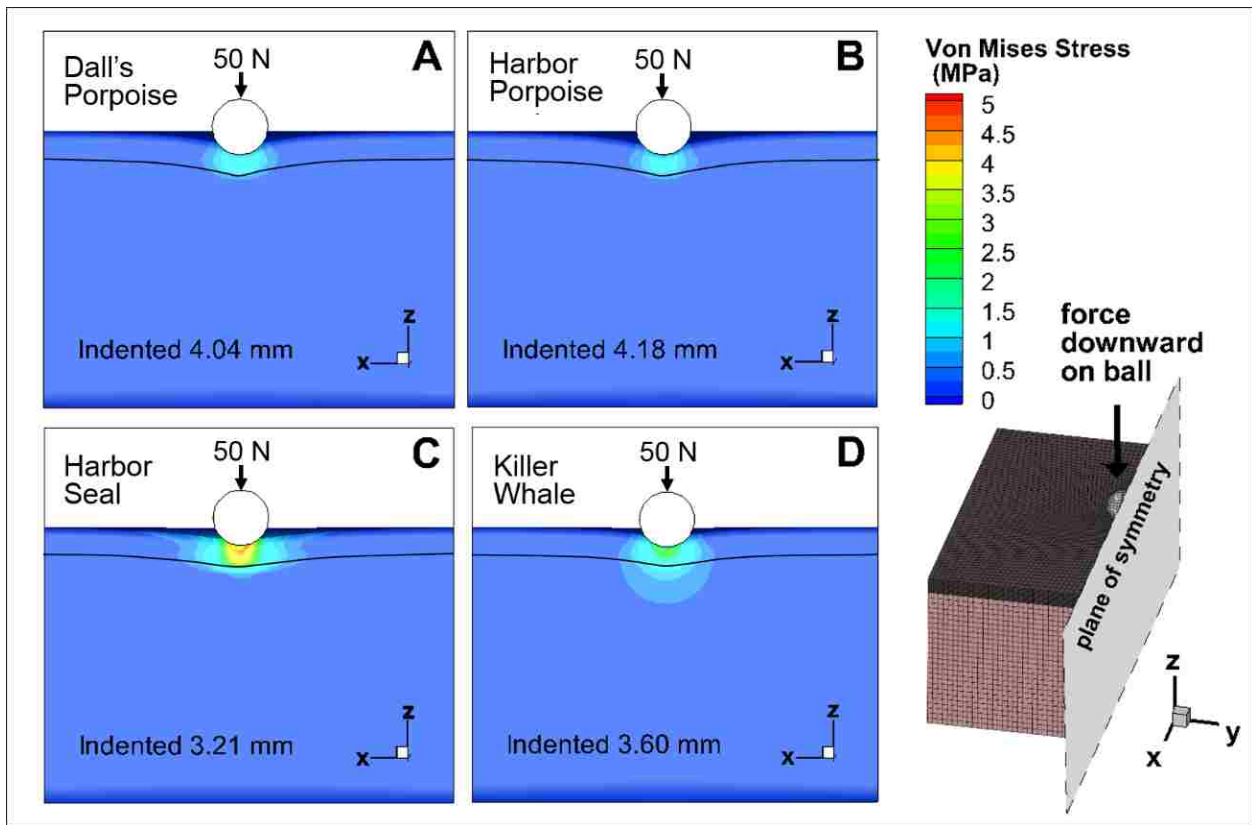


Figure 5.10: Von Mises stress, a formulation of the stress state used to predict the material failure, on a representative block of layered skin and blubber across four species. Inset illustrates the finite element method setup for the block of tissue, where a 10mm diameter rigid ball is indented with 50N of force into the block. Black line in A-D denotes interface of skin and blubber.

block of tissue. The depth of indentation depends on the stiffness of the composite and the stress distribution is affected by the difference between the stiffness of the layers. (Figure 5.10D). The indenter penetrates most deeply into the Harbor Porpoise, but the peak stresses are not very high. In contrast the harbor seal is not penetrated very deeply, but there are potentially dangerously high stresses in the skin because of the interaction between the layers.

## Chapter 6

### CONCLUSIONS AND FUTURE WORK

The goal of this dissertation was to characterize marine mammal soft tissue as an aid to understanding the potential injury from marine mammals colliding with tidal turbines. Characterization was completed across four animals and a battery of tests, adding a considerable amount of knowledge to a previously uncharacterized material. The laboratory testing allowed a numerical model of the material to be created and validated. With improved characterization and numerical models, the uncertainty of marine mammal skin and blubber material properties is greatly reduced. Improved material properties allow more confidence in modeling an encounter between a marine mammal and tidal turbine. With these material inputs, a specific turbine design could be modeled under the local operating conditions, like flow speed, to understand and evaluate the risk of collision. This chapter briefly summarizes the work accomplished in each chapter and important findings, concluding with future directions for the research.

#### **6.1 Summary and Major Findings**

##### *6.1.1 Tensile Testing*

The beginning of this research program was spent evaluating marine mammal skin and blubber material properties using tensile testing. Each animal was obtained opportunistically based on animals that stranded dead locally and in good condition. Using multivariate statistics across four species of marine mammal, the material did not show different material properties in different directions. This is an important result for finite element modeling, as it greatly simplifies the material model needed to represent the material numerically.

Statistical tests were also performed to evaluate the significance of test speed, age, and

freezing. In the comparison across all species, blubber material properties did not show a significant effect of test speed, while skin material properties were impacted by the test speed. Age and freezing effects were largely evaluated in the harbor seal data, as that dataset was the largest and most complete. There were differences between adult and pup material properties in all categories except skin elastic modulus. Freezing generally impacted the skin more than the blubber, with skin being stiffer and stronger after freezing and thawing.

The multivariate analysis showed that there was not a significant difference between toothed whale species skin, indicating a place where model simplifications may be employed. Similarity was also seen between harbor porpoise and Dall's porpoise blubber, but the harbor seal and Killer whale were significantly different from each other and the porpoises.

### *6.1.2 Indentation Testing*

The indentation testing showed that the stiffness of the blubber of harbor porpoise and killer whale is an order of magnitude less stiff than when measured using tension tests. The harbor seal was also less stiff in compression. In addition to providing an understanding of the behavior in compression, testing the material still intact, with the skin connected to the blubber provided a laboratory test that could be compared to a numerical model of the same test setup.

### *6.1.3 Bulk and shear modulus*

Bulk and shear modulus testing both required the development of new test setups to measure these quantities. Overall, skin had a higher bulk modulus than blubber. The result is unexpected, as the blubber might be expected to be more incompressible than skin. It is possible that this result is due to the skin's thinness making the test less accurate than the comparatively much thicker blubber specimens. Shear modulus testing gave lower results than what would be expected if the material behaved isotropically, but was similar to some measured tests of the behavior of rubber. The shear modulus testing in particular provides the largest case against modeling the blubber or skin as a linear elastic material.

#### 6.1.4 *Histology*

A brief foray into histology showed that the blubber of the harbor porpoise and killer whale have collagen fibers that are oriented in many different directions. The collagen of the killer whale blubber extends up into the skin; the distinction between skin and blubber appears more ambiguous in killer whale than in harbor porpoise. The blubber collagen fibers organization supports the findings that the material is isotropic, as the organization of collagen fibers has been linked to the differences in material properties in other mammals and fish.

#### 6.1.5 *Validation*

Validation of the material constitutive model was completed in the finite element solver Abaqus using the spherical indentation testing, both with blubber alone and with the skin still attached to the blubber. For the killer whale blubber only test, a reduced polynomial hyperelastic model with  $N=2$  using a specific trial of the indentation test (as opposed to an average) gave results in agreement with the laboratory data. This same method was applied to harbor porpoise testing and gave similarly good results, showing that this method is appropriate for capturing the blubber behavior in both species.

Using the skin and blubber laboratory data, a full model was created. Blubber material properties were varied numerically in some cases to understand the effects of blubber variation on the full model, but the majority of numerical models were created using the reduced polynomial hyperelastic model created with the blubber only validation. While blubber data collected in tension does not agree with the spherical indentation validation, the skin data in tension gives appropriate results.

An Ogden hyperelastic model with  $N=1$  for killer whale skin using coefficients generated from the bulk and shear modulus data gave the best results when combined with the reduced polynomial model for blubber.



### 6.1.6 *Parametric Studies*

A series of parametric studies were created with the motivation of understanding how much the natural variation across individuals of the same species (or multiple tests of the same individual) impacts the modeling result. Additionally, using average values from different species allows comparison across taxa, showing how the species' combinations of material properties vary.

The main conclusion from both sets of parametric studies is that injury is more likely if two layers are the same or if underlying layer is stronger and stiffer. A similar material between the two layers allows the force of impact to penetrate more deeply into the tissue. If all animals' geometry were exactly alike, with the same thickness of skin and blubber, the killer whale would have the force of the turbine penetrate deepest into its body. The harbor seal would likely be the most likely to break the skin, as the blubber is not as able to absorb as much of the impact force with the stiffer skin on top. However, since the killer whale is much more massive and has thicker skin, it is likely the least at risk of the animals presented in this study.

## 6.2 *Future Work*

### 6.2.1 *Constructing a complete model*

The work here makes a more accurate model of a specific turbine design and marine mammal of interest possible. With the knowledge gained from this research, a few suggestions for modeling the collision can be made as the immediate next steps in this research.

#### 6.2.1.1 *Skin element formulation*

Similar work has modeled skin in the shell formulation [20]. Though the skin layer is quite thin compared to the scale of the turbine and even the mammal itself, modeling in this way misses an opportunity to assess injury. The prototypical work completed in modeling the full animal and turbine collision shows that the skin experiences the most stress in the

bottom layer, at the interface between the skin and blubber (Figure 6.1). In fact, the skin elements directly under the blade in this particular simulation are not likely to be damaged. If underlying layers are damaged while the outermost layer stays intact and there is no open wound, the animal has a much higher likelihood of having a recoverable injury [3].

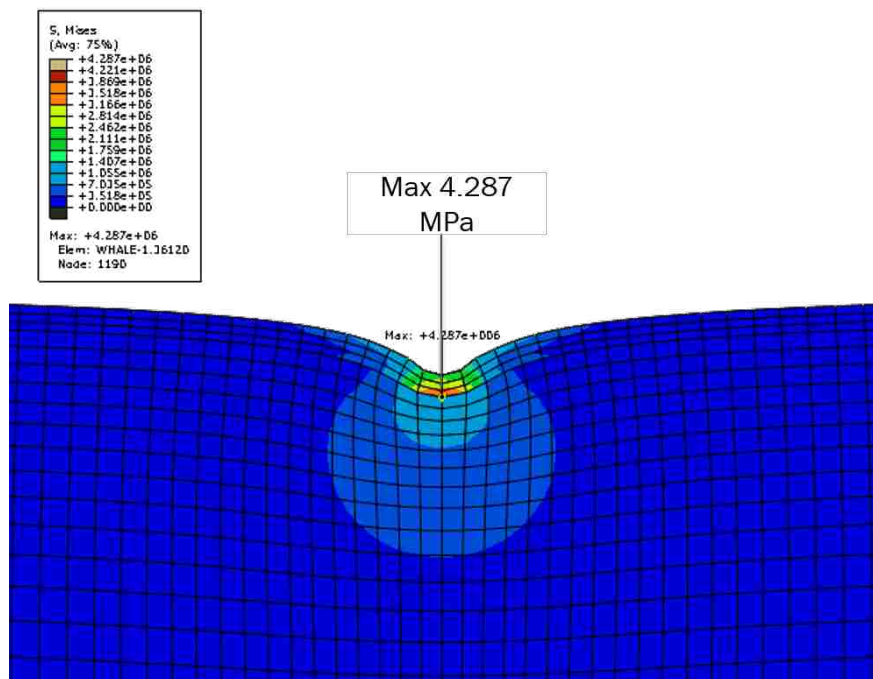


Figure 6.1: As the blade impacts a killer whale, based on material properties from the parametric study in Chapter 5, the skin experiences the highest stress at the interface between the skin and blubber.

### 6.2.1.2 Blade formulation and rotation

In the prototypical model of the animal and blade, there was interest in what would happen to the blade in addition to the stresses experience by the animal. While this question is still open, including what might happen to the blade if other debris were to hit it [71, 48], the added complexity of correctly modeling the blade material properties, as well as the stresses already on it from the surrounding water, make this line of questioning outside the scope of

understanding the impacts on a marine mammal. Thus, a rigid blade model is recommended for future modeling of this interaction.

In addition, several methods were examined to best apply the rotational force on the blade in a realistic method. Installed turbine blades have a control system as well as the forces applied by the surrounding water that would be impacted by a collision. In the absence of a control system, a killer whale may be able to actually slow the rotation of the blades, but in reality the control system may be likely to speed up the blades. There are many options to model this contradictory set of constraints: the blade simply has an initial velocity, the end of the blade could have a rotation, or the velocity could change as the simulation progresses. The simplest and most reasonable approach, especially given the likely control strategies, seems to be applying a rotational force at the end of the blade. This also gives the option of testing the same model at various points on the blade, where injury may be greater (at tip) or less (closer to base) likely.

#### *6.2.1.3 Addition of bones and spine*

Across testing of a few blade designs and typical rotation speeds, the regions of tissue that might be damaged generally did not penetrate deep into the animal. Still, in some regions, the bones are quite close to the outer layers and could be modeled. The literature has more data for whale bones than for soft tissue data, which could be incorporated into a model. A next step would be a simple spine model to give the mammal additional stiffness as it is pushed out of the way by the turbine.

#### *6.2.1.4 Water surrounding collision*

As the animal is pushed by the turbine, the surrounding water pushes back on the animal, adding more resistance than if the animal were in air. This force is certainly important and can be simulated in Abaqus with the addition of spring forces on the bottom of the animal. Some analytical calculations on the added mass and forces exerted by certain speeds of moving water on a cylinder would likely approximate the added force from water well.

### 6.2.2 *Material Testing*

Full characterization of the behavior of marine mammal skin and blubber across many scales and loads may in fact be a lifetime of work. Soft tissues in a living animal constantly experience complex loading and the uniaxial tension results likely overestimate the strain-to-failure and perhaps then underestimate the elastic modulus [63]. Similar uniaxial tests could be completed with a larger sample size to determine if cutting the pieces into smaller shapes impacted the material properties measured. Biaxial testing may further illuminate this complexity, testing the material with a load more similar to what is experienced in the living animal.

All testing was completed in the same region of the animal, in the thoracic region on the dorsal side. Cetacean flukes have been shown to have evidence of anisotropy at the very least in their geometry [30, 79], so it would be a worthwhile endeavor to understand how material properties vary across a marine mammal's body. Fish skin elastic modulus has been shown to vary along the body of the animal [49] and thus aid in locomotion. Understanding the role that skin and blubber plays in marine mammal locomotion is not as well characterized as it is in other swimming vertebrates, so may be an interesting area of future research.

### 6.2.3 *Additional Species*

Additional pinniped species would aid multivariate analysis of multiple species. The harbor seal was quite different from the cetaceans tested, but more pinnipeds would make for a more balanced comparison. The permits enclosed here (Appendix B) allow for collection of a Steller sea lion, which would be a natural extension of this work.

A larger whale species would be another good addition to the data set, especially for understanding the biomechanics and evolution of marine mammals; comparing material properties across many geometries would add the potential to generalize or contrast between a larger range of size classes. However, a whale much larger than a killer whale is unlikely to be present in constricted tidal channels.

#### 6.2.4 *Environmental Monitoring Applications*

Some early tidal turbines are likely to be equipped with robust monitoring systems. Monitoring systems are being developed that can detect an approaching marine mammal [22]. These systems typically use acoustic cameras, as well as optical cameras. As more tidal turbines and monitoring systems are installed, the likelihood of collision can be better understood. Monitoring systems can observe how marine mammals approach tidal turbines, delineating the likely regions of the body that an animal might be injured, like whether it is approaching from up or downstream of the turbine. In addition, monitoring systems may be able to interface with the tidal turbine control system to slow or stop the turbine automatically. The decision to slow the turbine could potentially be made using input from finite element models, slowing the turbine only to safe speeds as opposed to completely braking and risking damaging the turbine's systems.

#### 6.2.5 *Control Theory Applications*

The control system can be modified to slow the turbine if an animal is detected. Even better than detecting the animal with a monitoring system would be to detect the approaching animal with the controller alone. It is possible that the approaching animal could be detected by its wake and the resulting turbulence by the turbine's controller. A next step in this research would be to test these controllers at a laboratory scale to see if this controller detection is possible. Integrating marine mammal collision risk into the control of the tidal turbine is a way that tidal turbines could be designed to reduce environmental risk, as opposed to adding environmental mitigation on as an afterthought.

#### 6.2.6 *Stakeholder Engagement and Retiring Risk*

The issue of marine mammal collision is at least partly a problem of public perception. Though this approach is robust and thorough when applied correctly, it may not appeal to or allay the concerns of those who are likely to raise the issue. Adding in input from

regulators, like the National Oceanic and Atmospheric Administration, who oversee the enforcement of the Marine Mammal Protection Act, can strengthen the outputs created by this work. These resource managers are key stakeholders in ensuring this research is useful in permitting new devices. Additional stakeholders include wildlife conservation and animal-welfare non-profits.

Creating a plan to best communicate the results of this work could help retire the risk and allow the industry to move forward. ‘Retiring’ risk is a goal where the risk is removed from further consideration [18]. While collision risk is a concern that may always pose some potential problems for new tidal turbine designs, a consistent method for evaluating this risk would be a major step forward in permitting new devices.

## BIBLIOGRAPHY

- [1] J. Abanades, D. Greaves, and G. Iglesias. Coastal defence using wave farms: The role of farm-to-coast distance. *Renewable Energy*, 75:572 – 582, 2015.
- [2] K. Alexander, R. Janssen, G. Arciniegas, T. O’Higgins, T. Eikelboom, and T. Wilding. Interactive marine spatial planning: Siting tidal energy arrays around the mull of kintyre. *PLOS ONE*, 7(1):1–9, 01 2012.
- [3] M. Andersen, K. Forney, T. Cole, T. Eagle, R. Angliss, K. Long, L. Barre, L. Van Atta, D. Borggaard, T. Rowles, et al. Differentiating serious and non-serious injury of marine mammals: Report of the serious injury technical workshop. *NOAA Tech. Memo. NMFS-OPR*, 39:94, 2008.
- [4] T. Anderson and E. Madenci. Experimental investigation of low-velocity impact characteristics of sandwich composites. *Composite Structures*, 50(3):239 – 247, 2000.
- [5] A. Annaidh, K. Bruyere, M. Destrade, M. Gilchrist, and M. Ottenio. Characterization of the anisotropic mechanical properties of excised human skin. *Journal of the Mechanical Behavior of Biomedical Materials*, 5(1):139 – 148, 2012.
- [6] V. Arumugam, M. D. Naresh, and R. Sanjeevi. Effect of strain rate on the fracture behaviour of skin. *Journal of Biosciences*, 19(3):307–313, 1994.
- [7] F. Azar, D. Metaxas, and M. Schnall. A deformable finite element model of the breast for predicting mechanical deformations under external perturbations. *Academic Radiology*, 8(10):965 – 975, 2001.
- [8] D. Bates, M. Mächler, B. Bolker, and S. Walker. Fitting linear mixed-effects models using lme4. *Journal of Statistical Software*, 67(1):1–48, 2015.
- [9] G. Beck and T. Smith. Distribution of blubber in the northwest Atlantic harp seal, *Phoca groenlandica*. *Canadian Journal of Zoology*, 73(11):1991–1998, 1995.
- [10] M. Bennett, R. Ker, N. Imery, and R. Alexander. Mechanical properties of various mammalian tendons. *Journal of Zoology*, 209(4):537–548, 1986.

- [11] R. Billingham and P. Medawar. The freezing, drying and storage of mammalian skin. *Journal of Experimental Biology*, 29(3):454–468, 1952.
- [12] J. Bischoff, E. Arruda, and K. Grosh. Finite element modeling of human skin using an isotropic, nonlinear elastic constitutive model. *Journal of Biomechanics*, 33(6):645 – 652, 2000.
- [13] R. Campbell-Malone. *Biomechanics of North Atlantic Right Whale Bone: Mandibular Fracture as a Fatal Endpoint for Blunt Vessel-Whale Collision Modeling*. PhD thesis, Massachusetts Institute of Technology, 2007.
- [14] R. Campbell-Malone, S. Barco, P.-Y. Daous, A. Knowlton, W. McLellan, D. Rotstein, and M. Moore. Gross and histologic evidence of sharp and blunt trauma in north atlantic right whales (*Eubalaena glacialis*) killed by ships. *Journal of Zoo and Wildlife Medicine*, 39(1):37–55, 2008.
- [15] T. Carlson, M. Grear, A. Copping, M. Halvorsen, R. Jepsen, and K. Metanger. Assessment of strike of adult killer whales by an OpenHydro tidal turbine blade. *Report by Pacific Northwest National Laboratory (PNNL)*, page pp 124, 2014.
- [16] R. Chan and I. Titze. Effect of postmortem changes and freezing on the viscoelastic properties of vocal fold tissues. *Annals of Biomedical Engineering*, 31(4):482–491, 2003.
- [17] T. Chandler and J. Calambokidis. 2003 aerial surveys for harbor porpoise and other marine mammals off Oregon, Washington, and British Columbia. *Contract report to National Marine Mammal Laboratory*, page 25pp, 2003. (Report available from Cascadia Research, [www.cascadiaresearch.org](http://www.cascadiaresearch.org)).
- [18] A. Copping. The state of knowledge for environmental effects driving consenting/permitting for the marine renewable energy industry. 2018.
- [19] A. Copping and M. Grear. Applying a simple model for estimating likelihood of collision of marine mammals with tidal turbines. In *European Wave and Tidal Energy Conference*, Cork, Ireland, 2017.
- [20] A. Copping, M. Grear, R. Jepsen, C. Chartrand, and A. Gorton. Understanding the potential risk to marine mammals from collision with tidal turbines. *International Journal of Marine Energy*, 19:110–123, 2017.
- [21] A. Copping, N. Sather, L. Hanna, J. Whiting, G. Zydlewski, G. Staines, A. Gill, I. Hutchison, A. O’Hagan, T. Simas, J. Bald, Sparling C., J. Wood, and E. Masden. Annex IV 2016 State of the Science Report: Environmental Effects of Marine Renewable Energy Development Around the World. 2016.



- [22] E. Cotter, P. Murphy, and B. Polagye. Benchmarking sensor fusion capabilities of an integrated instrumentation package. *International Journal of Marine Energy*, 20:64–79, 2017.
- [23] I. Cowan. The Dall Porpoise, *Phocoenoides dalli* (true), of the Northern Pacific Ocean. *Journal of Mammalogy*, 25(3):295–306, 1944.
- [24] A. Cua, K. Wilhelm, and H. Maibach. Elastic properties of human skin: relation to age, sex, and anatomical region. *Archives of Dermatological Research*, 282(5):283–288, 1990.
- [25] D. A. Danielson. Human skin as an elastic membrane. *J. Biomechanics*, 6(5):539–546, 1973.
- [26] R. Dunkin, W. McLellan, J. Blum, and A. Pabst. The ontogenetic changes in the thermal properties of blubber from Atlantic bottlenose dolphin *Tursiops truncatus*. *Journal of Experimental Biology*, 208(8):1469–1480, 2005.
- [27] N. Erdsack, G. Dehnhardt, M. Witt, A. Wree, U. Siebert, and W. Hanke. Unique fur and skin structure in harbour seals (*Phoca vitulina*)— thermal insulation, drag reduction, or both? *Journal of The Royal Society Interface*, 12(104), 2015.
- [28] B. Finlay. Dynamic mechanical testing of human skin ‘in vivo’. *Journal of Biomechanics*, 3(6):557 – 568, 1970.
- [29] F. Fish. Transitions from drag-based to lift-based propulsion in mammalian swimming. *American Zoologist*, 36(6):628–641, 1996.
- [30] F. Fish, M. Nusbaum, J. Beneski, and D. Ketten. Passive cambering and flexible propulsors: cetacean flukes. *Bioinspiration & biomimetics*, 1(4):S42, 2006.
- [31] W. Folland, J. Newsted, S. Fitzgerald, P. Fuchsman, P. Bradley, J. Kern, K. Kannan, R. Remington, and M. Zwiernik. Growth and reproductive effects from dietary exposure to aroclor 1268 in mink (*Neovison vison*), a surrogate model for marine mammals. *Environmental toxicology and chemistry*, 35(3):604–618, 2016.
- [32] J. Gennisson, T. Baldeweck, M. Tanter, S. Catheline, M. Fink, L. Sandrin, C. Cornillon, and B. Querleux. Assessment of elastic parameters of human skin using dynamic elastography. *IEEE Transactions on Ultrasonics, Ferroelectrics, and Frequency Control*, 51(8):980–989, Aug 2004.

- [33] A. Gent. Rubber elasticity: basic concepts and behavior. In *Science and Technology of Rubber (Third Edition)*, pages 1–27. Elsevier, 2005.
- [34] M. Grear and M. Motley. Numerical Modeling of the Impact Response of Tidal Devices and Marine Mammals. In *European Wave and Tidal Energy Conference*, Nantes, France, 2015.
- [35] M. Grear and M. Motley. Tidal turbine collision assessment using the bulk and shear modulus of marine mammals' soft tissue. In *European Wave and Tidal Energy Conference*, Cork, Ireland, 2017.
- [36] M. Grear, M. Motley, S. Crofts, A. Witt, A. Summers, and P. Ditsche. Mechanical properties of harbor seal skin and blubber - a test of anisotropy. *Zoology*, 126:137–144, 2018.
- [37] M. Grear, M. Motley, P. Ditsche, and A. Summers. Comparative material properties of marine mammals skin and blubber. submitted.
- [38] M. Grujicic, B. Pandurangan, G. Arakere, W.C. Bell, T. He, and X. Xie. Seat-cushion and soft-tissue material modeling and a finite element investigation of the seating comfort for passenger-vehicle occupants. *Materials & Design*, 30(10):4273 – 4285, 2009.
- [39] E. Hamilton. Elastic properties of marine sediments. *Journal of Geophysical Research*, 76(2):579–604, 1971.
- [40] J. Hamilton, R. Dillaman, W. McLellan, and A. Pabst. Structural fiber reinforcement of keel blubber in harbor porpoise (*Phocoena phocoena*). *Journal of Morphology*, 261(1):105–117, 2004.
- [41] G. Hastie, D. Russell, P. Lepper, J. Elliott, B. Wilson, S. Benjamins, and D. Thompson. Harbour seals avoid tidal turbine noise: Implications for collision risk. *Journal of Applied Ecology*, 55(2):684–693, 2018.
- [42] M. Hebrank and J. Hebrank. The mechanics of fish skin: lack of an "external tendon" role in two teleosts. *The Biological Bulletin*, 171(1):236–247, 1986.
- [43] F. Hendriks, D. Brokken, J. Van Eemeren, C. Oomens, F. Baaijens, and J. Horsten. A numerical-experimental method to characterize the non-linear mechanical behaviour of human skin. *Skin research and technology*, 9(3):274–283, 2003.
- [44] C. Huang, A. Stankiewicz, G. Ateshian, and V. Mow. Anisotropy, inhomogeneity, and tension-compression nonlinearity of human glenohumeral cartilage in finite deformation. *Journal of Biomechanics*, 38(4):799 – 809, 2005.

- [45] J. Huggins, S Raverty, S Norman, J. Calambokidis, J. Gaydos, D. Duffield, D. and Lambourn, J. Rice, B. Hanson, S. Jeffries, B. Norberg, and L. Barre. Increased harbor porpoise mortality in the Pacific Northwest, USA: understanding when higher levels may be normal. *Diseases of Aquatic Organisms*, 115(2):93–102, 2015.
- [46] R. Inger, M. Attrill, S. Bearhop, A. Broderick, W. J. Grecian, D. Hodgson, C. Mills, E. Sheehan, S. Votier, M. Witt, and B. Godley. Marine renewable energy: potential benefits to biodiversity? an urgent call for research. *Journal of Applied Ecology*, 46(6):1145–1153, 2009.
- [47] A. Jensen and G. Silber. Large whale ship strike database. Technical report, NOAA Technical Memorandum NMFS-OPR-25, U.S. Department of Commerce, Washington, D.C., USA, 2004.
- [48] J. Johnson, J. Kasper, N. Hansen, P. Duvoy, and J. Schmid. The effects of river and debris diversion structure generated turbulence on the oceanic river energy converter. In *Proceedings of the 3rd Marine Energy Technology Symposium METS*, 2015.
- [49] C. Kenaley and A. Sanin. Mechanics of fish skin: contrasting material properties within and between functional systems. *Integrative and comparative biology*, 57:E311–E311, 2017.
- [50] E. Kipps, W. McLellan, S. Rommel, and D. Pabst. Skin density and its influence on buoyancy in the manatee, harbor porpoise, and bottlenose dolphin. *Marine Mammal Science*, 18:765–778, 07/02 2002.
- [51] D Klötzer, Ch Ullner, E Tyulyukovskiy, and N Huber. Identification of viscoplastic material parameters from spherical indentation data: Part II. experimental validation of the method. *Journal of materials research*, 21(3):677–684, 2006.
- [52] K. Komatsu, L. Mosekilde, A. Viidik, and M. Chiba. Polarized light microscopic analyses of collagen fibers in the rat incisor periodontal ligament in relation to areas, regions, and ages. *The Anatomical Record*, 268(4):381–387, 2002.
- [53] H. Koopman. Topographical distribution of the blubber of harbor porpoises (*Phocoena phocoena*). *Journal of Mammalogy*, 79(1):260, 1998.
- [54] H. Koopman, S. Iverson, and D. Gaskin. Stratification and age-related differences in blubber fatty acids of the male harbour porpoise (*Phocoena phocoena*). *Journal of Comparative Physiology B*, 165(8):628–639, 1996.

- [55] Y. Lanir and C. Fung. Two-dimensional mechanical properties of rabbit skin—II. experimental results. *J. Biomechanics*, 7(2):171–182, 1974.
- [56] W. Larrabee. A finite element model of skin deformation. I. Biomechanics of skin and soft tissue: A review. *The Laryngoscope*, 96(4):399–405, 1986.
- [57] V. Lesage, M. Hammill, and K. Kovacs. Functional classification of harbor seal (*Phoca vitulina*) dives using depth profiles, swimming velocity, and an index of foraging success. *Canadian Journal of Zoology*, 77(1):74–87, 1999.
- [58] D. Lin, D. Shreiber, E. Dimitriadis, and F. Horkay. Spherical indentation of soft matter beyond the hertzian regime: numerical and experimental validation of hyperelastic models. *Biomechanics and modeling in mechanobiology*, 8(5):345, 2009.
- [59] J. Long, M. Hale, M. McHenry, and M. Westneat. Functions of fish skin: flexural stiffness and steady swimming of longnose gar, *Lepisosteus osseus*. *Journal of Experimental Biology*, 199(10):2139–2151, 1996.
- [60] C. Malinka, D. Gillespie, J. Macaulay, R. Joy, and C. Sparling. First in situ passive acoustic monitoring for marine mammals during operation of a tidal turbine in ramsey sound, wales. *Marine Ecology Progress Series*, 590:247–266, 2018.
- [61] C. McKee, J. Last, P. Russell, and C. Murphy. Indentation versus tensile measurements of young's modulus for soft biological tissues. *Tissue Engineering*, 17(3):155–164, 2011.
- [62] MeyGen Limited. Meygen. <http://www.meygen.com/>, 2016.
- [63] L. Mihai, L. Chin, P. Janmey, and A. Goriely. A comparison of hyperelastic constitutive models applicable to brain and fat tissues. *Journal of The Royal Society Interface*, 12(110):20150486, 2015.
- [64] P. Motta. Anatomy and functional morphology of dermal collagen fibers in sharks. *Copeia*, pages 454–464, 1977.
- [65] S. Otani, Y. Naito, Akito K., M. Kawasaki, S. Nishiwaki, and A. Kato. Diving behavior and performance of harbor porpoises, *Phocoena phocoena*, in Funka Bay, Hokkaido, Japan. *Marine Mammal Science*, 14(2):209–220, 1998.
- [66] A. Pabst, S. Rommel, and W. McLellan. The functional morphology of marine mammals. In J Reynolds and S Rommel, editors, *Biology of Marine Mammals*, chapter 1, pages 15–72. Smithsonian Institution, Washington, DC, 1999.

- [67] C. Pailler-Mattei, S. Bec, and H. Zahouani. In vivo measurements of the elastic mechanical properties of human skin by indentation tests. *Medical Engineering and Physics*, 30(5):599–606, 2008.
- [68] V. Pavlov. Dolphin skin as a natural anisotropic compliant wall. *Bioinspiration and Biomimetics*, 1:31–40, 2006.
- [69] M. Pawlaczyk, M. Lelonkiewicz, and M. Wieczorowski. Age-dependent biomechanical properties of the skin. *Postep Der Alergol*, 5:302–306, 2013.
- [70] C. Pierpoint. Harbour porpoise (*Phocoena phocoena*) foraging strategy at a high energy, near-shore site in south-west Wales, UK. *Journal of the Marine Biological Association of the United Kingdom*, 88(6):1167–1173, Mar 2008.
- [71] B. Sanderson, A. Redden, and J. Broome. Sediment-laden ice measurements and observations, and implications for potential interactions of ice and large woody debris with tidal turbines in Minas Passage. *Publication No. 109 of the Acadia Centre for Estuarine Research*, 2012.
- [72] O. Shergold, N. Fleck, and D. Radford. The uniaxial stress versus strain response of pig skin and silicone rubber at low and high strain rates. *International Journal of Impact Engineering*, 32(9):1384 – 1402, 2006.
- [73] M. Soldevilla, M. McKenna, S. Wiggins, R. Shadwick, T. Cranford, and J. Hildebrand. Cuvier’s beaked whale (*Ziphius cavirostris*) head tissues: physical properties and CT imaging. *Journal of Experimental Biology*, 208(12):2319–2332, 2005.
- [74] C. Sparling, M. Lonergan, and B. McConnell. Harbour seals (*Phoca vitulina*) around an operational tidal turbine in Strangford Narrows: No barrier effect but small changes in transit behaviour. *Aquatic Conservation: Marine and Freshwater Ecosystems*, 28(1):194–204, 2018.
- [75] H. Stanley, S. Casey, J. Carnahan, S. Goodman, J. Harwood, and R. Wayne. World-wide patterns of mitochondrial DNA differentiation in the harbor seal (*Phoca vitulina*). *Molecular Biology and Evolution*, 13:368–382, 1996.
- [76] B. Stemper, N. Yoganandan, M. Stineman, T. Gennarelli, J. Baisden, and F. Pintar. Mechanics of fresh, refrigerated, and frozen arterial tissue. *Journal of Surgical Research*, 139(2):236 – 242, 2007.
- [77] U. Strandberg, A. Käkälä, C. Lydersen, K. Kovacs, O. Nielsen, H. Hyvärinen, and R. Käkälä. Stratification, composition, and function of marine mammal blubber: The

- ecology of fatty acids in marine mammals. *Physiological and Biochemical Zoology: Ecological and Evolutionary Approaches*, 81(4):473–485, 2008.
- [78] Michael P Summers and John P Parmigiani. The dynamic shear moduli of whale blubber. *Biorheology*, 51(6):399–408, 2014.
- [79] Q. Sun, H. Morikawa, K. Ueda, H. Miyahara, and M. Nakashima. Bending properties of tail flukes of dolphin. *Journal of Biomechanical Science and Engineering*, 6(1):15–25, 2011.
- [80] I. Tsukrov, J. C. DeCew, K. Baldwin, R. Campbell-Malone, and M. J. Moore. Mechanics of the right whale mandible: Full scale testing and finite element analysis. *Journal of Experimental Marine Biology and Ecology*, 374(2):93 – 103, 2009.
- [81] R. Vilarta and B. Vidal. Anisotropic and biomechanical properties of tendons modified by exercise and denervation: aggregation and macromolecular order in collagen bundles. *Matrix*, 9(1):55–61, 1989.
- [82] I. Visser. Propeller scars on and known home range of two orca (*Orcinus orca*) in New Zealand waters. *New Zealand Journal of Marine and Freshwater Research*, 33(4):635–642, 1999.
- [83] S. Wainwright, F. Vosburgh, and J. Hebrank. Shark skin: Function in locomotion. *Science*, 202(4369):747–749, 1978.
- [84] M. Wolman and F. Kasten. Polarized light microscopy in the study of the molecular structure of collagen and reticulin. *Histochemistry*, 85(1):41–49, 1986.
- [85] T. Wren, S. Yerby, G. Beaupré, and D. Carter. Mechanical properties of the human achilles tendon. *Clinical Biomechanics*, 16(3):245–251, 2001.
- [86] H. Yoshihara, Y. Kubojima, K. Nagaoka, and M. Ohta. Measurement of the shear modulus of wood by static bending tests. *Journal of wood science*, 44(1):15–20, 1998.
- [87] J. Zamon. Seal predation on salmon and forage fish schools as a function of tidal currents in the San Juan Islands, Washington, USA. *Fisheries Oceanography*, 10(4):353–366, 2001.
- [88] M. Zhang, Y. Cao, G. Li, and X. Feng. Spherical indentation method for determining the constitutive parameters of hyperelastic soft materials. *Biomechanics and modeling in mechanobiology*, 13(1):1–11, 2014.

## Appendix A

**TENSILE TESTING RESULTS**

Results of the tensile testing described in Chapter 2 are presented in full here.

Table A.2: Each animal tested in tension results in data for Elastic Modulus (E), Tensile Strength (TS), Yield Strength (YS), and Strain-to-Failure (STF). Blanks represent missing data. Each animal tested is shown in a different section, delineated by a line. The same animal tested fresh and frozen is also delineated.

<b>Animal</b>	<b>Condition</b>	<b>Tissue</b>	<b>Age</b>	<b>Angle</b> (degrees)	<b>E</b> (MPa)	<b>TS</b> (MPa)	<b>Speed</b> (mm/s)	<b>YS</b> (MPa)	<b>STF</b> (mm/s)
Seal Pup 1	Fresh	Blubber	Juvenile	0	0.351	0.138	10	0.098	0.590
Seal Pup 1	Fresh	Blubber	Juvenile	90	0.478	0.138	10	0.102	0.758
Seal Pup 1	Fresh	Skin	Juvenile	0	21.614	5.790	10	4.499	0.656
Seal Pup 1	Fresh	Skin	Juvenile	90	31.666	7.088	10	5.243	0.571
Seal Pup 1	Frozen	Blubber	Juvenile	0	0.584	0.166	10	0.109	0.684
Seal Pup 1	Frozen	Blubber	Juvenile	45	1.050	0.243	10	0.172	0.455
Seal Pup 1	Frozen	Blubber	Juvenile	90	0.876	0.248	10	0.174	0.575
Seal Pup 1	Frozen	Skin	Juvenile	0	18.372	12.521	10	9.789	0.767
Seal Pup 1	Frozen	Skin	Juvenile	45	25.897	15.557	10	10.996	0.668

Table A.1: Available morphometric data collected at necropsy for animal seal tested.

<b>Animal</b>	<b>Length (cm)</b>	<b>Weight (kg)</b>	<b>Blubber Thickness (cm)</b>
Seal 1	137	40	2.5
Seal 2	167	74	1.8
Seal 3	150	46	0.5
Seal Pup 1	78	14	2.5
Seal Pup 2	96	19	2.3
Harbor Porpoise 2	165	58	1.5
Harbor Porpoise 3			7.4
Orca J32	562		4.5

Seal Pup 1	Frozen	Skin	Juvenile	90	33.866	17.309	10	12.802	0.684
Seal Pup 2	Fresh	Blubber	Juvenile	0	0.296	0.366	10	0.252	0.608
Seal Pup 2	Fresh	Blubber	Juvenile	45	0.906		10		0.504
Seal Pup 2	Fresh	Blubber	Juvenile	90	0.486	0.278	10	0.203	0.584
Seal Pup 2	Fresh	Skin	Juvenile	0	10.577	8.333	10	6.331	0.769
Seal Pup 2	Fresh	Skin	Juvenile	45	14.280		10		0.812
Seal Pup 2	Fresh	Skin	Juvenile	90	15.360	10.186	10	7.834	0.486
Seal Pup 2	Frozen	Blubber	Juvenile	0	0.598	0.227	10	0.127	0.859
Seal Pup 2	Frozen	Blubber	Juvenile	45	0.807	0.345	10	0.214	0.625
Seal Pup 2	Frozen	Blubber	Juvenile	90	1.758	0.475	10	0.288	0.557
Seal Pup 2	Frozen	Skin	Juvenile	0	15.305	19.519	10	14.069	0.742
Seal Pup 2	Frozen	Skin	Juvenile	45	18.405	15.158	10	10.447	0.567
Seal Pup 2	Frozen	Skin	Juvenile	90	25.385	15.080	10	10.886	0.889
Dall Porpoise 1	Fresh	Blubber	Adult	0	0.513	0.138	1	0.084	0.374
Dall Porpoise 1	Fresh	Blubber	Adult	45	1.363	0.180	1	0.131	0.237
Dall Porpoise 1	Fresh	Blubber	Adult	90	1.019	0.188	1	0.084	0.337
Dall Porpoise 1	Fresh	Skin	Adult	0	3.763		10		0.550
Dall Porpoise 1	Fresh	Skin	Adult	45	4.269		10		0.379
Dall Porpoise 1	Fresh	Skin	Adult	90	5.750		10		0.429
Dall Porpoise 1	Fresh	Skin	Adult	0	2.446	1.844	1	1.379	0.516
Dall Porpoise 1	Fresh	Skin	Adult	45	4.676		1		0.381
Dall Porpoise 1	Fresh	Skin	Adult	90	5.284	1.467	1	1.220	0.315
Harbor Porpoise 1	Fresh	Blubber	Adult	0	0.175		10		0.425
Harbor Porpoise 1	Fresh	Blubber	Adult	0	0.127	0.100	1	0.057	0.805
Harbor Porpoise 1	Fresh	Blubber	Adult	45	0.541	0.100	1	0.072	0.332
Harbor Porpoise 1	Fresh	Blubber	Adult	90	0.464	0.100	1	0.062	0.333
Harbor Porpoise 1	Fresh	Skin	Adult	0	1.496		10		0.704
Harbor Porpoise 1	Fresh	Skin	Adult	0	1.699	0.938	1	0.822	0.745
Harbor Porpoise 1	Fresh	Skin	Adult	45	3.067	0.900	1	0.658	0.375
Harbor Porpoise 1	Fresh	Skin	Adult	90	3.286	1.171	1	0.949	0.374
Harbor Porpoise 2	Fresh	Blubber	Adult	0	0.457	0.200	10	0.119	0.486
Harbor Porpoise 2	Fresh	Blubber	Adult	45	0.669	0.300	10	0.229	0.295
Harbor Porpoise 2	Fresh	Blubber	Adult	90	0.577	0.220	10	0.185	0.416
Harbor Porpoise 2	Fresh	Blubber	Adult	0	0.383	0.200	1	0.121	0.489
Harbor Porpoise 2	Fresh	Blubber	Adult	45	0.432	0.167	1	0.078	0.398
Harbor Porpoise 2	Fresh	Blubber	Adult	90	0.475	0.220	1	0.129	0.439



Harbor Porpoise 2	Fresh	Skin	Adult	0	2.586	3.533	10	2.836	0.416
Harbor Porpoise 2	Fresh	Skin	Adult	45	6.334	2.125	10	1.650	0.274
Harbor Porpoise 2	Fresh	Skin	Adult	90	4.034	1.525	10	1.287	0.553
Harbor Porpoise 2	Fresh	Skin	Adult	0	1.942	3.014	1	2.472	0.507
Harbor Porpoise 2	Fresh	Skin	Adult	45	5.400	1.467	1	1.219	0.261
Harbor Porpoise 2	Fresh	Skin	Adult	90	3.089	1.257	1	1.013	0.386
Harbor Porpoise 2	Frozen	Blubber	Adult	0	0.874	0.260	10	0.209	0.432
Harbor Porpoise 2	Frozen	Blubber	Adult	45	0.976	0.300	10	0.271	0.287
Harbor Porpoise 2	Frozen	Blubber	Adult	90	0.614	0.260	10	0.237	0.443
Harbor Porpoise 2	Frozen	Skin	Adult	0	1.783	0.600	10	0.493	0.436
Harbor Porpoise 2	Frozen	Skin	Adult	45	4.284	1.350	10	1.230	0.443
Harbor Porpoise 2	Frozen	Skin	Adult	90	1.850	1.957	10	1.641	0.411
Harbor Porpoise3	Fresh	Blubber	Adult	0	0.661	0.500	10	0.476	0.449
Harbor Porpoise3	Fresh	Blubber	Adult	90	0.903	0.425	10	0.341	0.371
Harbor Porpoise3	Fresh	Blubber	Adult	0	0.454	0.550	1	0.339	0.554
Harbor Porpoise3	Fresh	Blubber	Adult	45	0.988	0.343	1	0.216	0.391
Harbor Porpoise3	Fresh	Blubber	Adult	90	0.798	0.400	1	0.294	0.372
Harbor Porpoise3	Fresh	Skin	Adult	0	2.508	0.925	10	0.697	0.650
Harbor Porpoise3	Fresh	Skin	Adult	90	2.096	1.750	10	1.466	0.446
Harbor Porpoise3	Fresh	Skin	Adult	0	1.347	0.533	1	0.367	0.569
Harbor Porpoise3	Fresh	Skin	Adult	45	7.186	1.888	1	1.303	0.377
Harbor Porpoise3	Fresh	Skin	Adult	90	1.857	1.633	1	1.380	0.371
Orca J32	Frozen	Blubber	Adult	0	3.715	0.713	10	0.470	0.646
Orca J32	Frozen	Blubber	Adult	45	2.003	0.400	10	0.308	0.349
Orca J32	Frozen	Blubber	Adult	90	3.514	0.838	10	0.658	0.289
Orca J32	Frozen	Blubber	Adult	0	4.271	0.313	1	0.194	0.481
Orca J32	Frozen	Blubber	Adult	45	3.582	0.386	1	0.228	0.455
Orca J32	Frozen	Blubber	Adult	90	3.034	0.588	1	0.422	0.337
Orca J32	Frozen	Skin	Adult	0	5.329	2.100	10	1.545	0.578
Orca J32	Frozen	Skin	Adult	45	10.575	2.029	10	1.431	0.501
Orca J32	Frozen	Skin	Adult	90	3.388	1.500	10	1.130	0.837
Orca J32	Frozen	Skin	Adult	0	2.310	0.900	1	0.554	0.889
Orca J32	Frozen	Skin	Adult	45	4.102	1.229	1	0.706	1.087
Orca J32	Frozen	Skin	Adult	90	11.048	2.440	1	1.651	0.426
Neonate Orca	Frozen	Blubber	Juvenile	0	1.404	0.740	10	0.556	0.570
Neonate Orca	Frozen	Blubber	Juvenile	90	1.491	0.467	10	0.315	0.813

Neonate Orca	Frozen	Blubber	Juvenile	0	1.135	0.485	1	0.286	0.659
Neonate Orca	Frozen	Blubber	Juvenile	45	2.587	0.392	1	0.256	0.619
Neonate Orca	Frozen	Blubber	Juvenile	90	1.368	0.415	1	0.254	0.672
Neonate Orca	Frozen	Skin	Juvenile	90	1.702	0.960	10	0.629	1.706
Neonate Orca	Frozen	Skin	Juvenile	0	8.017	1.720	1	1.195	0.615
Neonate Orca	Frozen	Skin	Juvenile	45	6.196	1.038	1	0.670	1.227
Neonate Orca	Frozen	Skin	Juvenile	90	2.959	1.178	1	0.705	1.077
Seal Adult 1	Fresh	Blubber	Adult	0	2.220	0.875	10	0.451	0.961
Seal Adult 1	Fresh	Blubber	Adult	45	1.801		10		0.987
Seal Adult 1	Fresh	Blubber	Adult	90	2.460	0.786	10	0.476	0.637
Seal Adult 1	Fresh	Blubber	Adult	0	1.904		1		0.943
Seal Adult 1	Fresh	Blubber	Adult	45	1.094		1		1.015
Seal Adult 1	Fresh	Blubber	Adult	90	2.084		1		0.733
Seal Adult 1	Fresh	Skin	Adult	0	19.144	11.663	10	8.749	0.806
Seal Adult 1	Fresh	Skin	Adult	45	23.426		10		0.795
Seal Adult 1	Fresh	Skin	Adult	90	15.391	16.013	10	14.455	0.915
Seal Adult 1	Fresh	Skin	Adult	0	14.378		1		0.763
Seal Adult 1	Fresh	Skin	Adult	45	16.972		1		0.609
Seal Adult 1	Fresh	Skin	Adult	90	17.824		1		0.743
Seal Adult 1	Frozen	Blubber	Adult	0	0.655	0.200	10	0.106	0.662
Seal Adult 1	Frozen	Blubber	Adult	90	0.932	0.352	10	0.230	0.576
Seal Adult 1	Frozen	Blubber	Adult	0	0.477	0.200	1	0.106	0.753
Seal Adult 1	Frozen	Blubber	Adult	90	0.938	0.296	1	0.186	0.487
Seal Adult 1	Frozen	Skin	Adult	0	19.590	14.987	10	11.459	0.782
Seal Adult 1	Frozen	Blubber	Adult	0	1.136	0.398	10	0.224	0.765
Seal Adult 1	Frozen	Blubber	Adult	45	2.107	0.485	10	0.365	0.469
Seal Adult 1	Frozen	Blubber	Adult	90	1.501	0.418	10	0.275	0.640
Seal Adult 1	Frozen	Skin	Adult	0	16.829	28.043	10	19.647	1.259
Seal Adult 1	Frozen	Skin	Adult	45	40.638	33.917	10	23.553	0.760
Seal Adult 1	Frozen	Skin	Adult	90	31.040	27.740	10	18.872	0.869
Seal Adult 2	Fresh	Blubber	Adult	0	1.326	0.950	10	0.663	0.563
Seal Adult 2	Fresh	Blubber	Adult	45		0.322	10	0.281	
Seal Adult 2	Fresh	Blubber	Adult	90	1.180	0.688	10	0.281	1.006
Seal Adult 2	Fresh	Blubber	Adult	0	0.884		1		0.697
Seal Adult 2	Fresh	Blubber	Adult	45	0.719		1		0.602
Seal Adult 2	Fresh	Blubber	Adult	90	0.996		1		0.618

Seal Adult 2	Fresh	Skin	Adult	0	8.393	7.167	10	5.836	0.583
Seal Adult 2	Fresh	Skin	Adult	45	13.870	9.113	10	7.568	0.481
Seal Adult 2	Fresh	Skin	Adult	90	8.563	9.925	10	8.822	0.555
Seal Adult 2	Fresh	Skin	Adult	0	4.551		1		0.446
Seal Adult 2	Fresh	Skin	Adult	45	8.436		1		0.538
Seal Adult 2	Fresh	Skin	Adult	90	6.887		1		0.479
Seal Adult 2	Frozen	Skin	Adult	0	29.541	26.392	10	19.744	0.740
Seal Adult 2	Frozen	Skin	Adult	45	33.490	30.440	10	22.001	0.563
Seal Adult 2	Frozen	Skin	Adult	90	34.702	32.930	10	24.649	0.727
Seal Adult 3	Fresh	Blubber	Adult	0	0.774	1.127	10	0.771	0.859
Seal Adult 3	Fresh	Blubber	Adult	45	2.185	0.937	10	0.654	0.772
Seal Adult 3	Fresh	Blubber	Adult	90	1.454	0.805	10	0.526	0.581
Seal Adult 3	Fresh	Blubber	Adult	0	1.843	2.494	1	1.497	0.927
Seal Adult 3	Fresh	Blubber	Adult	90	1.584	1.133	1	0.772	1.197
Seal Adult 3	Fresh	Skin	Adult	0	29.189	17.097	10	13.249	0.567
Seal Adult 3	Fresh	Skin	Adult	45	27.284	20.143	10	13.437	0.718
Seal Adult 3	Fresh	Skin	Adult	90	27.433	22.628	10	21.991	0.817
Seal Adult 3	Fresh	Skin	Adult	0	34.011	16.570	1	12.830	0.699
Seal Adult 3	Fresh	Skin	Adult	90	41.854	15.792	1	11.264	0.487
Seal Adult 3	Frozen	Blubber	Adult	0	1.085		10		1.112
Seal Adult 3	Frozen	Blubber	Adult	45	1.385		10		1.540
Seal Adult 3	Frozen	Blubber	Adult	90	0.946		10		0.839
Seal Adult 3	Frozen	Skin	Adult	0	43.594	24.617	10	18.128	0.694
Seal Adult 3	Frozen	Skin	Adult	45	36.016	22.194	10	18.194	0.734
Seal Adult 3	Frozen	Skin	Adult	90	41.455	25.506	10	19.268	0.659

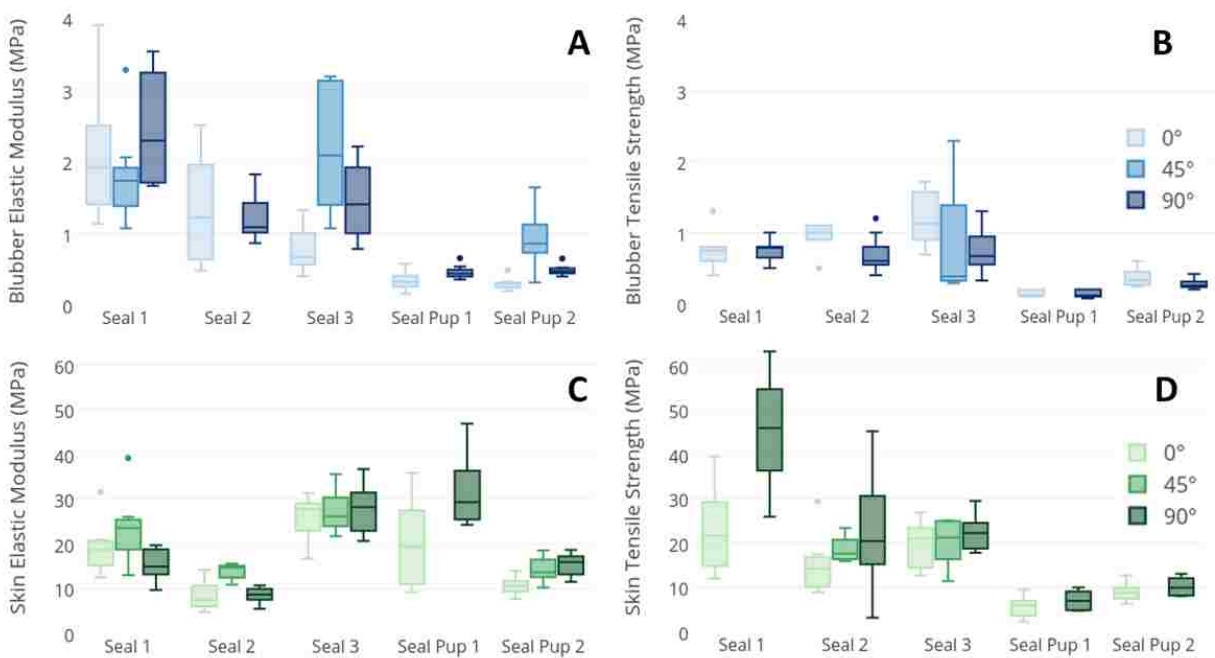


Figure A.1: Box plots show all tensile testing material results from fresh harbor seal (*Phoca vitulina*) tissue at a test speed of 10 mm/s. For each seal, tissue is tested at three orientations. Note that skin (A,B) and blubber (C,D) do not have the same y-scaling. Skin is an order of magnitude stiffer and stronger than the blubber across both the elastic modulus (A,C) and tensile strength (B,D) testing.

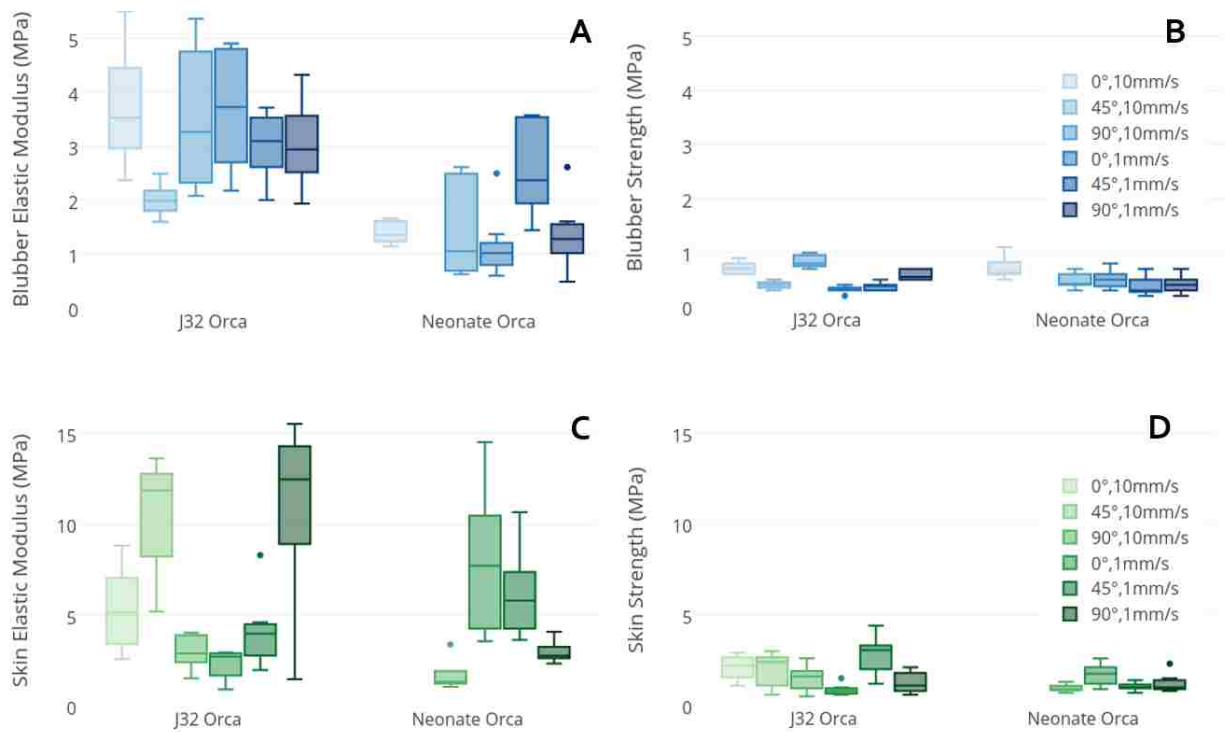


Figure A.2: Box plots show all tensile testing material results from frozen Killer whale (*Orcinus orca*) tissue at a test speed of 1 and 10 mm/s. For each whale, tissue is tested at three orientations. Note that skin (A,B) and blubber (C,D) do not have the same y-scaling. Skin is an order of magnitude stiffer and stronger than the blubber across both the elastic modulus (A,C) and tensile strength (B,D) testing.

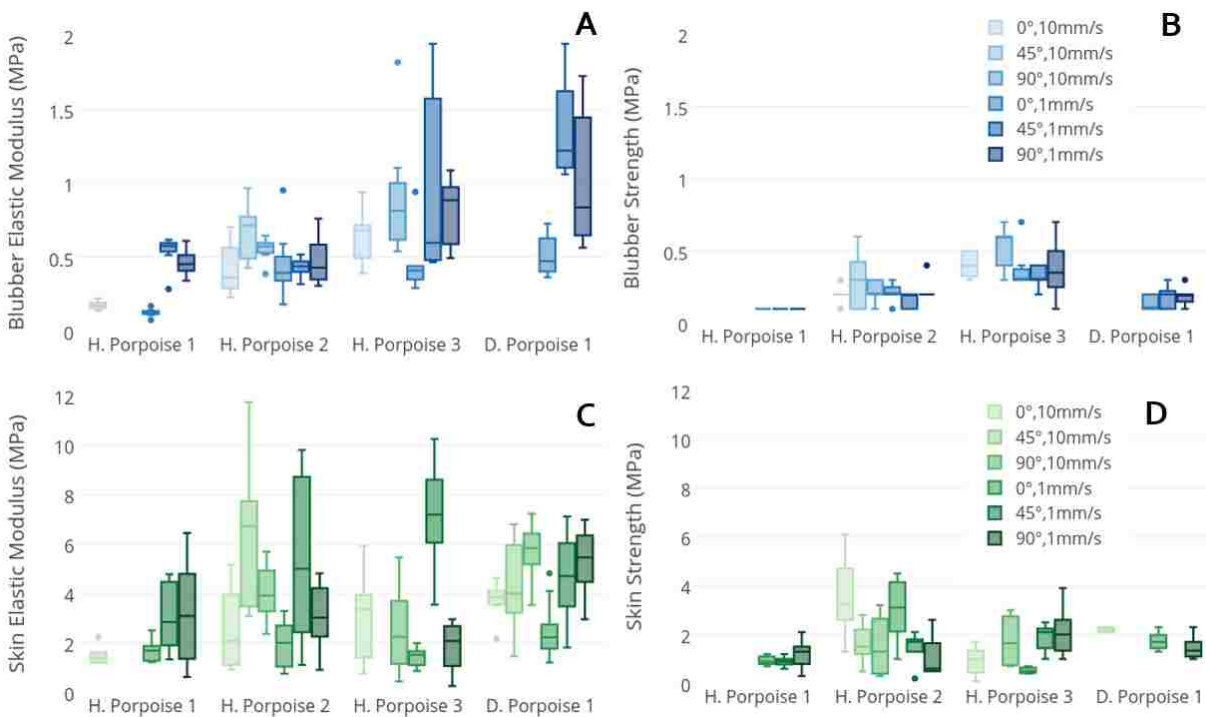


Figure A.3: Box plots show all tensile testing material results from fresh Harbor Porpoise (*Phocoena phocoena*) and Dall's Porpoise (*Phocoenoides dalli*), call "H. Porpoise" and "D. Porpoise" respectively. The tissue was tested at speed of 1 and 10 mm/s. For each whale, tissue is tested at three orientations. Note that skin (A,B) and blubber (C,D) do not have the same y-scaling. Skin is an order of magnitude stiffer and stronger than the blubber across both the elastic modulus (A,C) and tensile strength (B,D) testing.

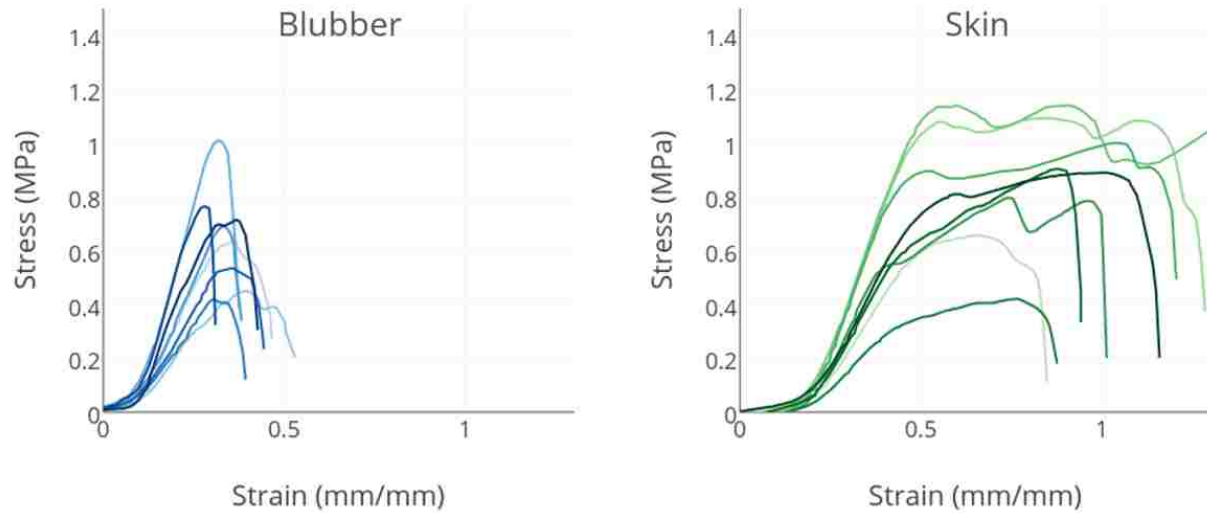


Figure A.4: Example stress strain curves for orca tensile testing in the  $0^\circ$  orientation at 10 mm/s, with blubber in blue and skin in green.

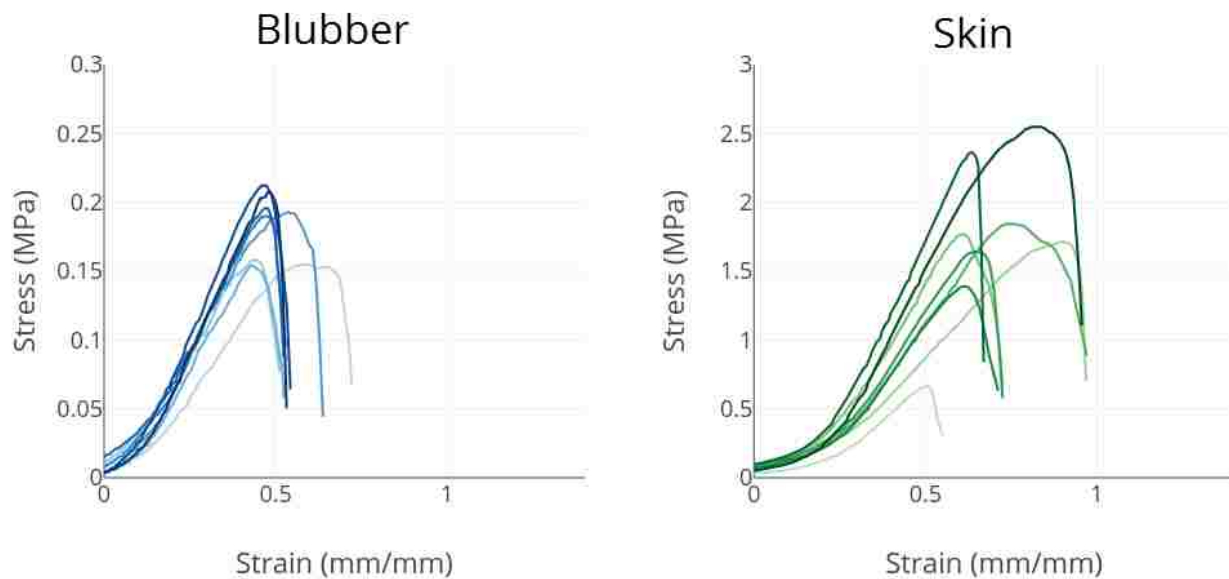


Figure A.5: Example stress strain curves for harbor porpoise tensile testing in the  $0^\circ$  orientation at 10 mm/s, with blubber in blue and skin in green. Note that the two plots are not on the same y-scale and in fact have a different order of magnitude.

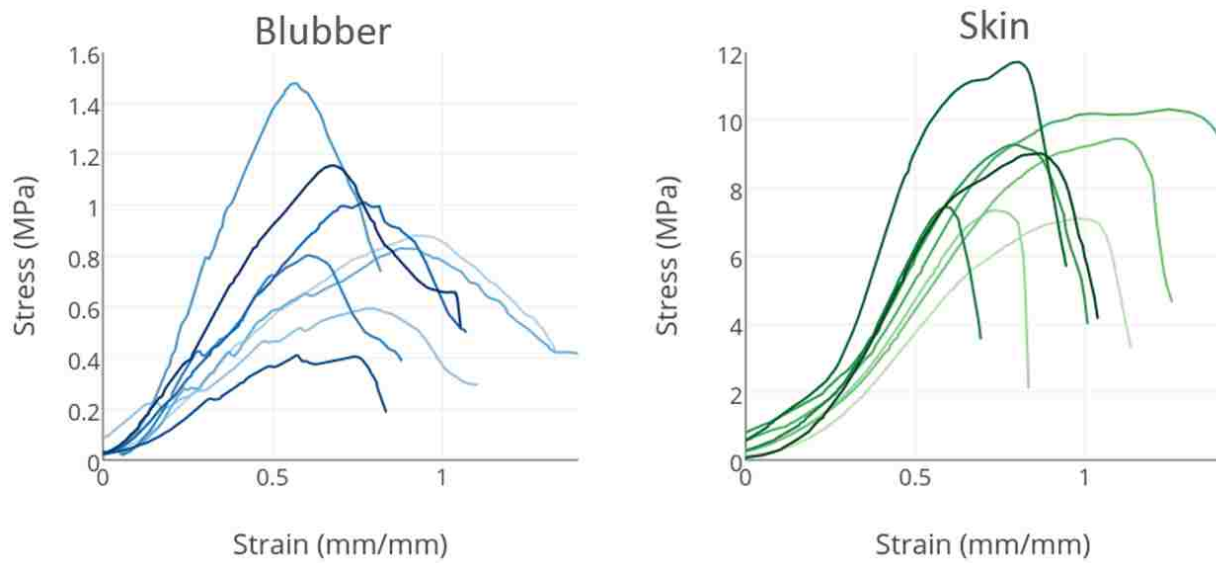


Figure A.6: Example stress strain curves for harbor seal tensile testing in the  $0^\circ$  orientation at 10 mm/s, with blubber in blue and skin in green. Note that the two plots are not on the same y-scale and in fact have a different order of magnitude.



## Appendix B

# MARINE MAMMAL PARTS PERMITS AND NECROPSY REPORTS

This appendix shows the requisite parts permits for completing testing on marine mammals.



UNITED STATES DEPARTMENT OF COMMERCE  
National Oceanic and Atmospheric Administration  
NATIONAL MARINE FISHERIES SERVICE  
Northwest Region  
7600 Sand Point Way N.E. Bldg 1  
Seattle, WA 98115

January 17, 2013

Dr. Michele Halvorsen  
Pacific Northwest National Laboratory  
902 Battelle Boulevard  
Richland, Washington 99352

Dear Dr. Halvorsen:

Thank you for your recent letter requesting authorization to receive marine mammal parts from the Northwest Marine Mammal Stranding Network (Network) for use in scientific research at the Pacific Northwest National Laboratory. We have reviewed your request for 12" x 12" sections of skeletal structure preferably from the head or rib areas to include the supportive tissues of muscle, fat, skin, and connective tissues to the bone from transient and resident killer whale (*Orcinus orca*), harbor porpoise (*Phocoena phocoena*), and harbor seal (*Phoca vitulina*). Due to the high interest in endangered Southern Resident Killer Whales please coordinate with our office when a sample becomes available. Pursuant to the marine mammal regulations at 50 CFR 216.22 and 50 CFR 216.37, this letter provides specific authorization for the transfer of marine mammal parts from the Network participants listed below. Marine mammal parts obtained under this authorization may not be subsequently transferred to other individuals or organizations without written authorization from this office. Copies of this response and your request have been forwarded to the Network for their information.

The regulations allow the transfer of marine mammal parts salvaged from stranded animals provided: (a) the parts have been registered by the Northwest Regional Office; (b) the person (facility) transmitting the parts does not receive remuneration of any kind; (c) the part is transferred for scientific research, curation in a collection, or educational purposes; and (d) the transfer has been authorized by written authorization from this office. Please be advised that provision of marine mammal parts by Network participants in response to your request is voluntary. If any of the participants listed transfer parts responsive to your request, the regulations require that they send notification of the transfer to this office within 30 days after the transfer. The notification should include the registration number and description of samples sent, and the name and address of the recipient. Marine mammal specimens and/or collections transferred or held pursuant to regulations at 50 CFR 216.22 or 50 CFR 216.37 must be produced upon request for inspection by the NOAA Office for Law Enforcement.




Figure B.1: PNNL Authorization from the National Oceanic and Atmospheric Association, which expires January 17, 2018.

2

If you have further questions regarding this response please contact Brent Norberg, of my staff, at 206-526-6550 or via email at [brent.norberg@noaa.gov](mailto:brent.norberg@noaa.gov). Marine mammal parts transfer notifications may be sent directly to Mr. Norberg.

Sincerely,



William W. Stelle, Jr.  
Regional Administrator

cc: Network Participant List (attached)

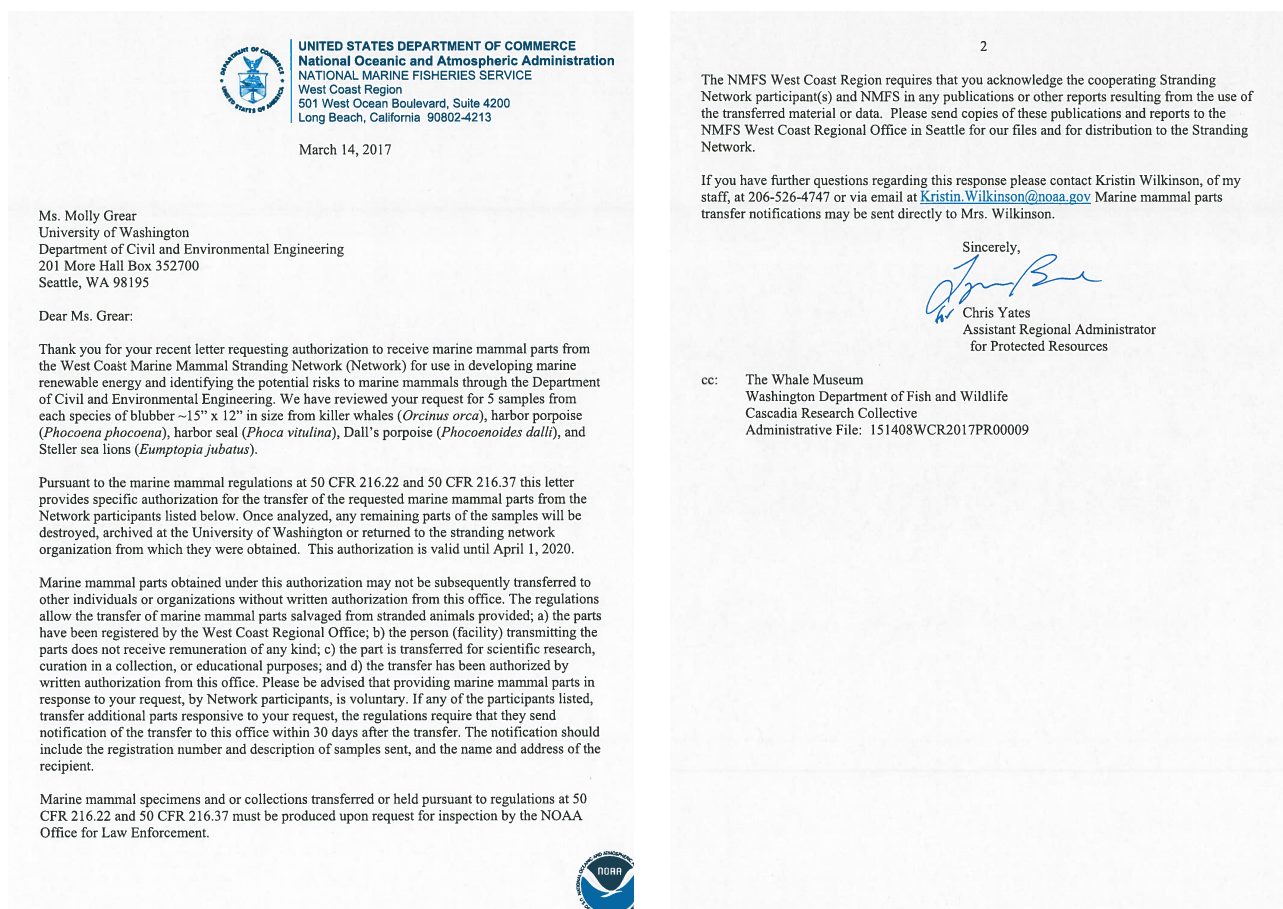


Figure B.2: UW Authorization from the National Oceanic and Atmospheric Association, which expires April 1, 2020

**MARINE MAMMAL INCIDENT RESPONSE FORM** (one form per animal)

Examination date Dec 6/14 Examiner(s) LNU, ES, BW (measured) Age Class Adult  
 Location Boies Beach Sex Female Juvenile/Subadult Yearling  
 Species KW SR CBD (could not be determined) Not assessed Pup/calving Not assessed  
 Response comments J32 pregnant Animal condition at time of initial exam Dead Alive

**DEAD ANIMAL** Weight Measured 562 Estimated 62 units lbs Length Measured 162 Estimated 168 units cm  
 External injuries few. Scap photos

**Carcass Condition** Freshly dead Advanced decomposition Extent of scavenging none - mib  
 Moderate decomposition Mummified/skeletal Unknown

**LIVE ANIMAL** Condition Other Measurements (estimated) Length N/A Weight N/A  
 Response actions taken (check all that apply) Left at site, no further action  
 Under observation Disentangled Transferred to rehab facility: Relocated Other

**EVIDENCE OF HUMAN INTERACTION** Yes (describe below) teeth on right lower jaw sawed off overnight  
 No CBD (could not be determined) Not assessed

**PHOTO DOCUMENTATION** Digital Video Photographer ES, BW  
 Whole body Head (incl. blowhole & ventral pleats) Dorsal fin (if applicable) Flippers Tail or hind flippers Genital area Pigmentation Injuries/scar Signs of human interaction Other:

**DISPOSITION** (incl. where and how stored) Collected carcass: Left on site (as is)  
 Collected gear/evidence: Collected samples: AWC, NOAA, DFO, RCMP, UBC  
 Disposed of: issues@landfill

**MARINE MAMMAL INCIDENT RESPONSE FORM** - Page 2

**CETACEAN MORPHOMETRICS** Units in cm Side Or L

Straightline length (from tip of upper jaw) 156.2  
 1 To fluke notch (row length) 16  
 2 To apex of melon 39  
 3 To gape of mouth 43  
 4 To centre of eye 49  
 5 To centre of blowhole 21.6  
 6 To anterior throat grooves (if applicable) 91  
 7 To anterior insertion of flipper 89.4  
 8 To anterior insertion of dorsal fin 92.3  
 9 To dorsal fin tip 89.4  
 10 To anterior genital slit 6.7  
 11 To anus 7.2  
 12 From fluke notch to anus 38

**APPENDAGES** 13 Dorsal fin height curved  
 14 Flipper, anterior length 43.3  
 15 Flipper, maximum width 14.2  
 16 Tail fluke width curved  
 17 At eyes 250  
 18 At posterior insertion of flipper 364  
 19 At maximum location 384  
 20 At anus 242

**VENTRAL THROAT PLEATS** (if applicable) Number of throat pleats 2 Length of longest throat pleat see below

**BLUBBER THICKNESS** 21 Dorsal see below  
 22 Lateral see below  
 23 Ventral see below

**PINNIPED / OTTER MORPHOMETRICS** Units in cm Or L

Length 1 Straightline - from tip of snout to tip of tail  
 2 Curvilinear - from tip of snout to tip of tail

**APPENDAGES** 3 Front flipper, anterior length  
 4 Back flipper, anterior length  
 5 At posterior insertion of front flipper  
 6 At maximum location  
 7 At anus

**BLUBBER THICKNESS** 8 Dorsal  
 9 Lateral  
 10 Ventral

**SEA TURTLE MORPHOMETRICS** Carapace length 1 Straightline - head end of shell to tip of tail  
 2 Curvilinear - head end of shell to tip of tail  
 Carapace width 3 maximum width

**ADDITIONAL COMMENTS** All blubber measurements summarized  

	Mid	Dorsal	Lateral	Ventral
Behind blow hole (nape)	4.1	4.5	5.5	5.5
Behind pectoral	4.0	5.6	5.5	

 ventral at anus - 4.8cm

Submit completed forms to Marine Mammal Response Coordinator by Fax: 250-756-7053 or Email: [lisa.spavan@dfmp.ca](mailto:lisa.spavan@dfmp.ca)

Revised February 23, 2014

cm. measurements on right side

**APPENDIX XVIII: Morphometric analysis of stranded killer whales**

Note: If time or tides are an issue, please collect at least the data points in **BOLD**

Observer Linda Nichol ES, BW Date Dec 6, 2014

Identification number J32 Gender F Weight

**MEASUREMENTS, BODY** (specify units of measure used)

1 Total straight length, snout to notch		13 Snout to genital slit	
2 Snout to center of eye (left)		14 Snout to anus	
3 Length of eye (left)		15 Eye to blowhole (center)(left)	
4 Snout to apex of melon		16 Projection of the lower jaw	
5 Snout to ear (left)	<u>6.7</u>	17 Blubber thickness*, mid dorsal	<u>2.8 cm</u>
6 Center of eye to ear (left)		18 Blubber thickness*, mid lateral	<u>3.2 cm</u>
7 Center of eye to angle of mouth	<u>1.3</u>	19 Blubber thickness*, mid ventral	<u>3.3 cm</u>
8 Center of eye to eye (curved - brow)	<u>2.2</u>	20 Girth at eye	
9 Snout to center of blowhole		21 Girth at axilla	
10 Snout to flipper (left)		22 Girth at leading edge of dorsal	<u>3x 19.8</u>
11 Snout to tip of dorsal fin	<u>86.7</u>	23 Girth at anus	
12 Snout to center of umbilicus	<u>83.4</u>	23a Girth cm before notch	

\*Blubber thickness is measured at line 22-just cranial to the dorsal fin

general snout tip  
 upper - 51  
 lower - 52  
 1cm

**MEASUREMENTS, APPENDAGES** (specify units of measurement)

29 Flipper length (ant) (left)		33 Length of dorsal fin base	
30 Flipper length (post) (left)		34 Width of flukes (straight)	
31 Maximum width of flipper (left)		35 Length of flukes (left)	
32 Height of dorsal fin		36 Depth of fluke notch	

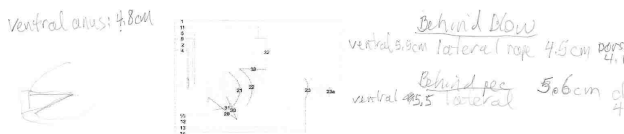


Figure B.3: Necropsy Report from J32, stranded in British Columbia, Canada in December 2014.

## MARINE MAMMAL MORTALITY INVESTIGATION

## FINAL REPORT

San Juan County Marine Mammal Stranding Network  
The Whale Museum  
P.O. Box 945  
62 First Street North  
Friday Harbor, WA 98250  
Telephone: (360) 378-4710; Fax: (360) 378-5790

The SeaDoc Society  
UC Davis Wildlife Health Center  
942 Deer Harbor Road  
Eastsound, WA 98245  
Telephone: (360) 376-3910  
Fax: (360) 376-3909

STRANDING CASE NUMBER: 2015-SJ022

DATE FOUND: July 22, 2015

DATE OF REPORT:

LOCATION FROM WHICH CARCASS WAS RECOVERED Buckhorn Beach, Orcas Island  
(48.708594, -122.869933)

(San Juan County, Washington)

SPECIES (NO.) Harbor Porpoise SEX Female AGE Adult WEIGHT 58 kg

## STRANDING HISTORY:

On July 22, 2015 a private citizen reported a dead harbor porpoise on Buckhorn Beach, Orcas Island. It was retrieved the same day by members of the San Juan County Marine Mammal Stranding Network and kept chilled until necropsy could be performed the next morning.

FINAL DIAGNOSIS: Thoracic mass: neoplasia vs. abscess (tentative)  
Parasitism  
Emaciation

## COMMENTS:

## MARINE MAMMAL IMPLICATIONS:

The top differentials for the mass include a neoplastic tumor with a necrotic center or an abscess. Neither of these is common among causes of harbor porpoise mortality. From 2000 to present, 1 out of 57 (1.7%) harbor porpoises necropsied by the SJCMMSN had an abscess. In that same sample, none of the porpoises had neoplasia. Parasites and emaciation are more commonly found (22/57, 38.5% and 8/57, 14.0%, respectively) among harbor porpoises within the Salish Sea at the time of death; however, the effects of the parasite burden are unclear. The emaciation is likely secondary to the thoracic mass and lung disease.

## PUBLIC HEALTH OR DOMESTIC ANIMAL IMPLICATIONS:

None known at this time

## APPROVED BY:

Joseph K. Gaydos, VMD, PhD  
SeaDoc Society, UC Davis Wildlife Health Center

Stephen Raverty, DVM, MSc, PhD  
British Columbia Ministry of Agriculture and Food

DISTRIBUTION LIST: SeaDoc Society, SJCMMSN, Baird, Balcomb, Calambokidis, Jeffries, Hanson, Lambourn, Mansfield, Norberg, Norman, Wilkinson Abernathy, Cottrell, Ford, Haulena, Raverty, Ross, Schwantje, Spaven, Stephen

## IMAGES:



Image 1: Multilobular mass extending from pericardium to the left lung, with larger pulmonary nodules visible in the right lung



Image 2: Caseous/liquefactive center of the mass

## PAGE 2 – SJCMMSN / SeaDoc Society - LABORATORY RESULTS

## FINAL REPORT

CASE NUMBER 2015-SJ022

## GROSS FINDINGS: (July 23, 2015)

This harbor porpoise is in fair postmortem condition and poor physical condition. The animal is cachectic with prominent dorsal and lateral spinous processes and wasting of the epaxial muscles. It measures 165 cm straight from the tip of its upper jaw to the deepest part of the fluke notch and has an axillary girth of 84 cm. Subcutaneous adipose tissue thickness measured at the mid thoracic level is 1.4 cm, 1.4 cm and 1.5 cm dorsally, laterally and ventrally, respectively. Teeth are present and worn to the gums in the caudal half of the dental arcade, suggesting the animal is older. Superficial dermal abrasions are present on the dorsal aspect of the beak, the right ocular region, the cranial aspect of the dorsal fin and the cranial aspects of the left and right sides of the fluke. Cutaneous and subcutaneous tissue is missing from the left side of the carcass from the gape of the mouth back to the level of the scapula and extending dorsally from the eye down to the level of the flipper. The left eye is missing. On the right side blood is present in the anterior chamber of the globe (hypphema). Light brown liquid can be expressed from the left nipple. Subcutaneous nodules are present craniodorsal to the genital slit, containing encysted nematode parasites. The lung parenchyma is diseased with multifocal firm, white nodules ranging in size (1-3 mm). The lungs are hyperemic and edematous. Roundworms (1-2 cm) are present within the airways of the lung. A large (14 cm by 10 cm), multilobulated thoracic mass is present that extends from the apex to the base of the heart. The mass is discrete from the heart and located primarily on the left side. It extends into the pericardium with a small section infiltrating the parenchyma of the left lung and another small portion (3 cm by 3 cm) extending towards the right lung, though it is discrete from the right lung. Blood supply is visible on the superficial surface of the mass. Many smaller masses extend cranially from this mass within the pericardium towards the cervical region and appear glandular. Upon dissection, the large mass has a liquefactive to caseous necrotic center that is pale yellow. The liver contains multiple firm, white nodules that contain trematode parasites. The uterus is involuting and highly vascularized. There is a follicle on each ovary. The forestomach is void of ingesta, but contains numerous small roundworms (~1 cm) and fewer larger roundworms (~3 cm). The glandular stomach and pylorus were not dissected, but were sent for stomach content analysis. Small nematodes are present in the peribullar tissue and the eustachion tubes and are surrounded by a dark red material (blood). The brain weighs 600 g. Gross lesions are not apparent in the brain, spleen, adrenals, kidneys, bladder or the remaining gastrointestinal tract.

MICROSCOPIC FINDINGS AND MORPHOLOGIC DIAGNOSIS: (Dr. Stephen Raverty, DVM, MSc, PhD, Veterinary Pathologist; British Columbia Ministry of Agriculture and Food, Abbotsford, BC)

## MICROBIOLOGIC RESULTS:

## TOXICOLOGIC RESULTS:

## PARASITOLOGIC RESULTS:

Nematodes noted in the subcutaneous adipose tissue are likely *Crassicauda* spp. Those present in the lung are likely *Anisakis* or *Halocercus* spp. Trematodes noted in the liver are likely *Camptula* spp. Two separate species noted in the stomach are likely *Anisakis*, *Pseudoterranova*, or *Hedvinius mironovi* spp. Nematodes from the peribullar tissue and eustachion tube are likely *Stenurus* spp. Parasites were collected, stored in 70% ethanol, and will be sent to the University of Florida for definitive identification.

## CEMENTUM ANALYSIS:

A tooth was submitted to NOAA's Southwest Fisheries Science Center for aging. Results are pending

Figure B.4: Necropsy Report from Harbor Porpoise, stranded on Orcas Island, Canada in July 2015.